

DECEMBER 2019

Ph.D. in Civil Engineering

SAMADAR SALIM MAJEED

T.C.

**HASAN KALYONCU UNIVERSITY
GRADUATE SCHOOL OF
NATURAL & APPLIED SCIENCES**

**PROPERTIES OF BASALT FIBER SELF-COMPACTED
CONCRETE AT ELEVATED TEMPERATURE**

**Ph.D. THESIS
IN
CIVIL ENGINEERING**

SAMADAR SALIM MAJEED

DECEMBER 2019

**Properties of Basalt Fiber Self-Compacted Concrete At
Elevated Temperature**

Ph.D. Thesis

in

Civil Engineering

Hasan Kalyoncu University

Supervisor

Prof. Dr. Mehmet KARPUZCU

Co-Supervisor

Asst. Prof. Dr. James H. HAIDO

By

Samadar Salim MAJEED

December 2019



© 2019 [Samadar Salim MAJEED]



**GRADUATE SCHOOL OF NATURAL &
APPLIED SCIENCES INSTITUTE
PhD ACCEPTANCE AND APPROVAL FORM**

Civil Engineering Department, Civil Engineering PhD (Philosophy of Doctorate) programme student **Samadar Salim MAJEED** prepared and submitted the thesis titled **PROPERTIES OF BASALT FIBER SELF-COMPACTED CONCRETE AT ELEVATED TEMPERATURE** defened successfully at the VIVA on the date of 11/12/2019 and accepted by the jury as a PhD thesis.

<u>Position</u>	<u>Title, Name and Surname</u> <u>Department/University</u>	<u>Signature</u>
Supervisor	Prof. Dr. Mehmet KARPUZCU Civil Engineering Department/ Hasan Kalyoncu University	
Jury Member	Prof. Dr. Mustafa GÜNAL Civil Engineering Department/ Gaziantep University	
Jury Member	Prof. Dr. Fevziye AKÖZ Civil Engineering Department/ Hasan Kalyoncu University	
Jury Member	Assoc. Prof. Dr. Nildem TAYŞI Civil Engineering Department/ Gaziantep University	
Jury Member	Asst. Prof. Dr. Adem YURTSEVER Civil Engineering Department/ Hasan Kalyoncu University	

This thesis is accepted by the jury members selected by the institute management board and approved by the institute management board.

Prof. Dr. Mehmet KARPUZCU
Director

I hereby declare that all information in this document has been obtained and presented in accordance with academic rules and ethical conduct. I also declare that, as required by these rules and conduct, I have fully cited and referenced all material and results that are not original to this work.

SAMADAR SALIM MAJEED

ABSTRACT

PROPERTIES OF BASALT FIBER SELF-COMPACTED CONCRETE AT ELEVATED TEMPERATURE

MAJEED, Samadar Salim

Ph.D. in Civil Engineering

Supervisor: Prof. Dr. Mehmet KARPUZCU

Co-Supervisor: Asst. Prof. Dr. James HAIDO

November 2019

136 pages

Inorganic based basalt fibers used in concrete production prevent the development of cracks and increase the service life of concrete structures. Similar to other industrial concrete fibers, basalt fibers can be utilized in self-compacted high strength concrete (SCHSC) with low permeability and proper workability. Because of this feature, basalt fiber concrete can be used in various infrastructure projects such as buildings, highways and bridges. Studies on the mechanical properties of this concrete are non-extensive; therefore, further investigations are considered essential in the direction of the efficiency of self-compacted basalt fiber concrete (SCBFC) in retrofitting deteriorated normal strength concrete.

In this study, effect of basalt fiber on the workability of fresh SCHSC has been measured in terms of slump flow, J-ring flow, V-funnel flow and L-box height ratio. In addition, the properties of hardened concrete such as compressive strength, splitting strength, modulus of elasticity, flexural strength and Poisson ratio were investigated for different temperatures between 25°C – 500°C. It was concluded that the fibers decreased the unit weight and compressive strength of the concrete and improved the tensile strength due to the arresting of micro cracks with increasing fiber ratio. The strength of SCHSC which has been exposed to high temperature was observed decrease. Permeability tests have been conducted as well and revealed that 0.25% volume fraction of basalt fibers is optimum value to get reasonable penetration of liquid within this concrete material.

In preparation of hybrid prism samples, it was prepared low strength concrete base to represent old and new repaired concrete and the surface of the new repaired concrete was coated with SCHSC. At the interfaces between these two parts, different roughening manners such as drilling (holes), grooving and sand blasting were applied. Slant shear test was performed to investigate adherence strength of samples. Surface improvement by grooving and sand blasting was found better than the other cases with taking into account the applied high temperatures. The effect of independent variables such as basalt fiber volume ratio and environmental temperature on the mechanical properties of concrete were evaluated statistically. According to the analysis outcomes, the roughening type of the interfacial surface

was found more important than fiber ratio and temperature changes on slant shear of hybrid concrete. Finally, modelling

has been performed with depending on gene expression programming for present experimental results and it is demonstrated that the predicted and experimental values from the models obtained are in suitable distribution on the agreement line with correlation coefficient more than 90%.

Keywords: Basalt Fiber Concrete; Slant Shear Strength; Self Compacted Fiber Concrete; Firing of Concrete; GEM modeling of concrete behavior.



ÖZET

YÜKSEK SICAKLIKTA BAZALT LİF İÇEREN KENDİLİĞİNDEN YERLEŞEN BETONUN ÖZELLİKLERİ

MAJEED, Samadar Salim
Doktora Tezi, İnşaat Mühendisliği
Tez Yöneticisi :Prof. Dr. Mehmet KARPUZCU
Eş Danışman: Asst. Prof. Dr. James HAIDO
Kasım 2019
136 sayfa

Beton üretiminde kullanılan inorganik kökenli bazalt lifler, çatlakların gelişimini engelleyerek beton yapıların servis ömrünü arttırmaktadır. Diğer endüstriyel beton lifleri gibi bazalt lifler de geçirimsizliği düşük ve uygun işlenebilirliği olan yüksek mukavemetli, kendiliğinden yerleşen betonlarda (KYBLB) kullanılabilir. Bu özelliği nedeni ile bazalt lifli betonlar, binalarda, otoyollar ve köprüler gibi çeşitli altyapı projelerinde kullanılabilir. Bazalt lifin betonun mekanik özelliklerine etkilerinin araştırıldığı çalışmalar kapsamlı değildir; bu nedenle düşük ve normal mukavemetli betonun güçlendirilmesinde kendiliğinden yerleşen, bazalt lifli betonların araştırılmasının gerekli olduğu düşünülmektedir.

Bu çalışmada, bazalt lifin KYBLB'nin taze betonun işlenebilirliğine etkileri slump akış, J-halkası akış, V-hunisi akış ve L-kutusu yükseklik oranı açısından ölçülmüş, basınç dayanımı, yarma dayanımı, elastisite modülü, eğilme dayanımı ve Poisson oranı gibi sertleşmiş beton özellikleri 25°C ile 500°C arasındaki farklı sıcaklıklar için araştırılmıştır. Liflerin, betonun birim ağırlığını ve basınç dayanımını azalttığı, çekme dayanımını ise lif oranının artırılmasıyla mikro çatlakları tutmasından dolayı iyileştirdiği sonucuna varılmıştır. Yüksek sıcaklık etkisine maruz kalan KYBLB'nun mukavemetinde genel olarak düşüş gözlenmiştir. Yapılan geçirimsizlik deneylerinde; bazalt liflerin hacim oranının %0.25 olduğu durumda beton içindeki sıvının etkili olduğu görülmüştür.

Hibrit prizma numunelerin hazırlanmasında; eski ve kötüleşmiş betonu temsilen düşük dayanımlı betondan altlık hazırlanmış, yeni onarılmış beton kısmını temsilen üst yüzeyine KYBLB ile kaplamama yapılmıştır. Bu iki kısım arasındaki arayüzeylerde delik açma, oluk açma ve kum püskürtme gibi farklı pürüzlendirme işlemleri uygulanmıştır. Numunelerde aderans dayanımının araştırılması için kayma testi gerçekleştirilmiş, yüksek sıcaklık etkisi dikkate alındığında oluk açma ve kum püskürtme işlemiyle yapılmış yüzey iyileştirmesinin diğerinden daha iyi olduğu gözlenmiştir. Bazalt lif hacim oranı ve çevre sıcaklığı gibi bağımsız değişkenlerin betonun mekanik özellikleri üzerine etkisi istatistiksel olarak değerlendirilmiş, analiz

çıktısına göre, hibrit betonun kayma dayanımında; arayüzeyin pürüzlendirme tipinin lif oranından ve sıcaklık değişiminden daha önemli olduğu görülmüştür. Gen ifadesiyle programlamaya bağlı olarak, deneysel sonuçlar üzerinde modelleme yapılmış ve modellerden elde edilen tahmini ve deneysel değerler arasında korrelasyon katsayısı %90'dan yüksek bir dağılım eğrisi elde edilmiştir.

Anahtar Kelimeler: Bazalt Lifli Beton; Eğimli birleştirmede Kayma dayanımı; Kendiliğinden Yerleşen Lifli Beton; Betonun yanması; Beton davranışının GEM Modellemesi





To the great family members, soul of my life...

ACKNOWLEDGEMENTS

I would like to express my special appreciation and thanks to my supervisor Prof. Dr. Mehmet KARPUZCU, you have been a tremendous mentor for me. Guiding and advising me from the first day to the finish makes me so grateful.

I would like to thank my research supervisor Asst. Prof. Dr. James H. HAIDO for his advice and for encouraging me during my study.

Friends with their kindness and encouragement being a light along with this far path. They really gives me power to continue this thesis facing all obstacles and challenges. Especially my dearest friend Asst. Prof. Dr. Adem YURTSEVER, who helped me to continue the working on this thesis. His existence were very important for me

A special thanks to my Wife and Little Elva. Words cannot express how grateful I am to my Mother and Father for all of the sacrifices that they did for me. Your prayer for me was what sustained me thus far.

Finally, I would like to express my gratitude to all those who participate in completion of this thesis especially universities of (Istanbul Technical University, Duhok University and Salahaldin University) for their huge laboratory support.

CONTENTS

	Page
ABSTRACT.....	v
ÖZET	vii
ACKNOWLEDGEMENTS	x
CONTENTS.....	xi
LIST OF TABLES	xv
LIST OF FIGURES	xvi
LIST OF SYMBOLS	xxi
CHAPTER 1	1
INTRODUCTION	1
1.1 General	1
1.2 Research Significance	4
1.3 Outline of the Thesis	5
CHAPTER 2	6
LITERATURE REVIEW	6
2.1 Introduction	6
2.2 Fiber for Concrete	8
2.2.1 Steel fiber.....	10
2.2.2 Glass fiber.....	11
2.2.3 Carbon fiber.....	11
2.2.4 Synthetic fiber.....	11
2.2.5 Basalt fiber.....	12
2.3 Mechanical Properties of HSC	15
2.4 Properties of Hybrid Concrete.....	20
2.5 Closing Remarks	24

CHAPTER 3	25
MATERIALS AND METHODS.....	25
3.1 Materials.....	25
3.1.1 Cement.....	25
3.1.2 Silica fume.....	26
3.1.3 Aggregate.....	27
3.1.4 Basalt fiber.....	29
3.1.5 Mixing water.....	30
3.1.6 Superplasticizer.....	31
3.2 Mixture Proportions	31
3.3 Concrete Production.....	32
3.4. Workability test methods and Casting.....	33
3.4.1 Slump flow test.....	34
3.4.2 V-funnel flow test.....	35
3.4.3 L-box test.....	37
3.4.4 J-ring flow test.....	39
3.4.5 Casting.....	40
3.5 Test Methods.....	44
3.5.1 Mechanical test methods	44
3.5.1.1 Compressive strength	44
3.5.1.2 Modulus of elasticity	46
3.5.1.3 Poisson's ratio.....	48
3.5.1.4 Splitting tensile strength	48
3.5.1.5 Flexural strength.....	49
3.5.1.6 Slant shear strength.....	50
3.5.2 Permeability test methods.....	52
3.5.2.1 Sorptivity index	52
3.5.2.2 Water penetration depth.....	53
3.5.2.3 Resistance to chloride ion penetration.....	55
3.5.3 Scanning Electron Microscopy (SEM).....	56

CHAPTER 4	57
RESULTS AND DISCUSSIONS	57
4.1 Workability tests.....	57
4.1.1 Slump flow diameter	57
4.1.2 J-ring flow diameter.....	59
4.1.3 T ₅₀ slump flow time	61
4.1.4 T ₅₀ J-ring flow time	62
4.1.5 V-funnel flow time	63
4.1.6 L-box height ratio	64
4.1.7 J-ring height difference.....	65
4.2 Mechanical tests	66
4.2.1 Compressive strength	66
4.2.2 Elastic modulus.....	70
4.2.3 Poisson's ratio.....	71
4.2.4 Splitting tensile strength	72
4.2.5 Flexural strength	74
4.2.6 Slant shear strength.....	76
4.3 Permeability tests	84
4.3.1 Sorptivity index	84
4.3.2 Water penetration depth.....	85
4.3.3 Resistance to chloride ion penetration.....	86
4.4 Scanning Electron Microscopy (SEM).....	88
CHAPTER 5	90
STATISTICAL ANALYSIS	90
5.1 Statistical Evaluation of Compressive Strength	91
5.2 Statistical Evaluation of Elastic Modulus	91
5.3 Statistical Evaluation of Poisson's Ratio.....	92
5.4 Statistical Evaluation of Splitting Tensile Strength	93
5.5 Statistical Evaluation of Flexural Strength.....	93
5.6 Statistical Evaluation of Slant Shear Strength.....	94

CHAPTER 6	96
MODELING	96
6.1 Introduction to Gene Expression Programming	96
6.2 Proposed Model.....	98
6.3 GEP Model for Elastic Modulus	101
6.4 GEP Model for Splitting Tensile Strength	105
6.5 GEP Model for Flexural Strength	110
6.6 GEP Model for Slant Shear Strength	113
CHAPTER 7	118
CONCLUSIONS.....	118
7.1 Fresh Workability:.....	118
7.2 Compressive Strength:	119
7.3 Modulus of Elasticity:	120
7.4 Poisson's ratios:.....	120
7.5 Splitting Tensile:	120
7.6 Slant shear strength:	121
7.7 Sorptivity Index:.....	122
7.8 Water Penetration Depth:	122
7.9 Resistance to chloride ion penetration:	122
REFERENCES	123

LIST OF TABLES

	Page
Table 2.1. Chemical composition of basalt fibers (Basaltex, 2019).....	14
Table 3.1. Chemical compositions and physical properties of ordinary Portland cement.....	26
Table 3.2. Sieve analysis and physical properties of river sand and crushed coarse aggregate.....	28
Table 3.3. Physical properties of basalt fiber.....	30
Table 3.4. Technical properties of superplasticizer.....	31
Table 3.5. Detailed mixture proportions for ordinary and self-compacting concretes (kg/m ³).....	32
Table 3.6. Classes and ranges for filling ability and passing ability for the SCC mixtures suggested by EFNARC (2005) committee.....	37
Table 4.1. Failure mode of slant shear strength test specimens.....	80
Table 4.2. Total charge passed according to ASTM C1202 (2019).....	85
Table 5.1. Statistical evaluation of compressive strength of SCC mixtures.....	88
Table 5.2. Statistical evaluation of elastic modulus of SCC mixtures.....	89
Table 5.3. Statistical evaluation of Poisson’s ratio of SCC mixtures.....	89
Table 5.4. Statistical evaluation of splitting tensile strength of SCC mixtures.....	90
Table 5.5. Statistical evaluation of flexural strength of SCC mixtures.....	91
Table 5.6. Statistical evaluation of flexural strength of SCC mixtures.....	92
Table 6.1. Input and output experimental data of elastic modulus, splitting tensile strength, and flexural strength for train and test set.....	96
Table 6.2. Input and output experimental data of slant shear strength for train and test set.....	97
Table 6.3. Parameters employed in model derivation.....	98

LIST OF FIGURES

	Page
Figure 2.1. Effect of fibers in concrete cracking and strength (Ghahremannejad et al., 2018).....	9
Figure 2.2. The fibers used in concrete (a) basalt fiber and (b) glass fiber (Kizilkanat et al., 2015).....	17
Figure 2.3. Slant shear test set-up for the composite concrete specimen (Tayeh et al., 2012).....	21
Figure 3.1. Photographic view of silica fume.....	26
Figure 3.2. Photographic view of: (a) river sand and (b) crushed coarse aggregate.....	28
Figure 3.3. Particle size distribution of: (a) river sand and crushed coarse aggregate and (b) aggregate mixture in comparison with A16-B16-C16 curves.....	29
Figure 3.4. Photographic view of basalt fiber.....	30
Figure 3.5. Slump flow test: (a) schematically illustration and (b) diameter measurement.....	35
Figure 3.6. V-funnel flow test: (a) schematically illustration and (b) performing test.....	36
Figure 3.7. L-box test (a) equipment types and (b) schematically illustration of equipment and pointing the fresh concrete heights (h_1 and h_2).....	38
Figure 3.8. J-ring flow test: (a) schematically representation of equipment and (b) typical height difference measurement.....	40

Figure 3.9. (a) Empty and (b) concrete-filled wooden moulds for slant shear strength test.....	41
Figure 3.10. A typical ordinary concrete part of slant shear strength test.....	42
Figure 3.11. Photograph of slant shear strength test: (a) after surface treatment and (b) after filling with SCC.....	43
Figure 3.12. Temperature exposure cycle.....	44
Figure 3.13. (a) Cylindrical test specimens for compressive strength and (b) specimens in oven for temperature exposure.....	44
Figure 3.14. (a) Sulfur capped cylindrical compressive strength test samples and (b) compressive strength test sample placed to the testing machine.....	45
Figure 3.15. Elastic modulus testing sample having horizontal and vertical strain gage	47
Figure 3.16. Test setup for flexural strength.....	49
Figure 3.17. The ordinary concrete part of slant shear strength test specimens having untreated surface texture.....	50
Figure 3.18. Slant shear strength test specimens including both old and new concretes.....	50
Figure 3.19. Sorptivity test specimens in the oven.....	51
Figure 3.20. Sorptivity test set-up simulation.....	52
Figure 3.21. Water penetration depth: (a) test set-up and (b) measurement.....	53
Figure 3.22. Rapid chloride permeability test set-up.....	54
Figure 3.23. Samples for SEM test.....	55
Figure 4.1. Variation in slump flow diameter of SCC mixtures concerning basalt fiber volume fraction.....	57
Figure 4.2. Photographic view of flowing of SCC mixture with 0.25% basalt fiber.....	58

Figure 4.3. Variation in J-ring flow diameter of SCC mixtures concerning basalt fiber volume fraction.....	59
Figure 4.4. Slump and J-ring flow diameter values versus basalt fiber volume fraction.....	59
Figure 4.5. Variation in T ₅₀ slump flow time of SCC mixtures concerning basalt fiber volume fraction.....	60
Figure 4.6. Variation in T ₅₀ J-ring flow time of SCC mixtures concerning basalt fiber volume fraction.....	61
Figure 4.7. T ₅₀ slump and J-ring flow time values versus basalt fiber volume fraction.....	62
Figure 4.8. Variation in V-funnel flow time of SCC mixtures concerning basalt fiber volume fraction.....	63
Figure 4.9. Variation in L-box height ratio of SCC mixtures concerning basalt fiber volume fraction.....	64
Figure 4.10. Variation in J-ring height difference of SCC mixtures concerning basalt fiber volume fraction.....	65
Figure 4.11. 7-day and 28-day compressive strength values of SCC mixtures versus basalt fiber volume fraction.....	66
Figure 4.12. Variation in compressive strength of SCC mixtures concerning basalt fiber volume fraction and temperature.....	67
Figure 4.13. Stress-Strain curve of SCC mixtures concerning basalt fiber volume fraction and temperature: (a) At ambient Temperature, (b) At 200°C Temperature, (c) At 300°C Temperature, (d) At 400°C Temperature and (e) At 500°C Temperature..	69
Figure 4.14. Variation in elastic modulus of SCC mixtures concerning basalt fiber volume fraction and temperature.....	70

Figure 4.15. Variation in Poisson’s ratio of SCC mixtures concerning basalt fiber volume fraction and temperature.....	71
Figure 4.16. Variation in splitting tensile strength of SCC mixtures concerning basalt fiber volume fraction and temperature.....	72
Figure 4.17. Variation in flexural strength of SCC mixtures concerning basalt fiber volume fraction and temperature.....	73
Figure 4.18. Splitting tensile and flexural strength values of SCC mixtures versus basalt fiber volume fraction.....	74
Figure 4.19. Slant shear strength values of SCC mixtures at ambient temperature versus basalt fiber volume fraction.....	75
Figure 4.20. Variation in slant strength of SCC mixtures concerning basalt fiber volume fraction and temperature: (a) as casted, (b) hole drilling, (c) groove, and (d) sand blast.....	78
Figure 4.21. Axial strengths of old concrete versus temperature.....	79
Figure 4.22. Photographically indication of typical failure modes occurring on slant shear strength test specimens: (a) before test and (b) after test.....	81
Figure 4.23. Sorptivity coefficients versus basalt fiber volume fraction.....	83
Figure 4.24. Water penetration depth versus basalt fiber volume fraction.....	84
Figure 4.25. Effect of basalt fiber volume fraction on chloride permeability of SCC mixtures in terms of total charge passed.....	85
Figure 4.26. SEM micrographs of concrete samples incorporating Basalt fiber.....	86
Figure 6.1. The flowchart presentation of a genetic programming paradigm (Koza, 1992).....	94
Figure 6.2. Typical configuration of expression tree.....	95
Figure 6.3. Expression trees for GEP model of elastic modulus: a) Function 1, b) Function 2, c) Function 3, and d) Function 4.....	99

Figure 6.4. Estimation performance of empirical GEP model concerning experimental result.....	100
Figure 6.5. Predicted versus experimental elastic modulus values for: a) train and b) test datasets.....	102
Figure 6.6. Expression trees for GEP model of splitting tensile strength: a) Function 1, b) Function 2, c) Function 3, and d) Function 4.....	104
Figure 6.7. Estimation performance of empirical GEP model concerning experimental result.....	105
Figure 6.8. Predicted versus experimental splitting tensile strength values for: a) train and b) test datasets.....	106
Figure 6.9. Expression trees for GEP model of flexural strength: a) Function 1, b) Function 2, c) Function 3, and d) Function 4.....	107
Figure 6.10. Estimation performance of empirical GEP model concerning experimental result.....	108
Figure 6.11. Predicted versus experimental flexural strength values for: a) train and b) test datasets.....	110
Figure 6.12. Expression trees for GEP model of slant shear strength: a) Function 1, b) Function 2, c) Function 3, and d) Function 4.....	111
Figure 6.13. Estimation performance of empirical GEP model concerning experimental result.....	113
Figure 6.14. Predicted versus experimental slant shear strength values for: a) train and b) test datasets.....	114

LIST OF SYMBOLS

B	Specimen width (mm)
BCF	Basalt concrete fiber
BET	Brunauer-Emmett-Teller
BF	Basalt fiber volume fraction
BFRSCC	Basalt fiber reinforced self-compacting concrete
C-S-H	Calcium-silicate hydrate
D	Specimen depth (mm)
E	Elastic modulus (GPa)
ECC	Engineered cementations composite
f_c	Compressive strength (MPa)
f_{flex}	Flexural strength (MPa)
FRC	Fiber reinforced concrete
FRPs	Fiber reinforced polymers
f_{slant}	Slant shear strength (MPa)
f_{split}	Splitting tensile strength (MPa)
GEP	Gene expression programming
GFRC	Glass fiber reinforced cement
h	Specimen height (mm)
HFC	Hybrid fiber concrete

HPFRCC	High performance fiber reinforced cement composites
HSC	High strength concrete
OC	Ordinary concrete
P	Failure load (N)
PCM	Phase change material
PET	Polyethylene terephthalate
S	Span length (mm)
SA	Slant area (mm ²)
SCC	Self-compacting concrete
SEM	Scanning electron microscopy
SIFCON	Slurry infiltrated fiber concrete
ST	Surface treatment method
UHP-FRC	Ultrahigh performance fiber reinforced concrete
T	Temperature level
\tan^{-1}	Arctangent
ϕ	Specimen diameter (mm)

CHAPTER 1

INTRODUCTION

1.1 General

In recent years, due to the increasing demand for infrastructure development, the consumption of concrete keeps growing (Dong et al., 2017). Concrete has many advantages such as formability, durability and required mechanical strength which gives it a merit over the other regular building materials but it has few drawbacks such as low strain capacity and tensile strength (S.T., Tassew and Lubell, 2014; Faiz, 2013; Jiang et al., 2014).

The economy growth for any country worldwide is highly affected by the needs of infrastructures in energy sector such as petrochemical terminals, liquefied natural gas projects, gasholders, units of oil product storage, gas risers and pipelines and marine infrastructures (offshore platforms, cargo wharves, piers, jetties, dry docks, bulkheads, fender systems, quays, floating barges etc.). These structures have high quality and durability requirements for the concrete which used in their construction as a key performance building material for the resistance of the special environmental conditions influencing long-term repairing of the infrastructure (Atutis et al., 2018).

Thus in the recent ages, civil engineering structures have their own durability and structural requirements; every concrete structure has an intended purpose and hence to meet this purpose, modification in traditional cement concrete has become mandatory. It has been found that different types of concretes were established. According to the aim of the construction, different constituents are mixed together to form the desired concrete material. Concrete technology had subjected to a major development in the last decades and it is virtually probable to fabricate job application aligned concrete mixes with common constructional material.

High and ultra-high strength concretes are examples of such fitted concrete with extremely high strength at early ages but also shows remarkable brittleness. Generally fibers are introduced in the cement matrix to enhance the fracture and mechanical properties and many researchers have launched to study the effects of fiber using in cement matrix with respect to the fiber type and content (Y. Uchida et al., 1995; D.Y. Yoo et al., 2015; Shahin and Köksal, 2011; D.Y. Yoo et al., 2013).

The utilization of fibers in concrete greatly affects its characteristics and different studies have demonstrated that these fibers produce significant improvement in the concrete mechanical properties such as the compressive strength, tensile strength, impact, abrasion resistance, fatigue, flexural strength, toughness, load bearing capacity of cracked concrete, and flexural strength (Mehta and Monteiro, 2006; Hsu, 1994; Banthia and Gupta, 1994). High-strength concrete (HSC) is defined based on its compressive strength at a given age. During 1970s, any concrete mixtures which showed 40 MPa or more compressive strength at 28 days were designated as high strength concrete. As the time passed, more and higher strength concrete such as 60 – 100 MPa, were developed which were used for the construction of long-span bridges, skyscrapers and others. High strength of concrete is achieved by reducing porosity in homogeneity and micro-cracks in the hydrated cement paste and the transition zone. Consequently, there is a reduction of the thickness of the interfacial transition zone in high-strength concrete. The densification of the interfacial transition zone allows for efficient load transfer between the cement mortar and the coarse aggregate, contributing to the strength of the concrete.

Somehow, when fibers added in specific percentage to concrete improves the mechanical properties, durability and serviceability of the structure and produced a high strength concrete. It is well known by finding out that one of the unique properties of Fiber Reinforced Concrete (FRC) is its superior resistance to cracking and crack propagation. Fiber reinforced concrete is concrete containing fibrous material which increases its structural integrity. It contains short discrete fibers that are uniformly distributed and randomly oriented. Fibers include steel fibers, glass fibers, synthetic fiber, basalt fiber and natural fibers – each of which provides varying properties to the concrete. In addition, the character of fiber reinforced concrete changes with varying concretes, fiber materials, geometries, distribution,

orientation, and densities. Fibers are usually used in concrete to control cracking due to plastic shrinkage and to drying shrinkage. They also reduce the permeability of concrete and thus reduce bleeding of water. Some types of fibers produce greater impact, abrasion, and shatter-resistance in concrete.

Marine constructions (e.g. marine and harbor structures) rank among the premier applications of concrete materials; which is considered as optimal option due to its strength, economy and durability. In the case of concrete immersed in water, a chemical aggression on the concrete structure is maximized in terms of reactivity between reactive aggregates and alkali in cement might be raised by accelerating corrosion of fibers which are susceptible to water. A chloride is the most aggressive serious element which is carried to the surface of concrete by the seawater. Hence and in order to withstand the aforementioned environmental conditions, durability of concrete assure a key role (Ghali, 2014; Tsinker, 1997; Gaythwaite, 2004). Deficiency of durability may address to corrosion, cracking, failure of the member and excessive deflection. Concrete members may also encounter cooling/heating, wetting/drying and freezing cycles, which also lead to concrete deterioration and subsequent corrosion of steel bars or steel fibers. Above-mentioned consequences promote many researches in UK, USA, Baltic States and Spain to find practicable means of using fiber reinforced polymers (FRPs) to decrease as much as the further repairing costs of concrete infrastructure (Abdelrahman and Rizkalla, 1997; Sen et al., 1998; Lees and Burgoyne, 1999; Torres et al., 2013; Atutis et al., 2015).

Non-metallic material such as fiber reinforced polymer possesses suitable long-range potential because it is nonmagnetic, non-corrodible and has a lower modulus of elasticity than steel fiber and consequently is less sensitive to shrinkage, anchorage and creep losses than steel fibers. So, fiber reinforced polymers might be a good alternative of conventional fibers of the concrete for manufactured facilities utilization mentioned above. Various sorts of fibers such as cellulose, asbestos, polypropylene, steel, carbon, aramid, polyethylene, glass, PVA, and basalt have been employed to reinforce concrete products (Hannant, 2003).

Somehow, when fibers added in specific percentage to concrete improves the mechanical properties, durability and serviceability of the structure and produced a high strength concrete. It is well known by finding out that one of the unique

properties of Fiber Reinforced Concrete is its superior resistance to cracking and crack propagation which decreases the structural integrity. This concrete contains short discrete fibers that are uniformly distributed and randomly oriented. In addition, the properties of fiber reinforced concrete changes with varying concretes, fiber materials, geometries, distribution, orientation, and densities. Fibers are usually utilized in concrete to control cracking due to plastic and drying shrinkages. They also reduce the permeability of concrete and thus reduce bleeding of water. Some types of fibers produce greater impact, abrasion, and shatter-resistance in concrete.

Basalt Fiber origin is basalt rock which is a volcanic rock and can be divided into small particles then formed into continuous or chopped fibers (Kizilkanat et al., 2015). Basalt fiber has a higher working temperature and has a good resistance to chemical attack, impact load, and fire with less poisonous fumes. Some of the potential applications of these basalt composites are plastic polymer reinforcement, soil strengthening, bridges and highways, industrial floors, heat and sound insulation for residential and industrial buildings, bullet proof vests and retrofitting and rehabilitation of structures. The production of basalt fibers is similar to the production of glass fibers. Basalt is quarried, crushed and washed and then melted at 1500° C.

In retrofitting purpose of deteriorated concrete, high strength concrete can be used to repair old concrete to produce hybrid concrete construction. Lack of permeability of new high strength concrete part will play great role in preventing decay of old concrete. Different materials are used according to their strengths and weaknesses to provide simple, workable and competitive high-quality structures that offer consistent performance. In-situ concrete toppings are often added to precast floors for additional strength, stiffness and toughness and produce a high strength concrete. However the effect of basalt fiber inclusion on the mechanical properties of concrete is still under debate.

1.2 Research Significance

The role of the modern basalt fibers has not been extensively investigated in producing high strength concrete (HSC) which can be used in improving the properties of hybrid concrete made with ordinary and high strength concretes. In

addition, more researches are considered essential to examine the effect of the treatment modes for interfacial surface, between ordinary and high strength concretes, on the mechanical properties of hybrid concrete under the effect of high temperatures. The study also included the investigation of the workability, mechanical, permeability properties and electron microscopic scanning of SCC mixtures.

1.3 Outline of the Thesis

Chapter 1 – Introduction: Purposes and objectives of the thesis were introduced.

Chapter 2 – Literature review and background: The literature review on self-compacting concrete was presented in detail. The previous researches on the experimentally investigating the effect of basalt fiber and temperature have been discussed and submitted.

Chapter 3 – Materials and methods: The materials used in the experimental program have been described and introduced. The testing methods have also been specified and submitted. In addition, these standards of these testing methods have been referenced.

Chapter 4 – Results and discussions: Indication, evaluation, and discussion of the experimental test results have been reported in this section. The results were compared with the previous study findings.

Chapter 5 – Statistical analysis: The statistical evaluation technique employed in the thesis presented herein was described. The results attained from the experimental study were statistically evaluated to see which input parameter has a remarkable impact on the testing parameters of self-compacting concrete.

Chapter 6 – The soft computing technique used in this thesis was explained and introduced. The details of the software used in the generation of the models on the basis of gene expression programming were described and explained. The models proposed by gene expression programming was given and defined.

Chapter 7 – Conclusions: Conclusions of the thesis and recommendations for future studies were presented.

CHAPTER 2

LITERATURE REVIEW

2.1 Introduction

Horse's hair has been used in plaster for increasing the strength of its tensile since 2500 B.C. Even straw and other vegetal fibers have also been used for strengthening the sunbaked bricks. In Finland, asbestos fibers were used also for enhancing the flexural and tensile strengths of ceramic. Short length and thin fibers are introduced into breakable materials in order to assist as crack arresting mechanisms for improving the concrete properties. Development works and research on fiber reinforced concrete (FRC) are initiated since about 40 years for numerous applied requests due to recognizing the enhanced properties of the products of the (FRC). For example, offshore structures, overlays of the bridge deck, pavements, and strengthened concrete structures. Endurance limits and fatigue behavior are significant. The reason behind that is these types of structures should be considered for fatigue loading, and they help most comparing to adding fibers to the concrete (Haido, 2011).

Under forceful environmental conditions and in terms of the strength, structural strengthened concrete members reveals unwanted performance. Therefore, in the study of (Tayeh et al., 2013) it was stated that the recovery methods of these weakened structures must be reliable, cost reasonable and active. We can achieve this objective by using concrete with low permeability and absorbency and high strength in retrofitting determinations (Habel, 2004; Rossi, 2002; Denarie, 2006; Bruhwiler, 2008; Farhat, 2010; Farhat, 2007; Alae, 2003). The humidity conditions of the line between new and old concretes and the configuration of recovery materials affect the link between them (Shin and Wan, 2010). Moreover, the surface of the present material roughness (old concrete) plays sensible role in the improvement of the link power of the interfacial surface between new and old concretes (Julio et al., 2004).

Few methods have been used in earlier studies for improving the surface roughness and therefore improve the link power. While several above-mentioned studies have been studying the performance of hybrid concretes with treated interfacial surfaces, tiny data is obtainable on the relationship to effective treated interfacial surface and hybrid (retrofitted) concrete beams (Tayeh et al., 2012; Santos and Julio, 2011; Harris et al., 2011; Sarkar, 2010; Austin et al., 1995; Emmons, 1994; Talbot et al., 1994; Abu-Tair et al., 1996; Saucier and Pigeon, 1991; Silfwerbrand, 1990; Hindo, 1990; Stoppenhagen et al., 1995; Rodriguez and Park, 1994; Ramirez et al., 1991; Alcocer, 1993; Alocer and Jirsa, 1990; Bett et al., 1988).

In any concrete structure that has been built or under construction, the engineers may face main problem in engineering history which is deterioration (Tayeh et al., 2012) of strengthened concrete material. Since the time they found out this problem, they have been searching for solutions to ensure the effective structural management. So, the suitable solution for this problem is represented by good bond repairing or retrofitting by a material with high compressive strength and reasonable durability. During a few years ago, researches launched to find solutions for concrete deterioration with a limited concentration on using of high strength concrete (HSC) as retrofitted material. HSC is among the trendiest promising cementitious materials that developed with possible to be a practical key to improve the maintainability and flexibility of the existed infrastructure due to its energy absorption capacity, durability and high strength comparing to ordinary concrete. High performance concretes are typically made by cement (basically with dosage more than conventional concrete), super-plasticizer, silica fume, fine sands (0.8 mm as maximum grain size) (Habel et al., 2006) with steel fibers as optional component (Sarsam et al., 2014). The superior compressive and tensile strengths of this concrete can be attributed to the presence of fine compounds. It was previously demonstrated in many studies (Graybeal, 2006; Pfeifer, 2009; Graybeal, 2009) that HSCs are highly strong to stand chloride penetration, freeze-thaw cycles, abrasion, and the chemical attack. Common sorts of HSC are fiber strengthened ultrahigh performance fiber reinforced concrete (UHP-FRC) (Wille et al., 2011), engineered cementations composite (ECC) (Li, 2003; Li et al., 2001), high performance fiber reinforced cement composites (HPFRCC) (Naaman et al., 2006), hybrid fiber concretes (HFC) (Markovic, 2006), multi-scale cement composite (MSCC) (Rossi, 1997), slurry

infiltrated fiber concrete (SIFCON) (Naaman, 1989), concretes (FRC) (Brandt, 2008). The retrofitting of deteriorated concrete with HSC material needs repairing new concrete required to place next to old defective one (Momayez et al., 2005). Accordingly, a weak bond will be arising between old and new concretes in hybrid concrete members (Momayez et al., 2005; Yuan and Marosszeky, 1991). Thus, to produce a durable and effective bond in these structures, proper repair is considered the main requirement (Ali et al., 1999; Mu et al., 2002). Some endeavors (Tayeh et al., 2012; Harris et al., 2011; Santos and Julio, 2011; Vaysburd and Emmons, 2000; Azad and Hakeem, 2013; Denarié and Brühwiler, 2006; Julio et al., 2004; Garbacz et al., 2005) have been started recently to investigate the behavior of hybrid concrete.

This chapter is dedicated to present the historical background and previous studies that devoted to study the behavior of fibrous reinforced concrete with focusing on the mechanical properties of basalt fiber reinforced concrete.

2.2 Fiber for Concrete

Nowadays industry economics promotes to use optimal engineering materials and construction techniques (Ramakrishnan et al., 1998). According to (Kamutha et al., 2017) the most used building substance all over the world concrete it uses cement, fine aggregate and coarse aggregate as its constituents. Concrete structures still are very competitive and successfully have been employed in the civil engineering industry. (Ramakrishnan et al., 1998; Arslan, 2016) consist that there are two main insufficiencies in the plain concrete; a low strain at fracture and low tensile strength (Tassew and Lubell, 2014; Faiz, 2013; Jiang et al., 2014). Plain concrete usually has many micro-cracks and therefore, the concrete tensile strength is very low. Applied stress is responsible for the low tensile strength of the substance. Thus, the propagation of these micro-cracks is so fast. These insufficiencies resulted in significant research aimed at developing new methods to modify the concrete brittle properties and its breaking. Moreover, concrete technology had experienced the most important development in the past forty years and it is nearly probable to create job request concerned with concrete combined with normal construction substances. High as well as ultra-high strength concrete are some instances of that designed concrete which display very high strength at early days even though they show rare fragility.

In the construction industry, the mechanical properties of a substance are considered to have the main role in the process of selecting a suitable substance. However, this is powerfully determined by on the knowledge of the components and microstructure of the substance. Yet, it is an essential objective for engineers to have strong knowledge to understand of how the microstructure is formed, and how the engineering properties are influenced when adding new materials (Warren, 2013), which can be achieved when we test the concrete mechanical properties. The materials mechanical properties show an important role in defining the concrete characteristic and are described as substance features, which are revealed when a mechanical loading is applied to that substance.

In order to improve the concrete mechanical properties, fibers should be added to the mixture of the concrete, and then the effect on the concrete mechanical properties of, like: workability, elastic modulus, flexural strength, tensile strength, and compressive strength must be determined. Different types of fibers are added to the concrete such as steel fibers, basalt fibers, glass fibers, and polypropylene fibers, to enhance the strength to the concrete (Kabay, 2014; Kizilkanat et al., 2015; Hannant, 2003). Fibers act as crack arrestors in concrete.

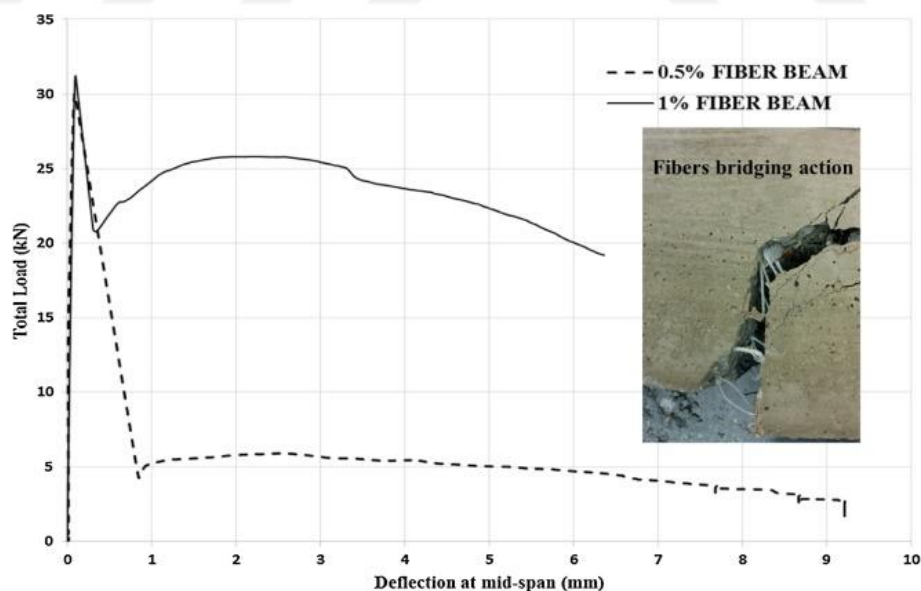


Figure 2.1. Effect of fibers in concrete cracking and strength (Ghahremannejad et al., 2018)

It has been demonstrated that the presence of fibers could increase the concrete strength (Y. Uchida et al., 1995; D.Y. Yoo et al., 2015; Shahin and Köksal, 2011; D.Y. Yoo et al., 2013) due to the sewing effect on the crack initiation (Fig. 2.1) and propagation, and also offer the concrete with enhanced ductility (Brigante, 2014; Jiang et al., 2014; F.U.A. Shaikh, 2013; Tassew and Lubell, 2014).

Basalt fiber is considered a promising new material. It has good strength characteristics, resistance to chemical attack, sound insulation properties. It has a wide range of applications like soil strengthening, bridges, and highways, industrial floors.

Most noticeable characteristics among the improved mechanical properties of fiber strengthened concrete are its superior fracture resistance and resistance to impact and impulsive or dynamic loads, they impart additional strength under all modes of loading which include, direct tension, shear, flexural and torsion loading (Jiang et al., 2014; Mehta and Monteiro, 2006). The degrees of improvement of the mechanical characteristics of fiber reinforced concrete (FRC) are influenced by specimen size, loading configuration, size and type of fibers (Ramakrishnan, 1997a). Based on the total volume of the concrete, different amount of fibers can be utilized with high, intermediate and low volume concentrations. Fiber dosage is considered high if it is 3-12%; while the fiber content range of 1-3% and 0.1-1.0% are intermediate and low, respectively.

Fibers have been produced from steel, plastic, glass and natural materials in various shapes and sizes. Fibers for commercial application of FRC have been of great variety (Ramakrishnan, 1997b); However, steel fiber, glass fiber, and polyethylene terephthalate (PET) fibers appear to reduce the workability of concrete (Lu and Hsu, 2006; Yan et al., 2013; Kral, 2009; Asokan and Osmani, 2009).

2.2.1 Steel fiber

The majority of the applications with steel fibers has been with mixes using normal weight concrete. For straight steel fibers, the primary factors which are controlling the composite properties were the aspect ratio of the fibers and fiber volume fraction. For each one cubic meter of concrete, the amount of fiber used is ranged from 89 to 119 kg. Workability and difficulty in mixing were the main complications came

across in the early steps. Fibers were balling up throughout the process of mixing at higher volume fractions. For longer fibers, this process named balling was found to happen often. The coarse aggregate size was typically controlled to avoid balling and to facilitate the use of short fibers.

Moreover, the concrete mortar fraction was improved to contest the problem of balling. With the fibers addition, there was always a lessening in workability. Hence, this is to affecting concrete quality in place, especially for higher fiber volume fractions (8 to 13).

2.2.2 Glass fiber

Experimentations using glass fibers were directed in the United States as early as the 1950s as well as in the United Kingdom and in Russia (Armelin and Banthia, 1997; Ashour et al., 1997). Glass fibers are primarily used for glass fiber reinforced cement (GFRC) sheets.

2.2.3 Carbon fiber

Until mid-1980`s the high cost of carbon fibers limited their use in Portland cement composites. More recently, low-cost carbon fibers were produced with coal. and petroleum pitch. With a gravity of about 1.9, carbon fibers are very light and inert to most of the chemical.s. Even though their cost is higher than polymeric fibers, carbon fibers have a potential for certain uses that need flexural strength and high tensile. Carbon fibers are obtainable in stands that have high elastic modulus similar to steel and stronger than steel 2 to 3 times and have up to 12,000 individual filaments and (Ramakrishnan, 1993; Adebar et al., 1997; Armelin and Banthia, 1997).

2.2.4 Synthetic fiber

In order to increase toughness and abrasion and impact resistance, and for reducing early plastic shrinkage crack, synthetic fibers are most generally addition to concrete for slab-on-grade structure. However, to precast concrete to improve resistance for stress handling, to pumped concrete for improving cohesiveness, and to shotcrete for reducing material waste and rebound, fibers may also be added.

Polypropylene fibers are mostly the synthetic fibers and they have been used since the early 1960s. The general forms of those fibers are tridimensional mat, fibrillated, twisted, and smooth mono-filamented. Polypropylene fibers do not have any influence on the requirements of mixing water and not absorbing water because they are hydrophobic. It has a low density and is also chemically inert.

Low melting point, combustibility, poor bond with cement matrix, and low modulus of elasticity are the major shortcomings of polymeric fibers. Treating the fiber surface or twisting several fibers together could improve their bond to the cement matrix.

The latest development in the field of synthetic fibers is polyolefin fibers, with a low aspect ratio similar to steel fibers for use in concrete. These fibers are available in various lengths and diameters and their addition will improve the structural properties of concrete like the steel fibers. However, engineers could easily mix them in large amounts with concrete, up to 20 % (by volume) without causing any increase in air entrainment in concrete, balling, or segregation.

It is possible to produce high volume fiber strengthened concrete using the regular concrete mixture proportions including coarse aggregates whereas high volume fiber concrete using steel fibers are produced using cement slurry instead of regular concrete. There are several advantages for polyolefin fibers, like no chemical inertness, corrosion potential, and no nuisance or hazardous conditions when fibers become loose or protrude from the surface of the concrete. Unlike steel fibers, these fibers are non-magnetic and non-corrosive.

2.2.5 Basalt fiber

At the surface of a planet, rapid chilling of lava formed a form of igneous rock called basalt, which considered the most common rock in the crust of the Earth. The features of Basalt differ from the historical contact to the elements, rate of cooling, and lava's source. Mixing uniform chemical makeup with high-quality fibers produced basalt deposits. The production processes of glass fibers and basalt are similar. The manufacturing the fiber requires only one raw material, which is crushed basalt rock. It is a continuous fiber made over melt drawing of igneous basalt rock at a temperature of about 2,700° F (1,500°C). Some studies stated that producing basalt

fiber needs less energy even though the temperature required to produce fibers from basalt is higher than glass. The reason for that is because of the consistency of its heating. On the other words, basalt fiber (BF), made from volcanic rock through melting process with environmentally friendly and non-hazardous nature (Borhan, 2012; Fiore et al., 2011; Sim et al., 2005).

Basalt fibers are made through melting pure raw material in a process of single-stage. They have high heat stability and insulating characteristics, have an elastic structure, non-toxic, and environmentally safe. They can be simply treated into the fabric of high consistency. Basalt fibers show special mechanical properties when they are used for composite materials. The modulus of elasticity of continuous basalt fibers is about 15-30% higher and the tensile strength is about double that of E-glass fibers. It was observed that the use of continuous basalt fibers improved the tensile strength of concrete more than E-glass fibers and gave a greater failure strain than the carbon fibers (Berozashvili, 2001). Basalt fibers in an amorphous state exhibit higher chemical stability than glass fibers. When exposed to water at 70°C, basalt fibers maintain their strength for 1200 hours, whereas the glass fibers do so only for 200 hours (Sim et al., 2005; Ludovico et al., 2010).

Basalt fiber is considered as a “multi-performance” fiber. For instance, it is resistant to acids and alkalis it insulates sound, electricity, and heat; its elongation is better than small carbon fiber, the strength of its tensile might be higher than large carbon fiber. The molecule of Basalt is a three-dimensional comparing to single sensitive linear polymeric fibers. It is cost-effectiveness, anti-aging, as well as other excellent Characteristics. Basalt rock is a volcanic rock and can be divided into small particles then formed into continues or chopped fibers with high working temperature and good resistance to chemical. attack, impact load, and fire with less poisonous fumes (Mingchao, 2008; Ramakrishnan, 1998; Wei et al., 2010; Lopresto, 2011; Fiore et al., 2011). It considered as a classic ceramic fiber when it is mixed with mortar and cement concrete, it disperses quickly. Basalt fiber used for concrete and cement is cheap; it competes for polyacrylonitrile fiber and polypropylene fiber. Thus, basalt fiber could protected concrete, serves the tasks of support, resists to the crack, and could extend the life of plant facilities, the coastal protection works, subway tunnels, ports, runways, urban elevated roads, railways, highways, bridges, construction in

the housing fields. Basalt fiber (BF) is a novel kind of inorganic fiber and does not contain any other additives, which makes it more economical. (Kizilkanat et al., 2015). Furthermore to high precise modulus, as well as highly precise strength, BCF (Basalt concrete fiber) also shows a very good cost performance, high availability, high shear strength, anti-compression strength, filtration, sound and thermal Insulation, anti-radiation, anti-oxidation, and excellent temperature resistance (-260~700°C). BCF (Basalt concrete fiber) could be found in nature as a non-metal inorganic substance. It has successfully satisfied the needs for developing the basic infrastructures due to the consideration that it is a high-tech fiber and new basic substance.

As shown in Table 1, the chemical composition for the basalt fibers was derived from the analysis of Van de Velde K. Using a cross-linking agent and coat the fibers has been firstly proposed in order to promote bonding between the cement and the fibers. Now, we will discuss the reason behind the chosen cross-linking agent. Calcium-Silicate Hydrate (C-S-H) reaction yields were particularly hard to be modeled and predicted. Nevertheless, current developments in this field (Pellen et al., 2009; Abdolhosseini et al., 2014) have unlocked the possible incorporation of chemically well-suited additives to the structures of hydrated cement gel.

Table 2.1. Chemical composition of basalt fibers (Basaltex, 2019)

Compound	% in basalt fibers
SiO ₂	51.6-57.5
Al ₂ O ₃	16.9-18.2
CaO	5.2-7.8
MgO	1.3-3.7
B ₂ O ₃	--
Na ₂ O	2.5-6.4
K ₂ O	0.8-4.5
Fe ₂ O ₃	4.0-9.5

Shahsaveri and Sakhavand (2016) deliver a brief summary of present investigation on integrating organic additives and polymeric into the nano-scale structures of C-S-H. In this regard, their study has concisely discussed and defined the following as potential possibilities; Poly vinyl alcohol PVA; Poly (4-vinyl benzyl trimethyl ammonium chloride); Poly (methacrylic acid) (PMA) (Sakhavand et al., 2013).

Basalt fibers, the latest generation of fiber strengthened polymer composites, are currently attracting the interest of the research community and construction industry. Many researchers (Serbescu et al., 2014; Dias and Thaumaturgo, 2005; Ma et al., 2011; Kabay, 2014; High et al., 2015; Hu and Shen, 2005) stated that the influence of the addition of BF is importantly improving the modulus of rupture, deformation resistance and toughness of concrete, as well as reducing the brittleness and improving the strength of the tensile.

A number of researchers (Sim et al., 2005; Palmieri et al., 2009; Wu et al., 2010; Lu et al., 2015) concluded that the continuous basalt fibers offer higher tensile strength than E-glass fibers, greater strain at failure than carbon fibers, as well as good resistance to chemical attack, high corrosion resistance, thermal stability, low water absorption, and high impact and fatigue resistance.

Some researchers (Brigante, 2014; Kabay, 2014; Sim et al., 2005) studied heat protection, thermal resistance, acoustic insulation and durability of the basalt fibers concrete. Remarkable improvement in these concrete properties has been observed with introducing basalt fibers. Even if basalt fibers have the aforementioned advantages, studies about them are limited (Jiang et al., 2014; Dias and Thaumaturgo, 2005; Li and Xu, 2009). Therefore further experimental studies should be carried out to determine the effects of basalt fibers on physical and mechanical properties of composites.

One of the major roles of fibers in concrete is to increase the fracture energy (Bayramov et al., 2004; Şahin and Köksal, 2011; Rezaie and Farnam, 2015). Even if many fiber types have been used in concrete (Bayramov et al., 2004; Rezaie and Farnam, 2015; Alberti et al., 2016; Michels et al., 2013) Knowledge related to mechanical properties, fracture behavior and microstructure of basalt fiber reinforced concrete (BFRC) is insufficient.

2.3 Mechanical Properties of HSC

Li and Xu (2009) investigated the impact of mechanical properties of geopolymeric concrete with basalt fibers. Three different concrete strengths were considered in the tests. Influence of strain rate on the concrete compressive strength under organic loads was also studied-outcomes show that dynamic impact properties of concrete

with basalt fibers exhibit linear increase with strain rate. Moreover, it was demonstrated that the steel fiber has great's role in improving energy absorption and deformation of the concrete material

Experimented tests were carried out by Arivalagan (2012) to study the split tensile and compressive strengths of basalt fiber concrete of M20 and M30 were selected at different curing ages of 7 days, 14 days and 25 days. Remarkable increasing in the tensile and compressive strengths of basalt fiber concrete has been observed in compression to that for control normal concrete by the range of 120%-125%.

Borhan (2013) examined the mechanical and thermal characteristics of basalt fiber concrete with basalt fiber contents of 0.1, 0.2, 0.3 and 0.5% by volume. Properties of concrete such as split tensile and compressive strengths and heat transfer were investigated in conclusions; it is proved that the increase in fiber content improves concrete strength. Furthermore, regards showed the lower amount in heat conductive of fiber concrete through its thickness in comparison to conventional concrete.

According to (Shi et al., 2014) study it were performed that experiments on effective thermal conductivity of basalt fiber composite concrete with dispersed phase change material (PCM). Paraffin was employed as PCM in a liquid state. The effective thermal conductivity of the samples is measured with a steady state approach. A numerical analysis model was developed to find the impact of the composite materials. Numerical outputs refer to that the thermal resistance of finite contact between concrete and PCM affects the conductivity of the composite at solid state with changing the volume of PCM with temperature. Good matching has observed between numerical and experimental result. Kizilkanat et al. (2015) carried out a comparative study to investigate the mechanical properties of high strength concrete with glass and basalt fibers (Fig. 2.2).

It is demonstrated from the experiments that there is no considerable effect of introducing fibers on the modulus of elastics and compressive strength. The tensile strength of basalt fiber concrete improves with increasing basalt fiber dosage while no remarkable increase was noted in the strength glass fibrous reinforced concrete with a glass fiber content of more than 0.5 %. Moreover, flexure strength of these composites is in the similar trend of compressive strength. Fracture energy was

investigated as well and it was concluded that it is improved significantly which increasing basalt fiber content beyond 0.25 % by volume. Hence, closing remarks were staffed that the basalt fiber is more effective than glass fiber in improving composite resistance.

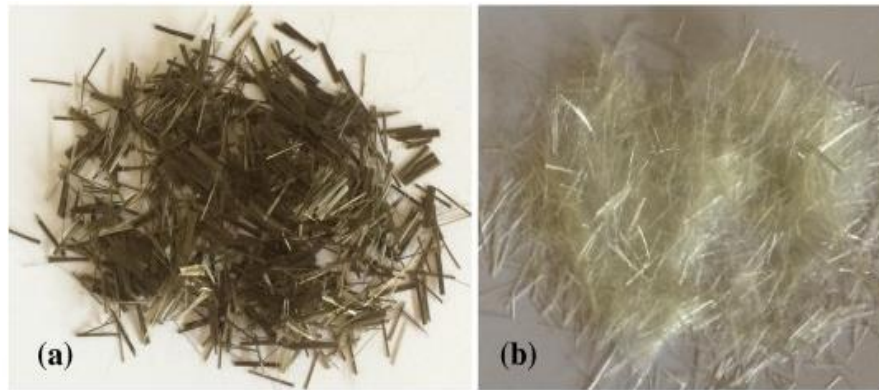


Figure 2.2. The fibers used in concrete (a) basalt fiber and (b) glass fiber (Kizilkanat et al., 2015)

High et al. (2015) provided an experimental study at using of chopped basalt fiber to enhance the concrete compressive strength and flexure of the capacity of concrete elements. Measurements revealed that these fibers have little influence on the concrete compressive strength while flexure of modulus was significantly improved.

Elshafie et al., (2016) examined the influenced of volume faction and length of the used basalt fibers on the mechanical characteristics of concrete. Best basalt fiber length and its content have been obtained depending on optimum effect on concrete. Conclusion and suggestion have been drawn to use blended fibers with a length of 12mm and 24mm to improve the mechanical properties of concrete. In addition, the authors proved that the optimum basalt fiber content is 0.25%.

Research deals with studying the fracture behavior of basalt fiber concrete was provided by (Arslan, 2016). There points bending test was performed with basalt and glass chopped fibers there volume fractions of these fibers were utilized namely 0.5, 1, 2, and 3 kg/m³. Fracture energy of these elements was measured by calculating load-crack mouth opening displacement. Moreover, microstructural analysis for three-dimensional components of aggregate, cement paste, glass and basalt fibers were carried out using scanning elector microscopy and examinations of energy-

dispersive X-ray spectroscopy. It is observed that there is a considerable effect of fiber content on fracture energy of concrete. Accordingly, flexural and tensile strengths of basalt and glass fiber dosage a slight drop was noticed in flexural strength of concrete with high fiber concrete.

Zhang et al., (2017) worked on the investigation of the effects of high strain rates, produced by specific split pressure bar machine, on the impact performance of basalt fiber reinforced concrete. Six fiber volume fractions were selected namely 0, 0.05, 0.1, 0.15, 0.2, and 0.25%. Dynamics compressive strength examined based on stress-strain curve found during the experiments. In additional, pore structure and micro properties of basalt fiber concrete was studied base on these experiments of outcomes, dynamic, constitutive, relationships (models) were derived according to an improved Zhu-Tang model.

Arunagiri et al., (2017) studied the mechanical properties of basalt fiber geopolymer concrete. Specimen contain different fiber concrete ranged by 0.5-2.5%. According to the comparison of results with control concrete without fibers, it is demonstrated that split tensile, compressive and flexural strength of basalt fiber concrete was increased by 2%.

Mechanical properties of geopolymer concrete made with fly ash and basalt fibers were examined by Kumutha et al., (2017). They utilized waste materials of fly ash and ground granulated blast furnace slag instead of ordinary cement in geopolymer concrete fabrication. Remarkable increasing 139% in flexural strength was observed with introducing basalt fiber in the concrete matrix.

Liu et al., (2017) examined the mechanical properties of basalt fibrous concrete with recycled aggregate. A total of 324 samples were chosen for their experimental work. Elastic modulus, compressive strength, splitting tensile strength of this concrete was investigated. Coarse aggregates in concrete were totally replaced by recycled aggregate. Results showed similar failure pattern was observed for ordinary and basalt fiber concretes. The mechanical behavior of basalt fiber can be effectively improved with using fiber content of 0.2%.

The microstructure and mechanical properties of basalt fiber concrete made with recycled earthquake waste were studied by Dong et al., (2017). Two main parameters

were considered in the experimental program such as replacement of coarse aggregate with this waste and fiber content. The influence of these parameters on ultimate strength, modulus of elasticity, Poisson's ratio, failure model, tensile strength and compressive strength was investigated. Scanning electron microscopy of concrete reveals that basalt fibers are accumulated on the surfaces of the attached cement mortar and in pores, can improve the microstructure of the interfacial transition zone.

Dias and Thaumaturgo (2005) examined the fracture toughness of geo-polymeric concrete with basalt fiber. Experiments of records show that geo-polymeric concrete with basalt fibers has better toughness basalt fiber reinforced by Portland cement.

The effect of using presoaked basalt fiber on strengthening and mechanical properties of concrete was investigated by Ma et al., (2011). Fiber volume as a variable in the Experimental tests it is demonstrated that the influence of introducing this fiber on tensile and compressive strengths was significantly and not noteworthy. Thus, the brittleness of concrete can be reduced accordingly.

Kabay (2014) reported the influence of basalt fiber on mechanical and physical properties of concrete. Two ratios of water cement of 0.45 and 0.6 were utilized to produce ten mixture of high and normal strengths concrete. Various sites of basalt fiber were incorporated in these mixes Experimental results showed that enhancement can be found in the abrasion resistance, fracture energy and flexural strength of basalt fibrous concrete even at low fiber content. A reasonable relationship was formulated between abrasive wear and flexural strength of concretes.

Jin et al., (2014) concluded Experimental work on freeze-thaw cycle tests to examine the behavior of basalt fiber concrete in terms of dynamic modulus of elasticity and qualify loss. Fiber dosages of 0%-0.3% were used for fabrication of four groups of concrete samples. Outcomes revealed that qualify loss and modulus of elasticity of basalt fiber concrete in thawing and freezing process is clearly better than those for plain ordinary concrete.

Ramakrishnan et al., (1998) studied the utilization of basalt fiber in improving the mechanical properties of concrete materials it was concluded that those fibers can be

mixed with concrete without any balling. A remarkable increase in post-cracking absorbed the energy of fibrous concrete and consequently enhancing its impact resistance.

Sim and Park (2005) performed experiments on tensile strength and toughness of basalt fiber concrete. It was concluded that the elongation and tensile strength were improved by 3-5 times and 0.5-1.0 time, respectively. Thus, the concrete toughness was increased too. The effect of the additional basalt fibers on ultimate compressive strength, bending strength and shrinkage at 28 days of cement mortar was investigated by Zielinski and Olszewski (2005). They found an optimum amount of this fiber to provide the best mechanical and physical properties of mortar.

2.4 Properties of Hybrid Concrete

The structural safety and functionality are highly affected by the bonding between deteriorated concrete members and a new overlay repairing materials. In order to enhance the resistance of interfacial surface against the penetration of harmful chemical material, an effective and good bonding is required at the interface between old and new concretes. Tayeh et al., (2012) examined experimentally the permeability and mechanical properties of the interfacial surface between old normal concrete substrate and new overlay concrete (see Figure 2.3) made with ultra-high performance steel fibrous concrete as repairing material.

Substrates fabricated by ordinary concrete were utilized with a different roughed surface to assess the mechanical characteristics of the interfacial bond using splitting tensile and slant shear test. Permeability properties were evaluated by water, gas and rapid chloride permeability tests.

Results prove that high bond strength was achieved by using new high strength concrete overlay which bonds in an efficient way with normal strength concrete substrate hybrid concrete specimens with sandblasted interfacial surface give best interfacial bonding in compression to other forms of interfacial surface preparation.

Scanning electron microscopy outcomes referred to very good bonding, between old and new concretes which improves the impermeability for these composite materials. Thus, it is conceived that the use of high strength concrete concomitant with proper

interfacial surface preparation of the normal concrete substrate should be effective to provide durable repair of concrete.



Figure 2.3. Slant shear test set-up for the composite concrete specimen (Tayeh et al., 2012)

Habel, 2004 investigated the behavior of concrete made with ordinary concrete and overlay high strength concrete under impact loading. The application of their material for overlay significantly enhanced the response of the element under an impact loading with none of crushing, spalling, and cracking while common for the ordinary concrete overlay.

The measurements confirmed that the applying of this type of hybrid concrete improves that the service stiffness, and minimize the deformation. Chui (2005), Lee (2006) and Denarie (2003) performed introductory study on the role of reactive powder concrete as a new repairing material. specimen were prepared for slant shear experiment to measure bond strength at include surface with 45° gloze, compressive strength pull out strength test of steel and test for relative dynamic modulus. Experimental results showed that the flexural strength and compressive strength with bonding reactive powder concrete longer of 10mm thick were 150-200% more than those bonding with normal concrete.

The abrasion coefficient of reactive powder concrete overlay was eight times greater than that made with ordinary strength concrete. A laboratory test was conducted by Harris 2011 and Sarkar 2010 to estimate the bond strength between normal strength concrete substrate and ultra-high strength concrete overlay. Various types of interfacial surface texture were used namely smooth, surface prepared by steel brush low roughness (0.04-0.09 in), high roughened surface prepared by transverse grooves.

Splitting tensile and slant shear tests have been carried out to investigate the bond, tensile, shear and compression strengths. The strength of hybrid concrete was evaluated in three points loading flexural test as well. The outcomes revealed that the interfacial failure consistently occurred in the sample with a smooth interface surface. A remarkable increase in bond strength was observed in slant shear tests with a prepared interfacial surface, while bond strength in splitting test was not very sensitive to the interfacial surface roughness.

Lee et al., 2006 investigated the performance of hybrid concrete made with regular and reactive powder concrete. Cylindrical specimens were used in the tests. The durability of these samples was examined via accelerated deterioration resulted from freezing-thawing cycle environments. Bond strength on slant shear strength for interfacial surface between two concretes was measured before and after this environmental aging. Experimental outcomes show that reactive powder concrete displaced remarkable retrofit and repair potentials. It is possessed high durability and strengthening than other concretes.

Experimental work was conducted by Santos and Julio (2011) to study the interfacial bond strength of hybrid concrete made with two concretes cast at different times (ages). Slant shear and splitting tests were considered in the laboratory tests. Many parameters were considered in the experiments namely, curing conditions for old and new concretes, a compressive strength of concrete and roughness of the interfacial surface in the concrete. It is concluded that the failure mode and bond strength of old to new concretes are highly affected by their curing conditions and differential shrinkage.

Tayeh et al., (2012) investigated the permeability and mechanical properties of the interfacial surface between ordinary concrete substrate and ultra-high strength fiber concrete overlay as are paring longer. The effect of the different roughened surface for substrate was quantified by splitting tensile and slant shear test. Moreover, the permeability properties were examined via rapid chloride permeability water and gas permeability tests. The measurement showed that the overlay ultra-high strength concrete produces an efficient bond with the normal concrete substrate. The best interfacial bonding is achieved by a substrate surface with sandblasting. The results for scanning electron microscopy reveal that ultra-high performance concrete overlay concomitant with proper interfacial surface preparation of substrate is able to provide durable concrete repair with improved impermeability.

The compressive stress-strain relationship and corresponding failure modes were investigated by Tayeh et al., (2013) for hybrid concrete prisms. These samples were fabricated by regular concrete and ultra-high strength concrete with the prepared roughened interfacial surface between them. The outcomes showed that the behavior of a hybrid specimen is closed to that for individual ordinary concrete sample especially with using the interfacial surface with sandblasting preparation.

Haido et al., (2018) utilized reactive and inert powders of silica fume and waste glass respectively to fabricate hybrid concrete prisms. These samples were manufactured by two parts namely ordinary concrete substrate and high strength overlay made with these silica fume, waste glass powder and a mixture of them-as given in the figure. The roughness of interfacial surface between ordinary and high strength concrete was improved in many ways such as holes, grooves and sandblast. It is demonstrated that the interfacial surface with grooves produced hybrid concrete with compressive strength equivalent to 89% of control concrete sample strength.

Julio at al., 2004 performed an Experimental study to assess the bond strength between two layers of old and new concretes. Various techniques for improving the roughness of interfacial surface between these concretes were selected. This surface was prepared by sandblasting, wire brushing, chipping with a jack-hammer and control case without any preparation. Slant shear test was carried out to quantity concretes bond strength in sheer action. It is concluded that highest bond strength for

hybrid concrete can be achieved by sandblasted interfacial surface between old and ordinary new concretes.

Garbacz et al., (2004) studied the influence of concrete surface roughness on adhesion in concrete repair system. Different ways of treatments for interfacial surface between new and old concrete were used, namely shot blasting, sandblasting, grinding, mechanical and hand milling. Repair mortar was applied with or without a bond coat to the substrates of concrete to measure adhesion. Result reveals that the roughness of concrete surface for substrate affects the adhesion mainly in the case of concrete overlays without the bond coat. The size and number of cracks are highly influenced by surface treatment, where sandblasting and shot blasting produce more crack in the hybrid concrete sample.

2.5 Closing Remarks

This chapter deals with discussing previous researches related to the mechanical properties of basalt fiber concrete and hybrid concrete made with ordinary and fiber reinforced concretes. According to the aforementioned review, it can be concluded that mechanical properties have not been investigated extensively. In addition, there is no study dealing with the performance of hybrid concretes substrate old part and new part of basalt fiber overlay concrete as retrofitting part. In other words, the role of basalt fiber high strength concrete in improving the strength this hybrid concrete has not been examined so far.

CHAPTER 3

MATERIALS AND METHODS

In order to accomplish the aims of current work, a number of experimental tasks were performed. The experimental part of the present study consist of manufacturing the basalt fiber reinforced self-compacting concrete (BFRSCC) and investigating the fresh, mechanical and permeability properties of these concretes. In addition, the microstructure of manufactured basalt fibered SCC mixtures was examined by employing the scanning electron microscope (SEM).

The fresh characteristics of BFRSCC mixtures were determined in terms of slump flow, V-funnel, L-box, and J-ring tests. On the other hand, the compressive strength, modulus of elasticity, Poisson's ratio, splitting tensile and flexural strengths, and slant shear strength of BFRSCC mixtures were measured to identify the mechanical properties while the rapid chloride penetration, water penetration, and sorptivity tests were conducted to determine the permeability characteristics of BFRSCC mixtures.

The following sections includes the material descriptions, detail of mix design, self-compacting concrete (SCC) manufacturing procedure, detailed curing program, and explanation of fresh and hardened test methods.

3.1 Materials

3.1.1 Cement

The ordinary Portland cement with specific gravity of 3.15 was employed in the production SCC mixtures as well as normal concrete mixture. The ordinary Portland cement was provided from Delta-Sulaimania Factory in Sulaimania, Iraq and its specific surface area was 327 m²/kg. The chemical compositions and physical properties of ordinary Portland cement have been submitted in Table 3.1.

Table 3.1. Chemical compositions and physical properties of ordinary Portland cement

Analysis report (%)	Ordinary Portland cement
CaO	62.15
SiO ₂	18.94
Al ₂ O ₃	3.90
Fe ₂ O ₃	4.77
MgO	1.52
SO ₃	2.37
Loss on ignition	2.18
Insoluble residue	0.65
Specific gravity	3.15
Specific surface area (m ² /kg)	338
Initial setting time (min)	181.7
Final setting time (min)	255

3.1.2 Silica fume

In the production of SCC mixtures, silica fume, which is commercially available, was used as pozzolanic material. The commercial name of silica fume was Microsilica 920D and it was procured from Dost Chemistry, Istanbul, Turkey.

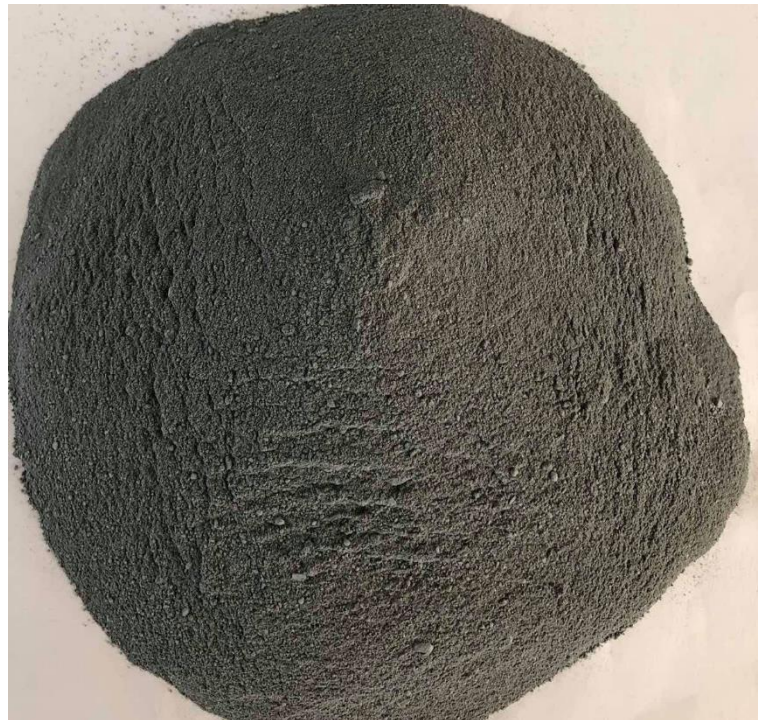


Figure 3.1. Photographic view of silica fume

The specific gravity and specific surface area values of silica fume were 2.2 and 369 m²/kg, respectively. The used silica fume consist of high amount of SiO₂, more than 90%. In addition, the specific surface area of silica fume measured regarding Brunauer-Emmett-Teller (BET) theory was between 15 and 28 m²/g. The photograph view of silica fume has been indicated in Figure 3.1.

3.1.3 Aggregate

The aggregate used in the normal and self-compacting concretes production was a mix of river sand with a specific gravity of 2.61 and crushed coarse aggregate with a specific gravity of 2.66. Both aggregate types conforming ASTM C127 and C128 were provided from local sources and their photographic views were demonstrated in Figures 3.2a and 3.2b, respectively.

The sieve analysis results for river sand and crushed coarse aggregate conducted regarding ASTM C136 were presented in Table 3.2 and Figure 3.3a. In addition, the particle size gradation of aggregate mixture achieved by mixing river sand and crushed coarse aggregate was plotted in Figure 3.3b with respect to A16-B16-C16 gradation curves.



(a)

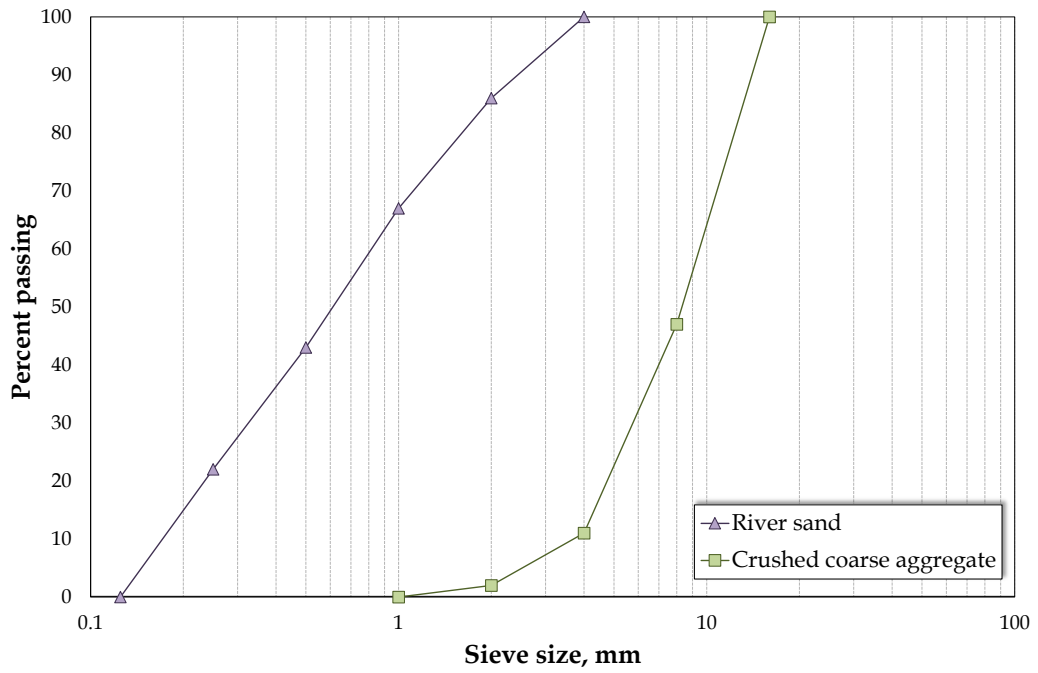


(b)

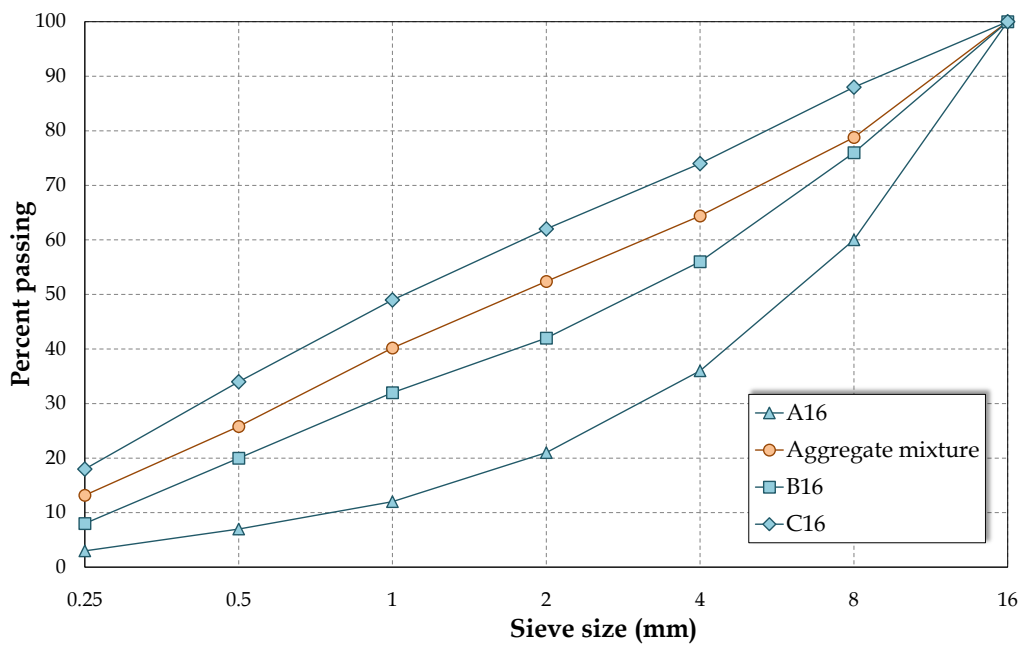
Figure 3.2. Photographic view of: (a) river sand and (b) crushed coarse aggregate

Table 3.2. Sieve analysis and physical properties of river sand and crushed coarse aggregate

Sieve size (mm)	River sand	Crushed coarse aggregate
16	100	100
8	100	47
4	100	11
2	86	2
1	67	0
0.5	43	0
0.25	22	0
Fineness modulus	1.82	5.40
Specific gravity	2.61	2.66



(a)



(b)

Figure 3.3. Particle size distribution of: (a) river sand and crushed coarse aggregate and (b) aggregate mixture in comparison with A16-B16-C16 curves

3.1.4 Basalt fiber

The basalt fiber having high performance was provided from Construction Vision Chemicals (CVC) Company, Turkey, with the commercial name of Fiber MF

Concrete. The diameter of basalt fiber employed in this study was 16 ± 2 μm and its length was about 24 mm. The properties of basalt fiber are submitted in Table 3.3 and the photograph of basalt fiber has been presented in Figure 3.4.

Table 3.3. Physical properties of basalt fiber

Properties	Fiber MF Concrete	Unit
Fiber length	24	mm
Fiber diameter	16 ± 2	μm
Density	2.80	g/cm^3
Elastic modulus	89	GPa
Melting temperature	1450	$^{\circ}\text{C}$
Break extension	3.15	%
Raw materials	Basalt	
Color	Dark grey/Smoked	



Figure 3.4. Photographic view of basalt fiber

3.1.5 Mixing water

Generally, it is suggested that drinkable water must be used in concrete production. Besides, if there is no drinkable water reservoir near to the production plant, water

from the stream, lake, and river may also be used. However, in the second condition, the water sample should be taken from the source and then should be analyzed for suitability to use in the concrete production. In this study, the drinkable water was used in the concrete production.

3.1.6 Superplasticizer

In this study, Hyperplast PC200, which is polycarboxylic polymers based and commercially available chemical admixture, was used in the concrete production to obtain desired workability. The technical properties of the superplasticizer are presented in Table 3.4.

Table 3.4. Technical properties of superplasticizer

Properties	Fiber MF Concrete
Form	Liquid
Color	Light yellow
Specific gravity	1.05±0.02
Water solubility	Soluble
Freezing temperature	-3 °C

3.2 Mixture Proportions

In the current study, two different concrete types, which are normal and self-compacting concretes, were designed. The normal concrete, which is named ordinary concrete in this study, was only utilized for the preparation of samples of the slant shear strength test. The design of ordinary concrete was done according to the concrete compressive strength. For this reason, many trial batches were produced and they were tested for 7-day and 28-day compressive strength. The mixture proportions for ordinary concrete mixture given in Table 3.5 belong to the trial batch that performed the desired 28-day compressive strength values of 30 MPa.

In addition to ordinary concrete, the study herein mainly investigates the influences of basalt fiber utilization in the self-compacting concrete (SCC) production on the workability, mechanical, and permeability properties. For this reason, four SCC mixtures were designed and produced. The total binder content of 570 kg/m³ and water-to-binder ratio (w/b) of 0.3 were designated in all four mixtures. The silica

fume, which was employed as 10% of total binder content by weight, was used as cementitious material instead of cement. In the production of SCC mixtures, four basalt fiber volume fractions of 0, 0.25, 0.5, and 1% were assigned by total concrete volume. The detailed SCC mixture proportions are presented in Table 3.5.

Table 3.5. Detailed mixture proportions and compressive strength for ordinary and self-compacting concretes (kg/m³)

Mix ID	OC	SCC	SCC25	SCC50	SCC100
Binder content	-	570.0	570.0	570.0	570.0
Portland cement	314.0	484.5	484.5	484.5	484.5
Silica fume	-	85.5	85.5	85.5	85.5
water-to-binder ratio	0.65	0.30	0.30	0.30	0.30
Water	204.1	171.0	171.0	171.0	171.0
River sand	941.0	936.3	936.3	936.3	936.3
Crushed coarse aggregate	941.0	671.7	671.7	671.7	671.7
Superplasticizer	-	5.7	11.4	17.1	22.8
Basalt fiber	-	-	7.0	14.0	28.0
Density	2398	2340	2320	2290	2265
28-day compressive strength values (MPa)					
Ambient temperature	30.5	101.9	94.5	90.8	85.5
200 °C		96.6	92.3	84.6	78.4
300 °C		89.0	83.8	73.9	69.3
400 °C		84.8	82.0	69.4	66.9
500 °C		77.0	67.9	65.2	60.5

The OC and SCC letters given in Mix ID row were the abbreviations of ordinary concrete and self-compacting concrete. Also, the number given in this row was used to denote the basalt fiber volume fractions. For instance, SCC25 mixture is the self-compacting concrete mixture manufactured with 0.25% basalt fiber.

3.3 Concrete Production

In the current study, a power-driven rotating drum mixer having 50-liter capacity of 50 liters was used in the production of concrete mixtures. ASTM C192 (2018) was followed in the production of ordinary concrete whereas the SCC mixtures were mixed and batched according to a special procedure since extra care and effort are

required in the production sequence and duration of SCC. However, there is a little difference between the production sequence and duration of SCC without and with basalt fiber. By this special production procedure, it was targeted to procure the same uniformity and homogeneity in all SCC mixtures. The order of this special production procedure for SCC mixture without basalt fiber can be listed as follows:

1. Put the aggregate mixtures into the drum,
2. Let the drum revolving for 1 minute to achieve aggregate mixed homogenously,
3. Pour the quarter of water onto the aggregate mixture,
4. Let the drum revolving for extra one minute,
5. Leave the aggregate mixture to absorb the water for one minute after extra one-minute finished,
6. Add the dry powder binder (cement and silica fume) material on the wetted aggregate,
7. Revolve the drum for extra two minutes to obtain powder material coated aggregate,
8. Mix the superplasticizer with remained water,
9. Pour the superplasticizer-water mixture onto the aggregate-powder material mixture,
10. Proceed the revolving of drum for extra three minutes,
11. Let the fresh SCC mixture to rest for two minutes after an extra three-minute revolving finished.

The aforementioned mixing order was applied on the plain SCC mixture, namely the mixture without basalt fiber. The SCC mixtures involving basalt fiber were also manufactured according to the process given above, but, before Step 8, the basalt fiber was added and the mixing time in Step 10 was prolonged to five minutes. Afterwards, the fresh SCC mixtures were mixed for two minutes and the workability tests were carried out.

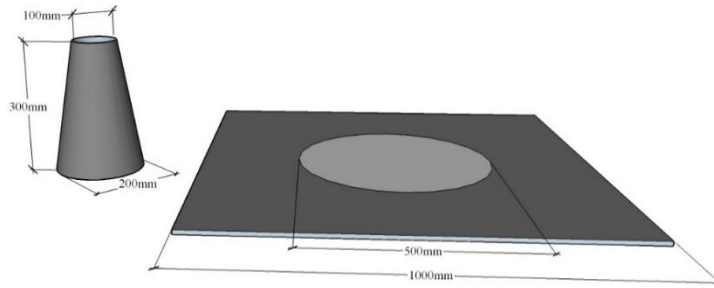
3.4. Workability test methods and Casting

Slump flow diameter and time, V-funnel flow time, L-box height ratio, and J-ring flow diameter and time tests were carried out to examine the workability characteristics of SCC mixtures produced in this study. The slump flow diameter and

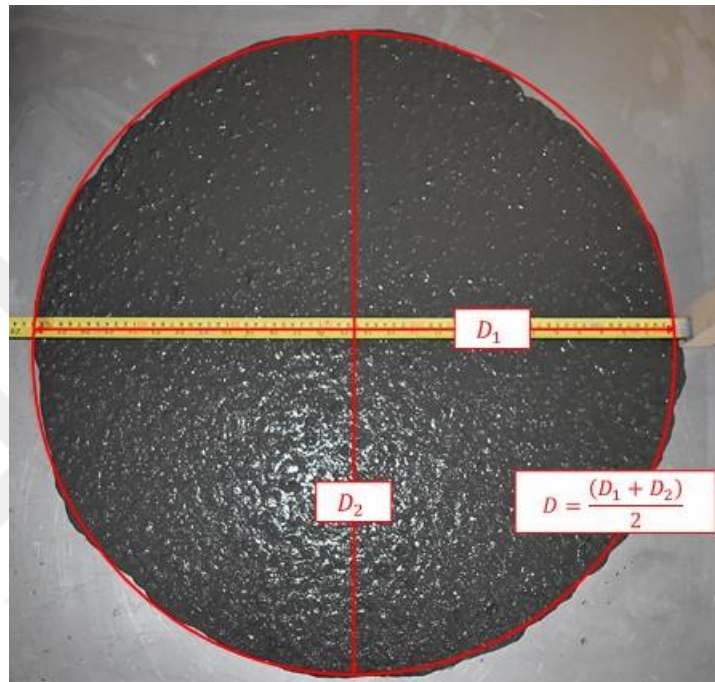
J-ring flow diameter tests were performed to indicate the flowability (in unconfined condition) of SCC mixtures. In addition to L-box test, the J-ring test method is also a good technique for identifying the passing ability class of SCC. Therefore, the J-ring and L-box tests were carried out to identify the passing ability class. Moreover, the viscosity of SCC mixtures was measured in terms of the slump flow time and V-funnel flow time tests. During the performing the slump flow, V-funnel, and L-box tests, the guidelines and specifications suggested by EFNARC (2005) committee were followed whereas the J-ring test was carried out regarding ASTM C1621 (2017).

3.4.1 Slump flow test

By performing this test, two different characteristics of SCC mixture can be identified, flowability and viscosity. Slump flow diameter representing the flowability and T_{50} flow time representing the viscosity of SCC mixture can be measured by this slump flow test. This test is the primary check to describe the workability performance of SCC mixtures and the flowability characteristics of SCC can only be identified by this test. Therefore, it should be carefully carried out. The equipment illustration and dimensions for this test have been given in Figure 3.8a. According to the EFNARC (2005) committee guidelines, the fresh SCC mixture is firstly poured into the slump cone and it is released to flow till the flowing stopped. Then the diameter of flowed SCC is measured from two points as indicated in Figure 3.8b and their average is given as slump flow diameter. Apart from flowability, visual observation in this test also provides an opportunity to comprehend the uniformity and segregation resistance of SCC mixture. In addition, the viscosity of the SCC mixture can be also measured by performing slump flow test. T_{50} slump flow time measurement that is the measuring of time passing during the flowing of the fresh SCC mixture from releasing to reaching 50-cm diameter circle as shown in Figure 3.8b can give an idea about the viscosity. However, it should be noted that this is an indirect viscosity measurement.



(a)



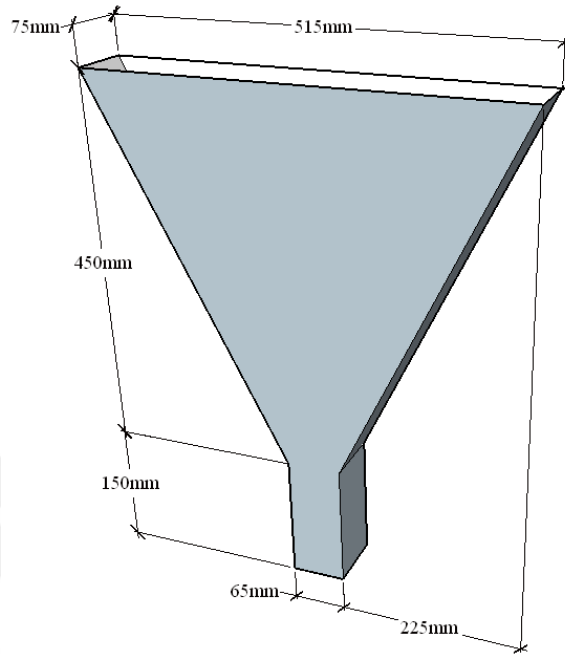
(b)

Figure 3.5. Slump flow test: (a) schematically illustration and (b) diameter measurement

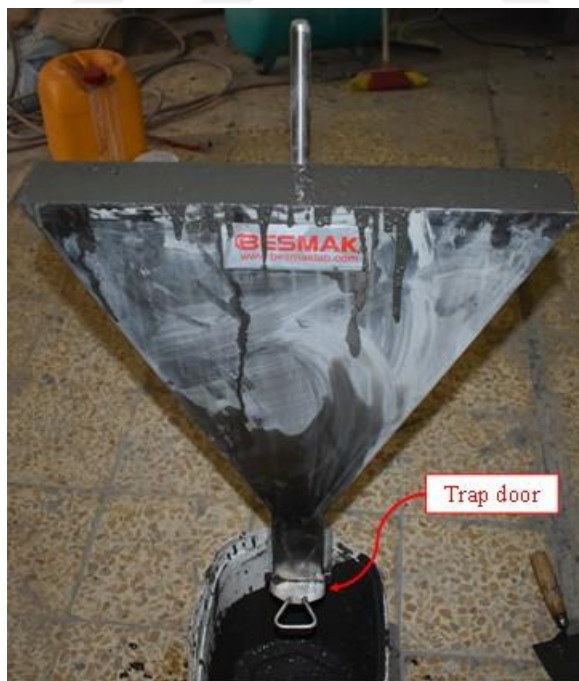
3.4.2 V-funnel flow test

This test is used only to describe the indirect viscosity characteristic of the SCC mixtures, herein, the term indirect viscosity means the viscosity characteristic achieved from this test is based on the flowing rate. A V-shaped funnel, of which schematically illustration and dimensions have been given in Figure 3.6a, is utilized during the conducting of V-funnel flow time test. The fresh SCC mixture is firstly poured into the funnel (as indicated in Figure 3.6b) and then the trap door placed at the bottom of the funnel is opened and flowing out of the SCC mixture from the funnel is allowed in this way. The time measured in the V-funnel flow test is the elapsed time between the beginning and end of flowing of the SCC from the funnel.

In order to assess the segregation in the SCC mixtures, V-funnel flow time test was repeated after first time carrying out the test, however, during the second time the fresh SCC mixture was kept in the funnel for 5 minutes and then it was permitted to flow out through the trap gate.



(a)



(b)

Figure 3.6. V-funnel flow test: (a) schematically illustration and (b) performing test

The difference between the first and second V-funnel flow times was used to assess the segregation degree in the SCC mixtures produced in this study. It has been stated in the EFNARC (2005) guidelines and specifications that there are three slump flow and two viscosity classes that are used to describe the filling ability of the SCC mixtures. These classes are tabulated in Table 3.6 for easy understanding.

Table 3.6. Classes and ranges for filling ability and passing ability for the SCC mixtures suggested by EFNARC (2005) committee

Description	Classes	Tests and ranges	
Filling ability	Slump flow classes	Slump flow diameter (mm)	
	SF1	550-650	
	SF2	660-750	
	SF3	760-850	
	Viscosity classes	T ₅₀ time (s)	V-funnel time (s)
	VS1/VF1	≤2	≤8
VS2/VF2	>2	9 to 25	
Passing ability	Passing ability classes	L-box height ratio	
	PA1	≥ 0.8 with two rebars	
	PA2	≥ 0.8 with three rebars	

3.4.3 L-box test

Another important workability test for the SCC is the L-box test since it directly describes the passing ability performance of the fresh SCC. There are two different L-shaped test equipment, containing two or three rebars as demonstrated in Figure 3.7a. The confined spaces are simulated by using L-box test equipment with two reinforcing bars and narrow openings are simulated by employing L-box test equipment involving three reinforcing bars. The fresh SCC mixture flows through the rebars on the test equipment that represent the narrow openings and localized spaces and as a result, the SCC mixture does not lose its uniformity and does not segregate and does not cause the blocking. All these states the filling ability characteristic of the SCC mixture.

The fresh SCC mixture in the vertical box is allowed to flow through the rebars to the horizontal box. When the flowing of the fresh SCC mixture stopped, the height ratio (h_2/h_1) as shown in Figure 3.7b is determined to evaluate the passing ability performance of the SCC mixture. Figure 3.7b also demonstrates the dimensions of L-

box test equipment. According to the EFNARC (2005) guidelines, there are two classes used to express the passing ability of the SCC mixtures as presented in Table 3.6.

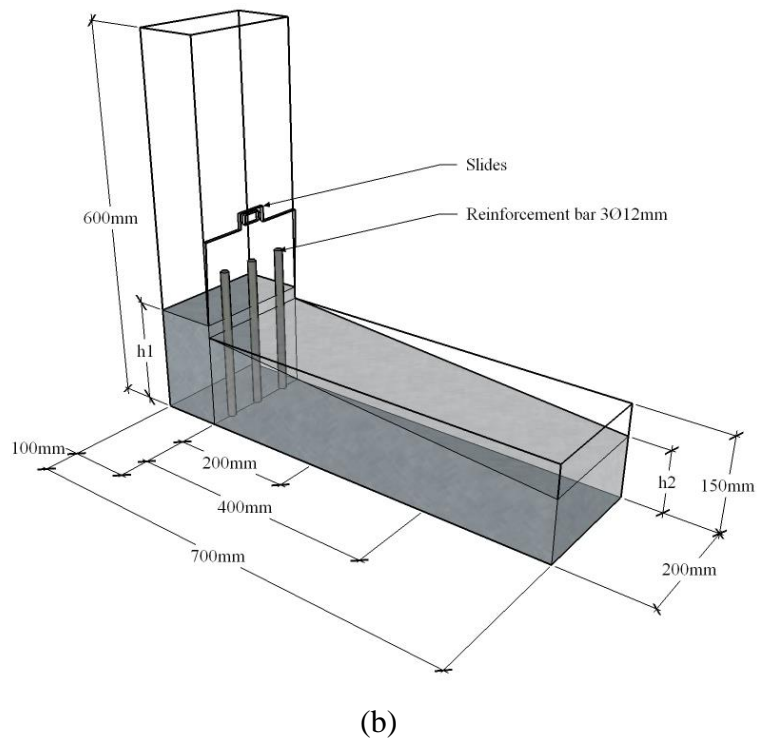
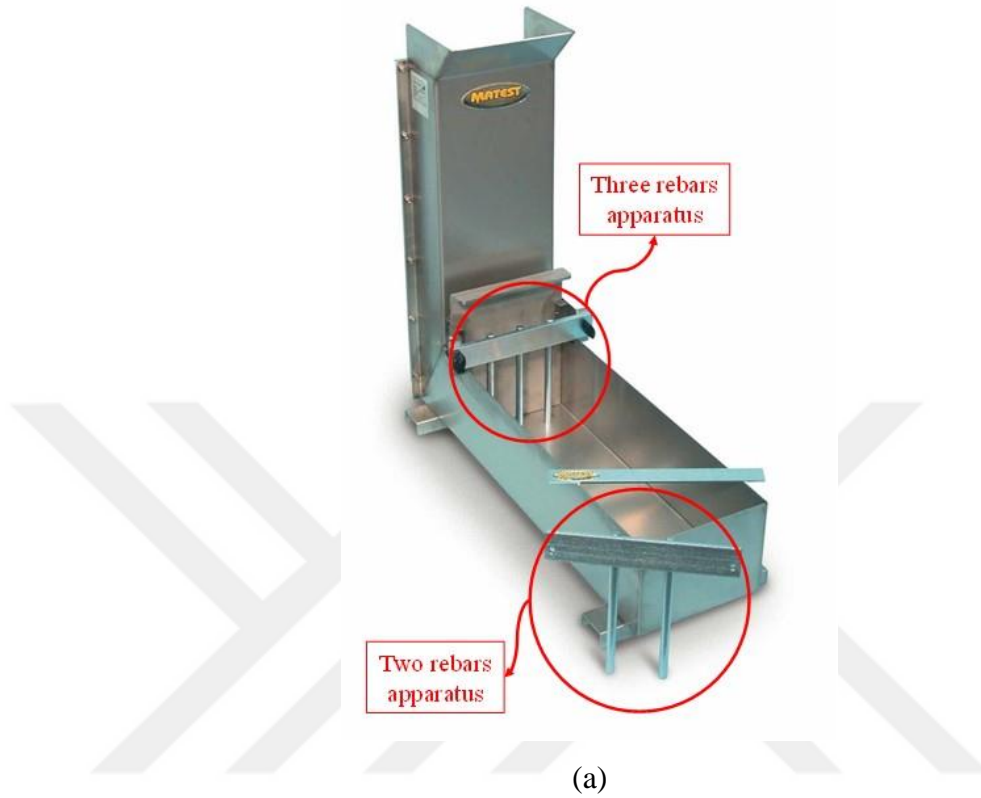


Figure 3.7. L-box test (a) equipment types and (b) schematically illustration of equipment and pointing the fresh concrete heights (h_1 and h_2)

3.4.4 J-ring flow test

J-ring flow test was performed with respect to ASTM C1621 (2017). The test apparatus consists of sixteen equally spaced 16-mm rebars on a 300-mm diameter circle and a ring with a thickness of 25 mm placed on these 100-mm height rebars. The schematically illustration of the J-ring test apparatus has been given in Figure 3.8a. It was aimed to measure the passing ability of the SCC mixtures produced in this study by this test. The flow diameter, T_{50} flow time, and height difference in flowed SCC mixture were measured to assess not only the passing ability but also flowability and filling ability of the SCC mixture. Therefore, the J-ring flow test can be considered the support for other workability measurement tests. In this test, the slump cone was also used for filling of concrete. Then, the flow diameter as in slump flow diameter were measured. At the same time, T_{50} J-ring flow time was measured as in T_{50} slump flow time test. As a result, the height difference between the concrete remained in the ring and flowed outside of the ring was measured as indicated in Figure 3.8b.

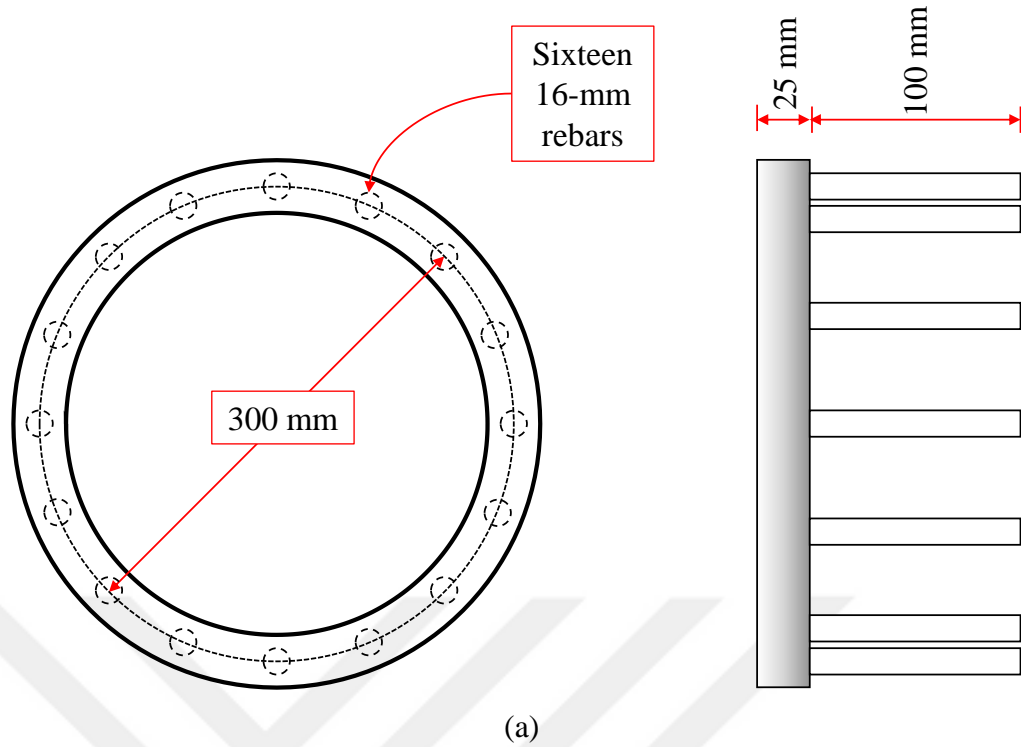


Figure 3.8. J-ring flow test: (a) schematically representation of equipment and (b) typical height difference measurement

3.4.5 Casting

As soon as the workability tests were ended, the fresh mixtures were molded and the molded specimens were wrapped with plastic sheets for 24 hours. For one day, the specimens were kept in the casting room, in which the temperature was 20 ± 2 °C. Then, the demolded specimens were putted in water pool for curing. The steel and plastic molds were used for the hardened and permeability test except slant shear strength test specimens.



(a)



(b)

Figure 3.9. (a) Empty and (b) concrete-filled wooden moulds for slant shear strength test

The wooden molds were employed in the preparation of slant shear strength test specimens as indicated in Figure 3.9. The specimens for this test were produced by using ordinary concrete representing old concrete and self-compacting concrete

representing new concrete. The wooden molds were firstly filled with ordinary concrete, of which one surface is inclined surface with angle of 60° . During the filling of first part, a rod was used to compact ordinary concrete. The ordinary concrete was poured in two layers and each layer was rodded 25 times to achieve good compaction. These parts of specimens were wrapped with plastic sheet and kept in the laboratory condition. After one day, they were demolded and 28-day water curing was applied. A typical ordinary concrete part has been indicated in Figure 3.10 after 28-day water curing period.



Figure 3.10. A typical ordinary concrete part of slant shear strength test

After 28-day water curing, four different surface treatments were applied to inclined surface which are (As casted, Sand blasting, drilled hole and Grooved). By this way, four different inclined surfaces were obtained as shown in Figure 3.11a and the specimens were again molded from these surfaces and filled with SCC as shown in Figure 3.11b. The mechanical and permeability tests were performed on three specimens and the average of them was presented as a test result.



(a)



(b)

Figure 3.11. Photograph of slant shear strength test: (a) after surface treatment and (b) after filling with SCC

3.5 Test Methods

This study covers the investigation of the workability, mechanical, and permeability properties of SCC mixtures. Therefore, the testing methods followed in this study were explained in three sub-sections.

3.5.1 Mechanical test methods

Compressive strength, modulus of elasticity, splitting tensile strength, flexural strength, and slant shear strength tests were conducted to investigate the mechanical properties of SCC mixtures manufactured in this study. The effect of temperature on the mechanical properties of the SCC mixtures were also examined in the current study. Therefore, 4 temperature levels except from ambient were designated to investigate the temperature effect on the mechanical properties of the SCC mixtures. The temperatures were exposed to the SCC mixture samples according to the cycle indicated in Figure 3.12.

3.5.1.1 Compressive strength

The recommendations and specifications provided in ASTM C39 (2018) were followed for performing the compressive strength of the normal concrete and SCC mixtures. Besides, to reveal the strength development by time and to see the silica fume effect on the compressive strength, the test was carried out at the ages of 7th, 14th, 28th, and 56th day. The $\phi 100 \times 200$ -mm cylindrical specimens were taken to conduct the compression test as shown in Figure 3.13a. Also, the main objective of this study was to investigate the temperature effect on the mechanical properties of the SCC mixtures.

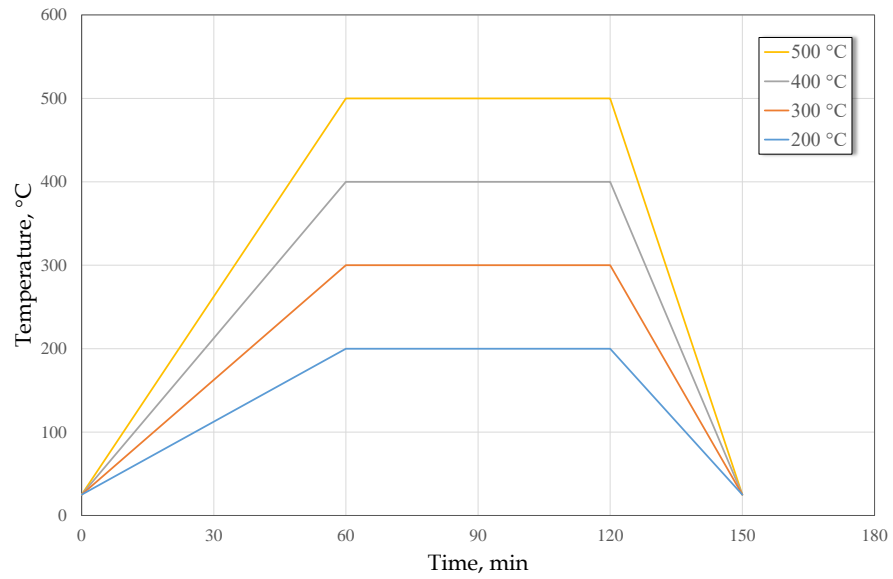


Figure 3.12. Temperature exposure cycle



(a)



(b)

Figure 3.13. (a) Cylindrical test specimens for compressive strength and (b) specimens in oven for temperature exposure

For this reason, the compressive strength test performed on the 28th day was carried out on the specimens exposed to 200, 300, 400, and 500°C temperature apart from specimens kept in the ambient temperature. The cylindrical specimens putted in oven to exposure the temperature has been shown in Figure 3.13b. In the current study, the

results reported for the compressive strength of the SCC mixtures are the average of three compressive strength values for each mixture. Before performing the compressive strength test, the samples were capped with sulfur as shown in Figure 3.14a and they were tested in the uniaxial testing machine with capacity of 3000 kN as indicated in figure 3.14b.



(a)



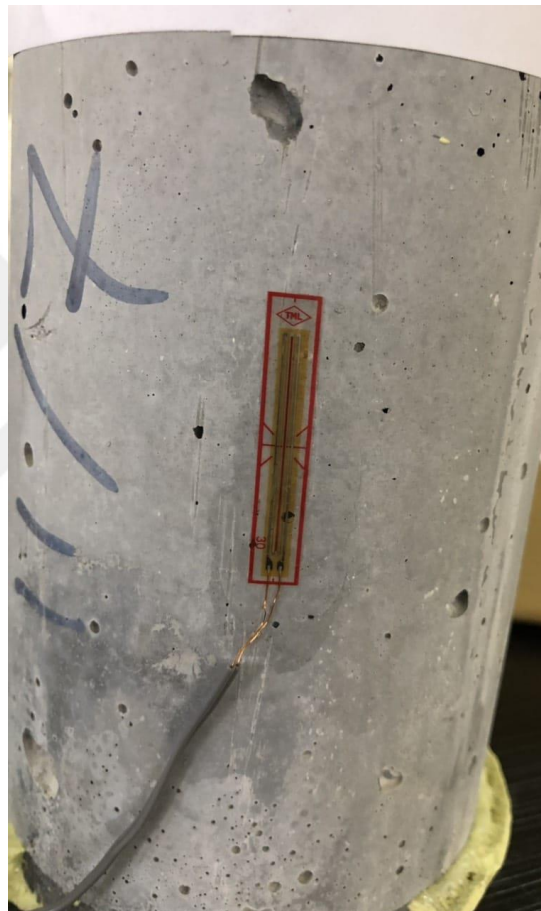
(b)

Figure 3.14. (a) Sulfur capped cylindrical compressive strength test samples and (b) compressive strength test sample placed to the testing machine

3.5.1.2 Modulus of elasticity

Static elastic modulus of the SCC mixtures was appointed regarding ASTM C469 (2014). The cylinder specimens were handled to conduct the testing procedure stated

in ASTM C469 (2014). A strain gages was used to handle the axial deformation of the test specimen as shown in Figure 3.15a. The test was performed on three specimens and their average was submitted as the result of elastic modulus for each mixture. In addition, since the main objective of this study was to investigate the temperature effect on the mechanical properties of the SCC mixtures, the elastic modulus test performed on the 28th day was carried out on the specimens exposed to 200, 300, 400, and 500°C temperature apart from specimens kept in the ambient temperature.



(a)



(b)

Figure 3.15. Elastic modulus testing sample having horizontal and vertical strain gage

3.5.1.3 Poisson's ratio

Poisson's ratio of the SCC mixtures was appointed regarding ASTM C469 (2014). The cylinder specimens were handled to conduct the testing procedure stated in ASTM C469 (2014). The test for determination of Poisson's ratio was carried out on three cylindrical specimens and their average was submitted as the result of Poisson's ratio for each mixture. The samples for this test included two strain gages placed vertically and horizontally as shown in Figures 3.15a and 3.15b. In addition, since the main objective of this study was to investigate the temperature effect on the mechanical properties of the SCC mixtures, the Poisson's ratio test performed on the 28th day was carried out on the specimens exposed to 200, 300, 400, and 500°C temperature apart from specimens kept in the ambient temperature.

3.5.1.4 Splitting tensile strength

Splitting tensile strength test was conducted in accordance with ASTM C496 (2017). The cylindrical specimens with diameter of 150-mm and height of 300-mm were employed to perform this test. The test was carried out on three specimens and the splitting tensile strength result for each mixture reported in this study is the average of these three specimens. Besides, the main objective of this study was to investigate the temperature effect on the mechanical properties of the SCC mixtures. For this reason, the splitting tensile strength test performed on the 28th in water day was

carried out on the specimens exposed to 200, 300, 400, and 500°C temperature apart from specimens kept in the ambient temperature. The following equation was used to compute the splitting tensile strength:

$$f_{split} = \frac{2P}{\pi h\phi} \quad 3.1$$

where;

f_{split} is the splitting tensile strength (MPa),

P is the failure load (N),

h is the specimen height (mm), and

ϕ is the specimen diameter (mm).

3.5.1.5 Flexural strength

Three point bending test was considered to evaluate the flexural strength of the SCC mixtures. The test was conducted regarding to ASTM C78 (2018). From each mixtures, three 100x100x400-mm prismatic specimens were tested and their average was submitted as the result for flexural strength. The prismatic specimen placed into the three point bending test machine has been shown in Figure 3.16. Moreover, the main objective of this study was to investigate the temperature effect on the mechanical properties of the SCC mixtures. For this reason, the flexural strength test performed on the 28th day was carried out on the specimens exposed to 200-, 300-, 400-, and 500-°C temperature apart from specimens kept in the ambient temperature. The following expression was used to compute the flexural strength of the SCC mixtures:

$$f_{flex} = \frac{3PS}{2BD^2} \quad 3.2$$

where;

f_{flex} is the flexural strength (MPa),

P is the failure load (N),

S is the span length (mm),

B is the specimen width (mm), and

D is the specimen depth (mm).



Figure 3.16. Test setup for flexural strength

3.5.1.6 Slant shear strength

ASTM C882 (2013) was followed to carry out the slant shear strength test. The test was performed on the prismatic specimens having a square cross-section. In the current study, it was firstly aimed to investigate the effect of surface characteristics on the slant shear strength between two different concrete types. For this reason, four different surface textures were designated at the beginning. The surface textures depicted in this study were control surface as cast (without surface roughening), hole drilled surface, grooved surface, and sandblasted surface textures as shown in Figure 3.7a. Then, an ordinary concrete with a compressive strength value of 30 MPa was produced regarding ACI 211 (2002) criteria. This ordinary concrete was produced to represent the old concrete in the old buildings as indicated in Figure 3.17.

Therefore, the 28-day water curing period was applied to these concrete samples and after that, the specimens were kept in the laboratory for two months. Afterward, the SCC mixtures manufactured in this study were used in the preparation of the slant shear strength test specimens to represent the new concrete as shown in Figure 3.18. Apart from the effect of the surface texture, the effect of fiber content in the SCC mixtures and the temperature that the specimens were exposed were also investigated. For each mixture, temperature level, and surface texture, the test was

conducted on three specimens and their average was reported as the slant shear strength.

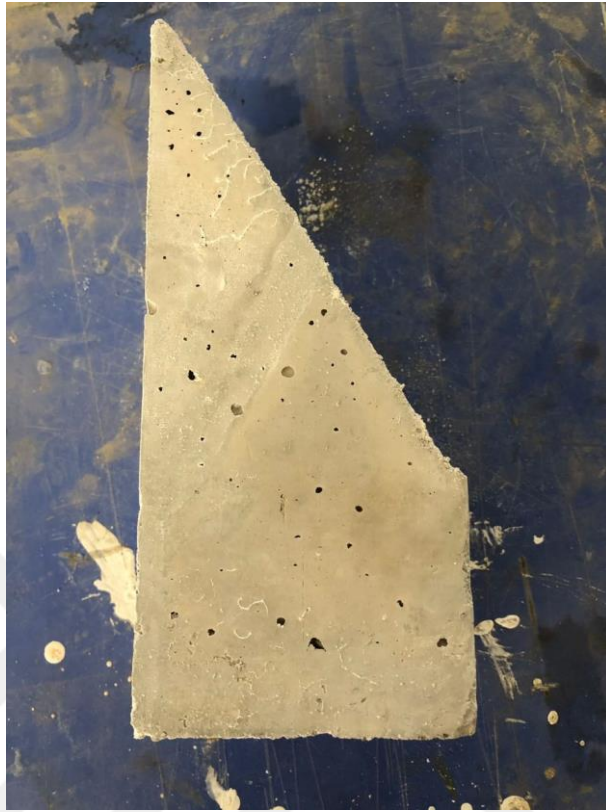


Figure 3.17. The ordinary concrete part of slant shear strength test specimens having untreated surface texture



Figure 3.18. Slant shear strength test specimens including both old and new concretes

The following expression was handled to determine the slant shear strength of the mixtures:

$$f_{slant} = \frac{P}{SA} \quad 3.3$$

where;

f_{slant} is the slant shear strength (MPa),

P is the failure load (N), and

SA is the slant area (mm²).

3.5.2 Permeability test methods

Sorptivity index, water penetration depth, and rapid chloride permeability tests were performed to examine the permeability characteristics of SCC mixtures manufactured in this study.

3.5.2.1 Sorptivity index

The amount of water pass through the capillary pores of the concrete was measured by the sorptivity test. This test was performed on the specimens with 100-mm diameter and 50-mm height that were attained by cutting the $\phi 100 \times 200$ -mm cylindrical specimens. In order to achieve reliable results from performing this test, the specimens are kept in an oven to attain oven-dry state specimens until the mass of the specimens become constant. To prevent crack occurrence due to the temperature, the oven has a temperature of 50 ± 5 °C as shown in Figure 3.19.



Figure 3.19. Sorptivity test specimens in the oven

The rounded sides of the specimens are covered with paraffin to prevent water absorption from the sides and the cut surface is exposed to the water during the conducting of the test as schematically demonstrated in Figure 3.20.

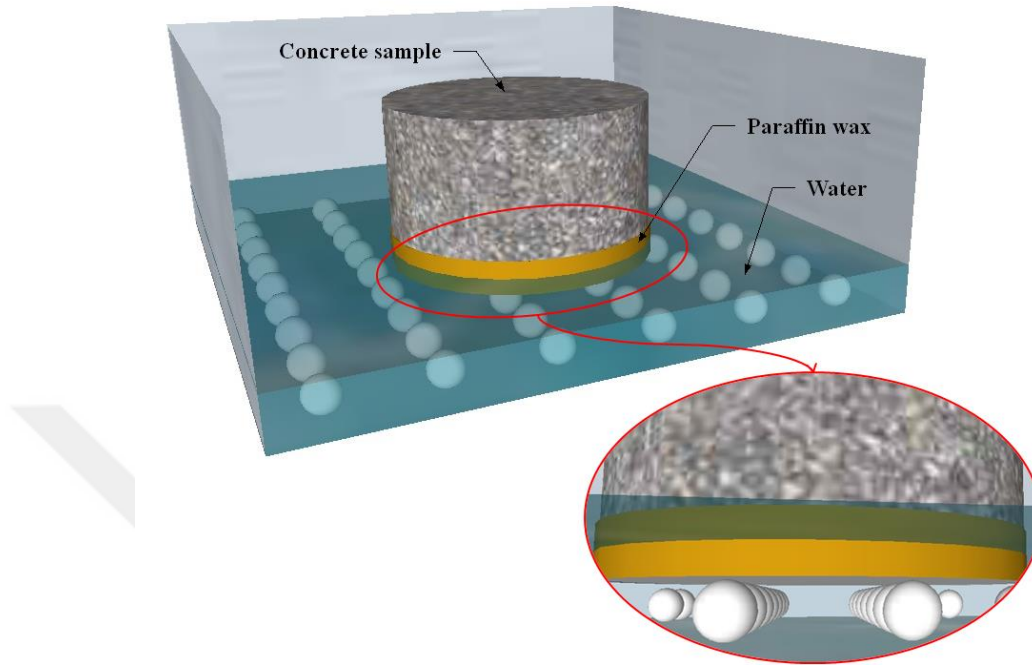


Figure 3.20. Sorptivity test set-up simulation

As shown in the figure, the test specimen is put into the tray filled with water of which elevation does not exceed the alignment of the paraffin. Then, the specimen is weighed to determine the gained mass due to water suction after lifting the specimen from the tray at particular time intervals. This process maintains for 64 minutes, subsequently, the volume of water absorbed by the specimen at these particular time intervals is calculated by dividing the mass gain to the water density and the specimen's nominal surface area. Finally, the sorptivity index of the SCC mixtures is computed by plotting the absorbed water volume versus the square root of time intervals by regarding the slope of best fit line. The test is carried out on 6 specimens and their average has reported as the result of each mixture.

3.5.2.2 Water penetration depth

The water penetration depth of the SCC mixtures was measured according to TS EN-12390-8 (2002). The test was conducted on three cylindrical specimens and their average were reported as the result. The cylindrical specimens are exposed to 500 ± 50 -kPa downward pressure water for 72 hours as indicated in Figure 3.21a. The

specimens are knapped into two pieces from the middle after a 72-hour water pressure application. Afterwards, the highest water penetration depth on the knapped surfaces is measured for each specimen as demonstrated in Figure 3.21b. If the concrete is going to keep in touch with aggressive media and moderately aggressive media, the water penetration depth should be more than 30 and 50 mm, respectively.



(a)



(b)

Figure 3.21. Water penetration depth: (a) test set-up and (b) measurement

3.5.2.3 Resistance to chloride ion penetration

The resistance of the SCC mixtures to chloride penetration was measured regarding ASTM C1202 (2019). The top and bottom parts of $\phi 100 \times 200$ -mm cylindrical specimens were used in the sorptivity test while the middle part of these specimens were used in the conducting of the rapid chloride permeability test. For this reason, the test was carried out on three 50-mm disk specimens and their average was submitted as the result. To eliminate the defects arising from the segregation and/or bleeding, the samples taken from the middle portion of the specimen are employed in the test. The preparation of the 28-day water cured specimens for the test is made with respect to recommendations provided in ASTM C1202 (2019). Then, the prepared specimens are placed between the sodium hydroxide (NaOH) and sodium chloride (NaCl) contained cells. In this context, the faces of the specimens are kept in touch with 0.3 N NaOH and 3% NaCl solutions. After placing the specimens between these cells, a direct current of 60 ± 0.1 volts is applied to the faces for the 6-hour period. During the test, the current traversing through the specimen is recorded and then, the total charge passed through the specimen is calculated by applying the Simpson's integration. As a result, the total charge in terms of coulombs is determined from the recorded current and the time history. The typical rapid chloride permeability test photo has been presented in Figure 3.22.



Figure 3.22. Rapid chloride permeability test set-up

3.5.3 Scanning Electron Microscopy (SEM)

SEM has been used in current research to show the microcracks in both parts of hybrid concrete. Moreover, the perfect bond at interfacial surface will be confirmed with detecting the cracking at this surface.

The distribution of basalt in the overlay strata was observed as well. Samples as shown in Figure 3.22 for SEM test were taken by dimension of 4cm length and 2, 2 cm thickness and width.



Figure 3.23. Samples for SEM test

CHAPTER 4

RESULTS AND DISCUSSIONS

The results and discussions part presented in this thesis consists of four sections. The test results for workability characteristics of the SCC mixtures were presented in the first part whereas the test results carried out to investigate the mechanical and permeability properties of the SCC mixtures were submitted in the second and third sections, respectively. Besides, the results and discussions about scanning electron microscopy (SEM) image analysis were given in the last section.

4.1 Workability tests

4.1.1 Slump flow diameter

The slump flow diameter results for the SCC mixtures manufactured in this study have been presented in Figure 4.1. The results indicated that the plain SCC mixture that produced without basalt fiber had a slump flow diameter value of 740 mm, which can be classified as SF2 flow class according to the EFNARC (2005) specifications. As stated in the EFNARC (2005) guideline, this type of SCC mixtures can be utilized for the many types of normal applications such as walls, columns, etc. The results also revealed that the utilization of basalt fiber in the SCC production worsened the flowing performance of the SCC mixtures. After the basalt fiber volume fraction of 0.25%, the SCC flowability class changed from SF2 to SF1. Namely, the slump flow diameter of the SCC mixtures dramatically dropped below the 650 mm when the basalt fiber volume fraction increased from 0.25 to 0.50 or 1.00%. This is an expected impact of fiber utilization in concrete production. The similar findings about the effect of fiber utilization on the concrete workability were reported by many researchers (Algin and Ozen, 2018; Dias and Thaumaturgo 2005; Kabay, 2014).

The main reason for the reduction in the slump flow diameter by the basalt fiber using can be explained as the basalt fiber particles absorb mixing water and also make the cement paste much more cohesive since the basalt fiber particles are in micro-scale particles. The SCC mixtures produced in this study, which were classified in the flowing class of SF1 according to EFNARC (2005) specifications, can be used in the members of structures that contains slight reinforcement or no reinforcement such as slabs of houses. In addition, this type of concrete may be used in the construction of the members that have the small sections to prevent horizontal flow such as deep foundations or piles.

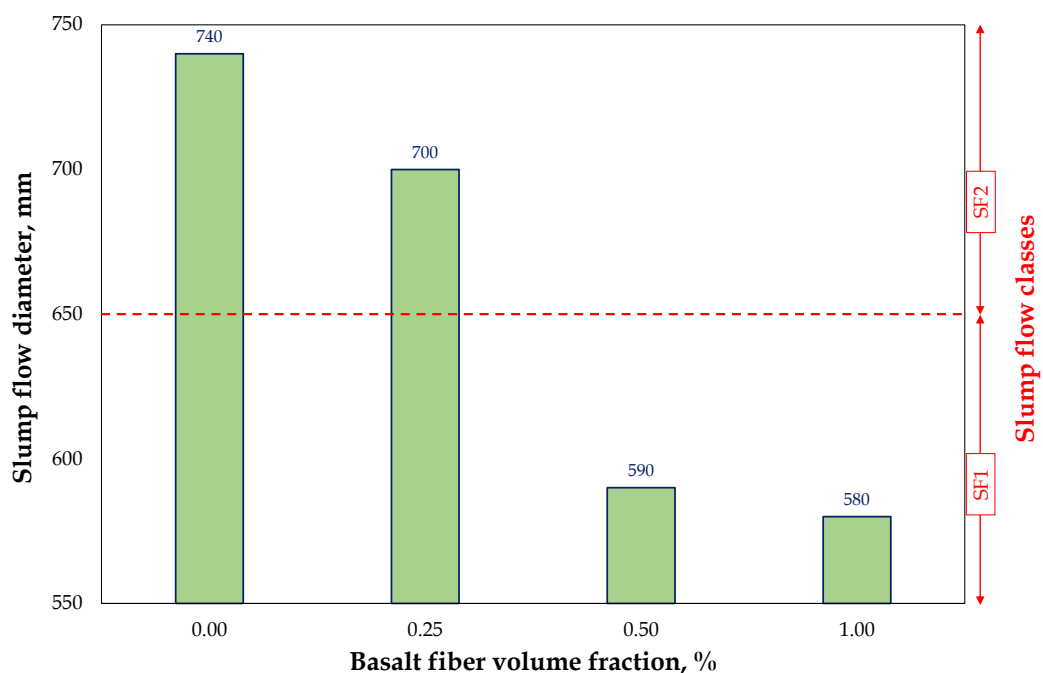


Figure 4.1. Variation in slump flow diameter of SCC mixtures concerning basalt fiber volume fraction

Moreover, the segregation and bleeding in the SCC mixtures were visually examined in this study. For this, the fresh concrete on the slump flow table was used. After the slump flow diameter and time tests finished, a little time was waited to observe there is segregation and bleeding or not. The typical photographic view of the SCC mixture on the slump flow table has been indicated in Figure 4.2. The photograph belongs to the SCC mixture produced with 0.25% basalt fiber volume fraction and when the photograph is examined, it can be easily seen that there is no segregation and bleeding in the concrete. The same results were beheld in all mixtures.

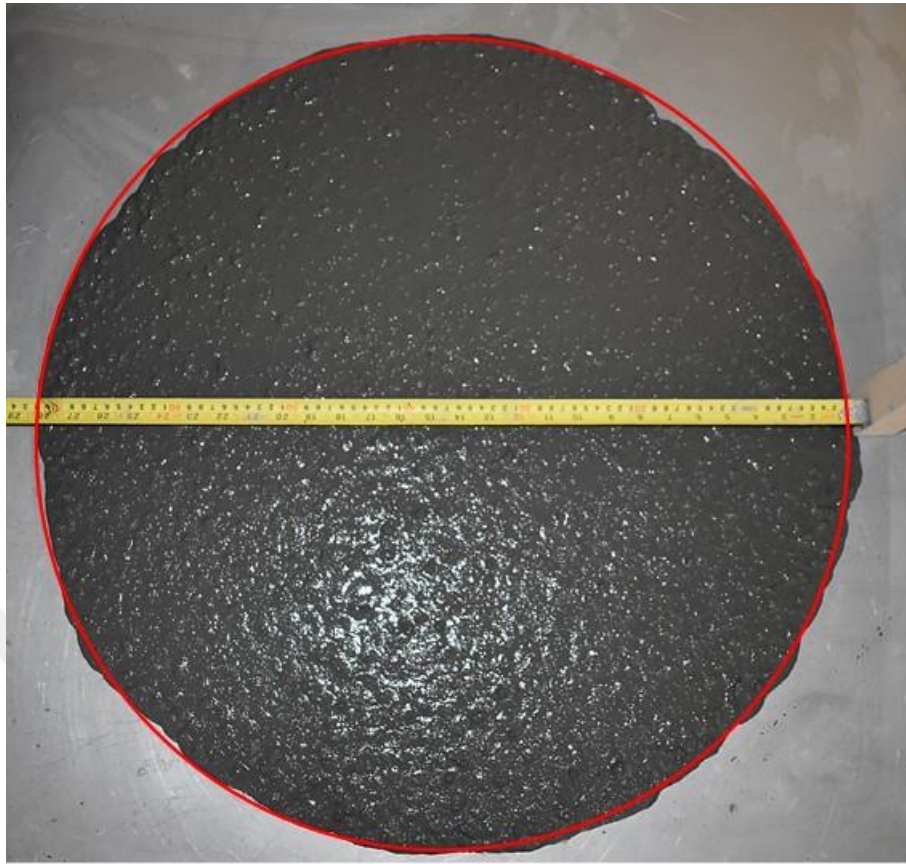


Figure 4.2. Photographic view of flowing of SCC mixture with 0.25% basalt fiber

4.1.2 J-ring flow diameter

Another flow diameter test for the SCC mixture is the J-ring flow diameter test. In order to express the reliability and robustness of the study and test results, J-ring flow diameter test was also carried out. The variation in the J-ring flow diameter of the SCC mixtures versus the basalt fiber volume fraction has been shown in Figure 4.3. The results procured from this study supported the findings attained in the slump flow diameter test. The utilization of the basalt fiber in the SCC production decreased the flowability performance. Especially, after the basalt fiber volume fraction of 0.25%, the amount of decrement in the flowability performance was increased. The main reason for this is the utilization of the mixing water by the basalt fiber particles and that caused both the decreasing of the workability and the increasing of the cohesiveness of the cement paste. This test also provide information about the passing ability performance of the SCC mixtures, since the SCC flows

among the rebars. For this reason, decreasing in the slump flow diameter means not only worsen of the flowing ability but also worsen of the passing ability.

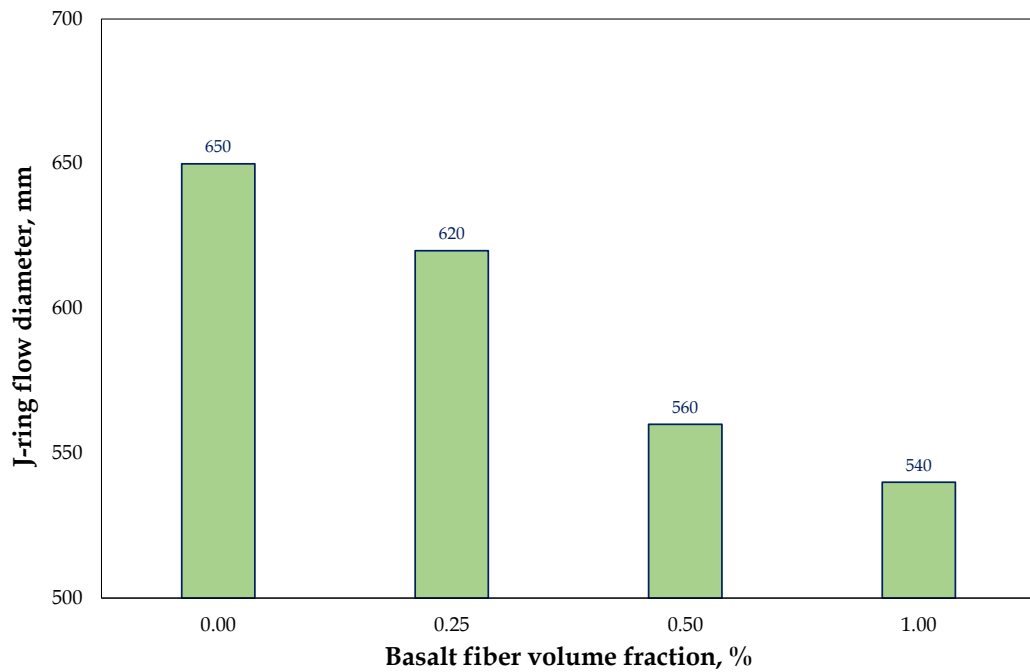


Figure 4.3. Variation in J-ring flow diameter of SCC mixtures concerning basalt fiber volume fraction

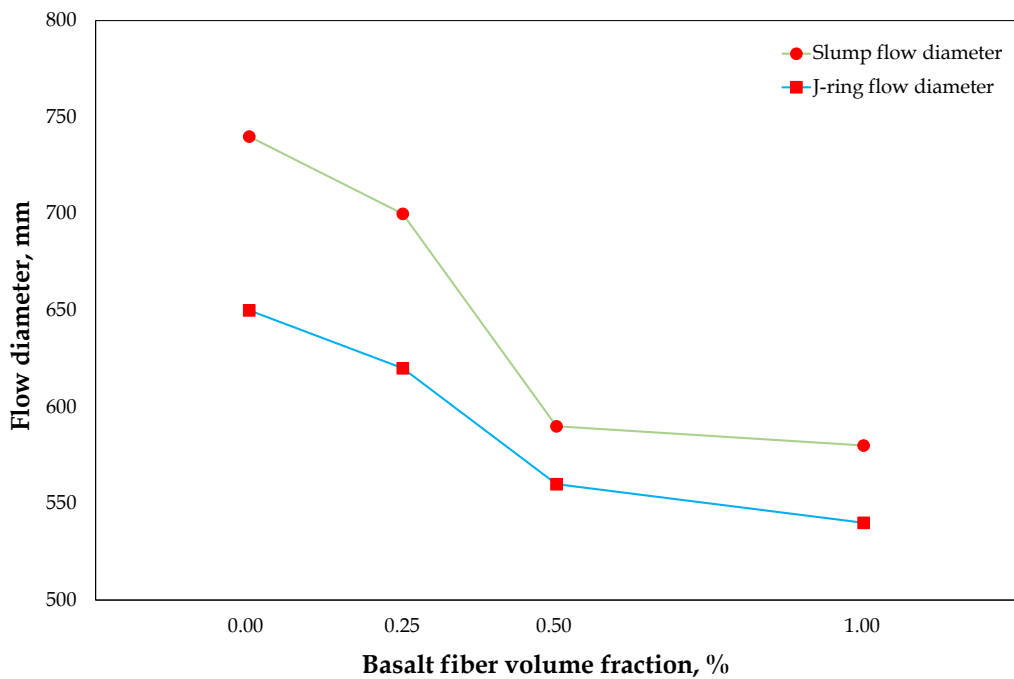


Figure 4.4. Slump and J-ring flow diameter values versus basalt fiber volume fraction

Figure 4.4 clearly indicates the variation trend in both slump and J-ring flow diameter concerning the basalt fiber volume fraction. The dramatical reduction in the flow diameters after 0.25% basalt fiber volume fraction utilization can be obviously seen in this figure. The figure also reveal the robustness and reliability of the both tests conducted in this study.

4.1.3 T_{50} slump flow time

The similar effect of the basalt fiber utilization as observed in slump flow diameter can be seen in T_{50} slump flow time. The variation in the T_{50} slump flow time with respect to the basalt fiber volume fraction has been indicated in Figure 4.5. The increment in the T_{50} slump flow time was observed by increasing the basalt fiber volume fraction. The plain SCC mixture that produced without basalt fiber has the T_{50} slump flow time of 2.1 s whereas the SCC mixtures produced at the basalt fiber volume fractions of 0.25, 0.50, and 1.00% have the T_{50} slump flow time values of 3.2, 3.9, and 4.2, respectively. The main reason for the delaying in the flowing time is due to high cohesiveness in the cement paste caused by fiber particles. According to this test results, all SCC mixtures produced in this study can be classified as viscosity class of VS2 regarding the EFNARC (2005) guideline.

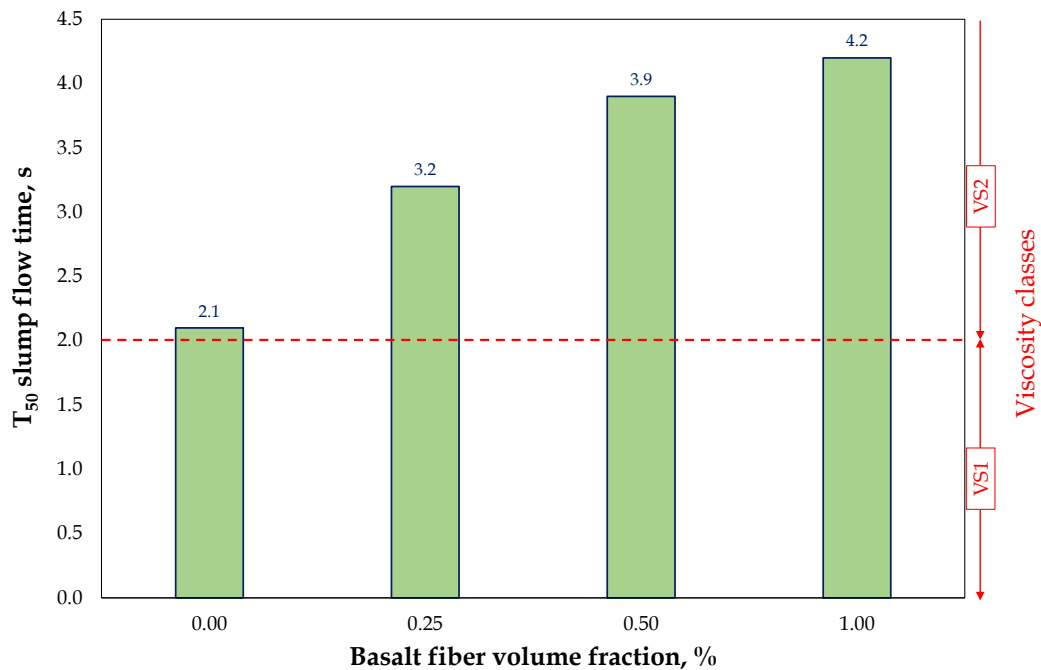


Figure 4.5. Variation in T_{50} slump flow time of SCC mixtures concerning basalt fiber volume fraction

4.1.4 T₅₀ J-ring flow time

The T₅₀ flow time values procured from the J-ring test indicated an increasing trend by the increasing of the basalt fiber volume fraction. The plain SCC mixture that does not include basalt fiber has the T₅₀ J-ring flow time of 2.4 s whereas the SCC mixtures produced with the basalt fiber volume fractions of 0.25, 0.50, and 1.00% have the T₅₀ J-ring flow times of 4.0, 5.1, and 6.4 s, respectively. A similar increment was observed in the slump flow time test. This is directly related to the decrement in the cohesiveness of the cement paste by basalt fiber addition. Since there is no definite classification for J-ring flow time provided by the EFNARC (2005) committee, presenting the result of this test will provide a piece of extra information about the indirect viscosity of the SCC mixtures. Therefore, Figure 4.7 has been also submitted to graphically illustrate the relation between T₅₀ slump and J-ring flow times versus the basalt fiber volume fraction. By performing of this test, it is also examined the passing ability performance of the SCC mixtures, since the SCC flows among the rebars. For this reason, increasing in the slump flow time means not only worsen of the filling ability but also worsen of the passing ability.

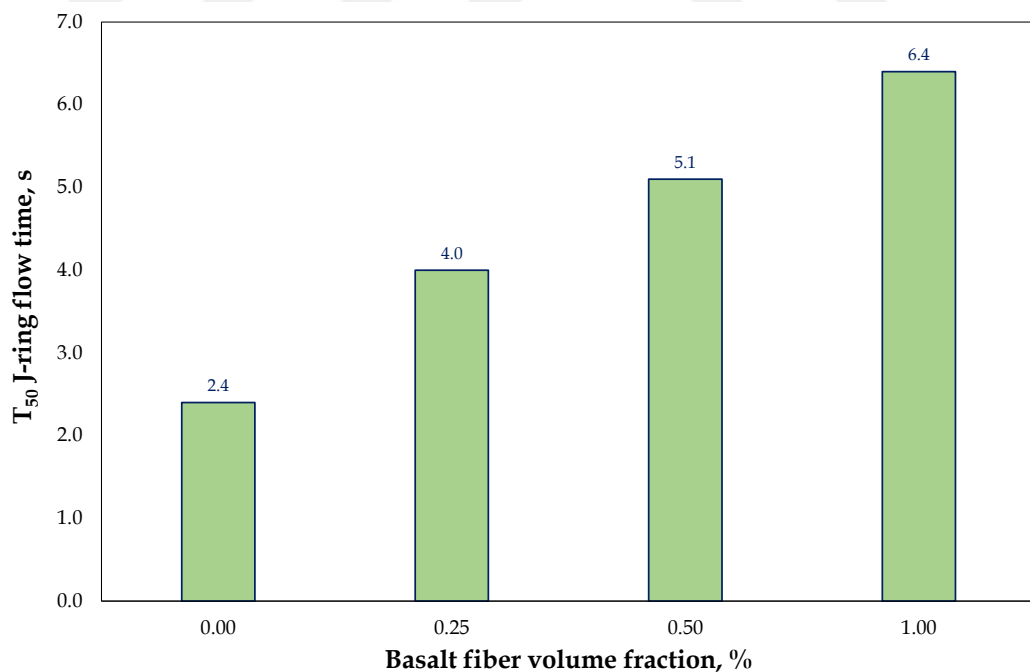


Figure 4.6. Variation in T₅₀ J-ring flow time of SCC mixtures concerning basalt fiber volume fraction

Figure 4.7 obviously shows the variation in both slump and J-ring flow time with respect to the basalt fiber volume fraction. The systematical increment in the flow times by the utilization of the basalt fiber in the concrete production can be examined in this figure. The figure also reveal the robustness and reliability of the both tests conducted in this study. Namely, the test supports the results achieved by other test.

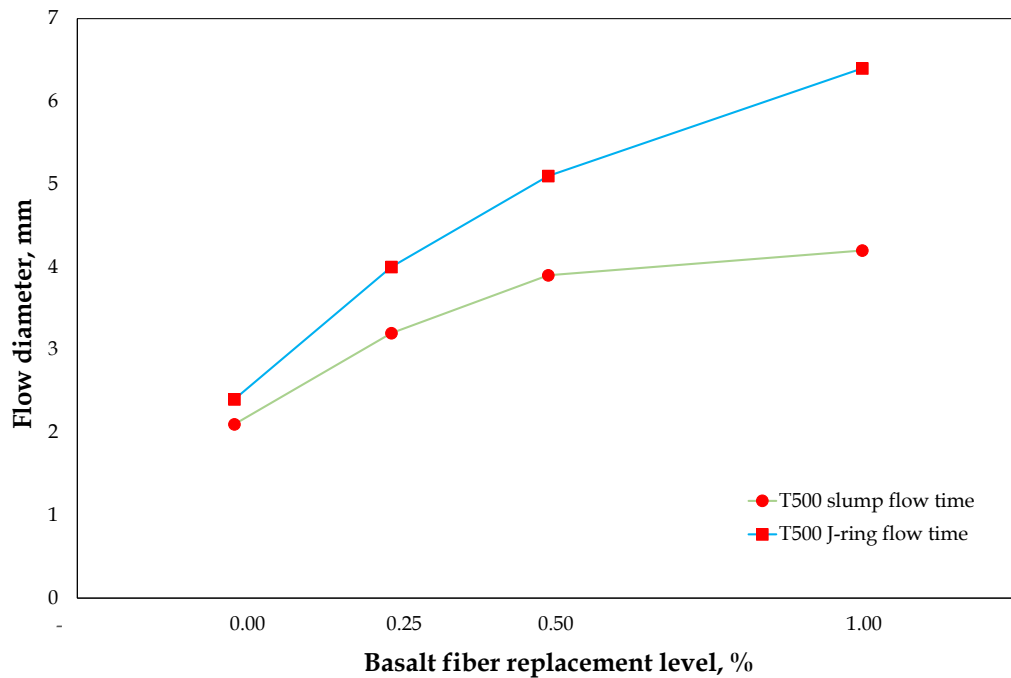


Figure 4.7. T₅₀ slump and J-ring flow time values versus basalt fiber volume fraction

4.1.5 V-funnel flow time

The T₅₀ slump flow and V-funnel flow times are both used to describe the indirect viscosity of the SCC mixtures. For this reason, the results of both test should support each other. When the results achieved in this study were investigated, it can be clearly seen the delaying in the V-funnel flow time by the increasing of the basalt fiber volume fraction. The variation in the V-funnel flow time of the SCC mixtures produced in this study versus the basalt fiber volume fraction has been shown in Figure 4.8. The plain SCC mixture, namely the mixture without basalt fiber, and the SCC mixture produced with basalt fiber volume fraction of 0.25% have the V-funnel flow time of 6.0 and 7.4 s. According to these V-funnel flow time values, these two SCC mixtures can be regarded in the viscosity class of VF1 according to the EFNARC (2005) specifications. However, the SCC mixtures manufactured with the basalt fiber volume fraction more than 0.25% can be classified in the viscosity class

of VF2 according to the EFNARC (2005) specifications. The use of basalt fiber more than 0.25% volume fraction changed not only the flowing class but also the viscosity class.

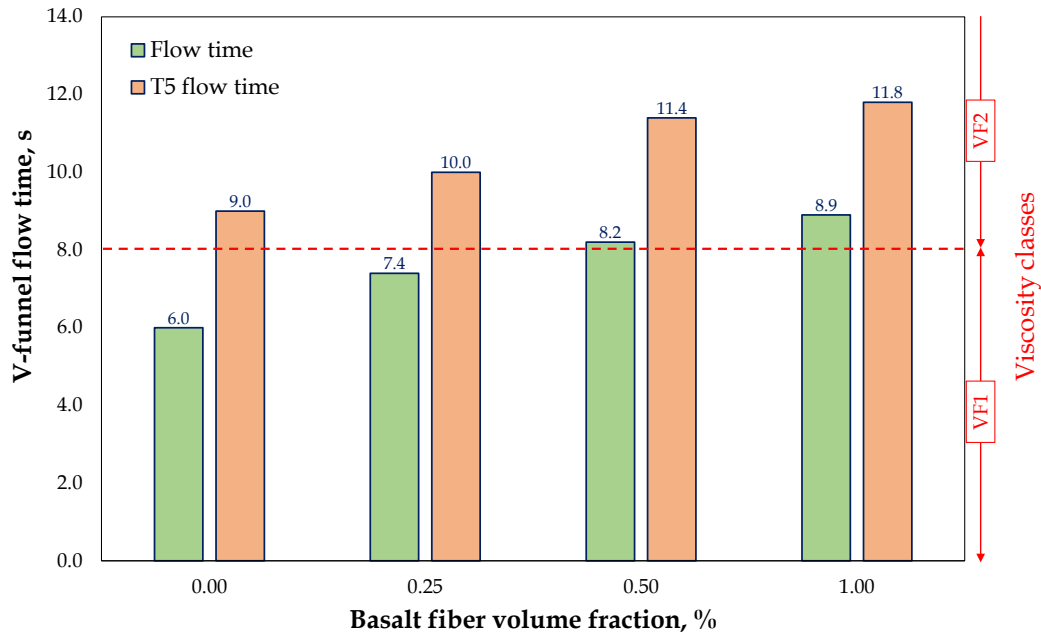


Figure 4.8. Variation in V-funnel flow time of SCC mixtures concerning basalt fiber volume fraction

Besides, the V-funnel flow time after keeping the fresh SCC in the funnel for 5 minute was also measured to examine the segregation in the mixture. The results achieved from this test were also presented in Figure 4.4. The basalt fiber utilization also caused retardation in the V-funnel T5 flow time. The difference between the V-funnel flow time and T5 flow time indicated that there is segregation in the SCC mixtures produced in this study since the difference between two flow times is about 3 s in all mixtures.

4.1.6 L-box height ratio

The passing ability class of the SCC mixtures manufactured in this study was determined regarding the L-box height ratio that was performed according to the specifications provided in the EFNARC (2005) committee. The results achieved from this test have been graphically presented in Figure 4.9. It can be easily seen from the figure that the plain concrete, without fiber, has the L-box height ratio of

0.88 and the using of basalt fiber in the concrete production caused systematical reduction in the L-box height ratio. Besides, the results indicated that all SCC mixtures can be regarded in the passing ability class of PA2 except the SCC mixture produced with basalt fiber of 1.0% volume fraction. Although the mixture produced with fiber volume fraction of 1.0% is grouped at the out of passing ability class, its L-box height ratio is 0.78.

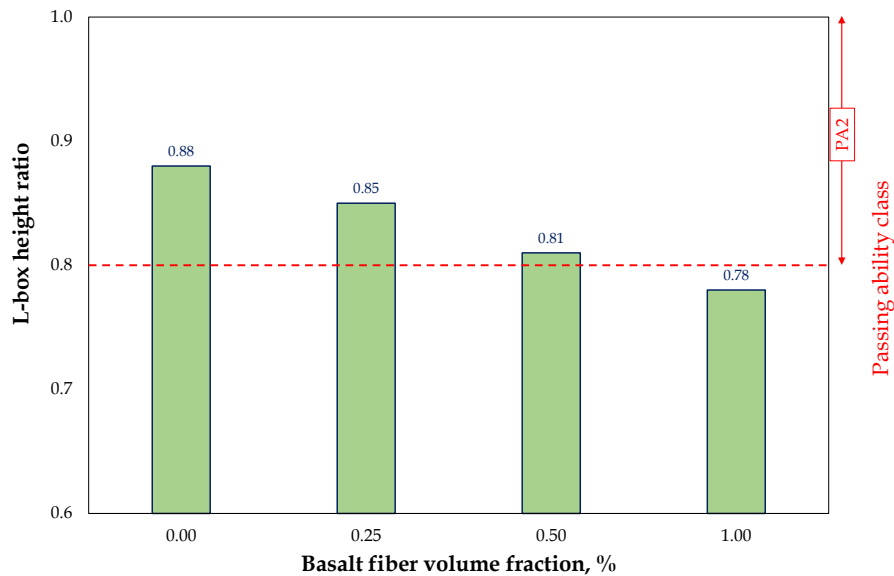


Figure 4.9. Variation in L-box height ratio of SCC mixtures concerning basalt fiber volume fraction

4.1.7 J-ring height difference

J-ring height difference, which is the difference between the highest and lowest concrete levels after the slump cone was removed and the SCC flowed, was measured to indicate the passing ability characteristics of the SCC mixtures manufactured in this study. The test results in accordance with basalt fiber volume fraction have been graphically presented in Figure 4.10. The results indicated that the utilization of the basalt fiber caused the decreasing of the passing ability performance of the concrete. The highest J-ring height difference was measured in the SCC mixture including 1.00% basalt fiber while the lowest value was achieved in the plain SCC mixture. For this reason, it can be concluded that the addition of the basalt fiber and increasing its content causes certain decreasing levels in the flowing, filling, and passing ability of the SCC mixtures. However, visual observation of the

slump and J-ring flow tests revealed that using basalt fiber in the SCC production made the concrete more cohesive that means better segregation and bleeding resistance characteristics.

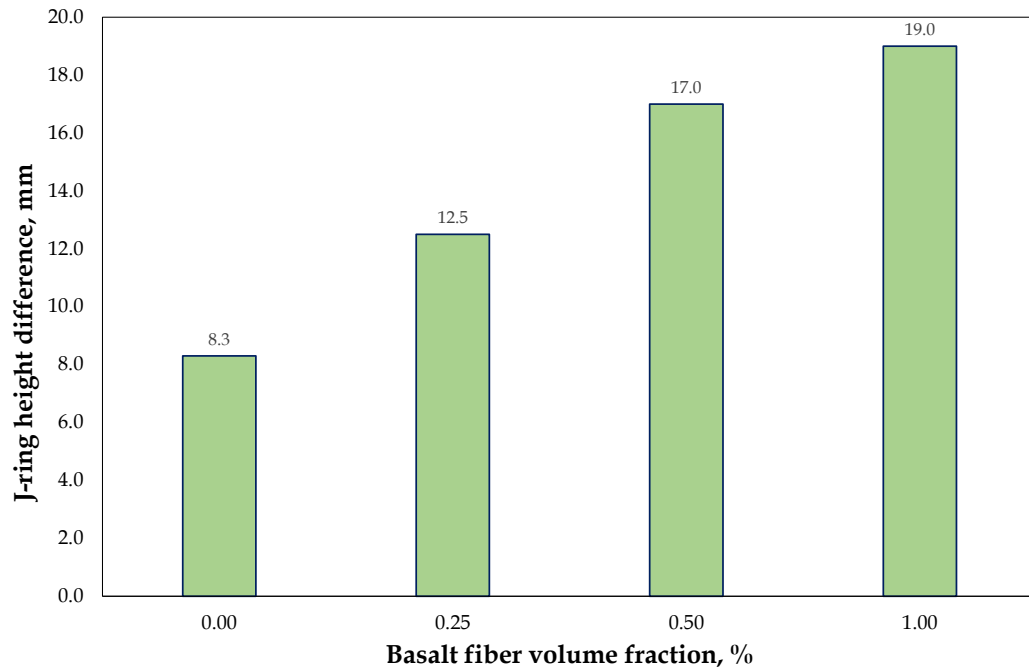


Figure 4.10. Variation in J-ring height difference of SCC mixtures concerning basalt fiber volume fraction

4.2 Mechanical tests

4.2.1 Compressive strength

Variation in 7-day and 28-day compressive strengths of the SCC mixtures with respect to basalt fiber volume fraction has been shown in Figure 4.11. The results revealed that the 7-day compressive strength values of the SCC mixtures are about $75\pm 5\%$ of the 28-day compressive strength values. In addition, it was observed that the basalt fiber addition to the SCC decreased the compressive strength values at both ages. The similar effect of fiber on the compressive strength of the concrete was reported by researchers (Borhan, 2013; Dias and Thaumaturgo, 2005; Jun and Ye, 2010; Li et al, 2004). However, in the literature, there are some studies, which found the exact opposite results of the aforementioned findings that the compressive strength of concrete was increased by fiber addition (Algin and Ozen, 2018; Arslan, 2016; Dong et al., 2017; Jiang et al., 2014; Kizilkanat et al., 2015; Sivakumar and

Santhanam, 2007). Therefore, it is hard to state any certain conclusion about the influence of microfibers on the compressive strength of concrete.

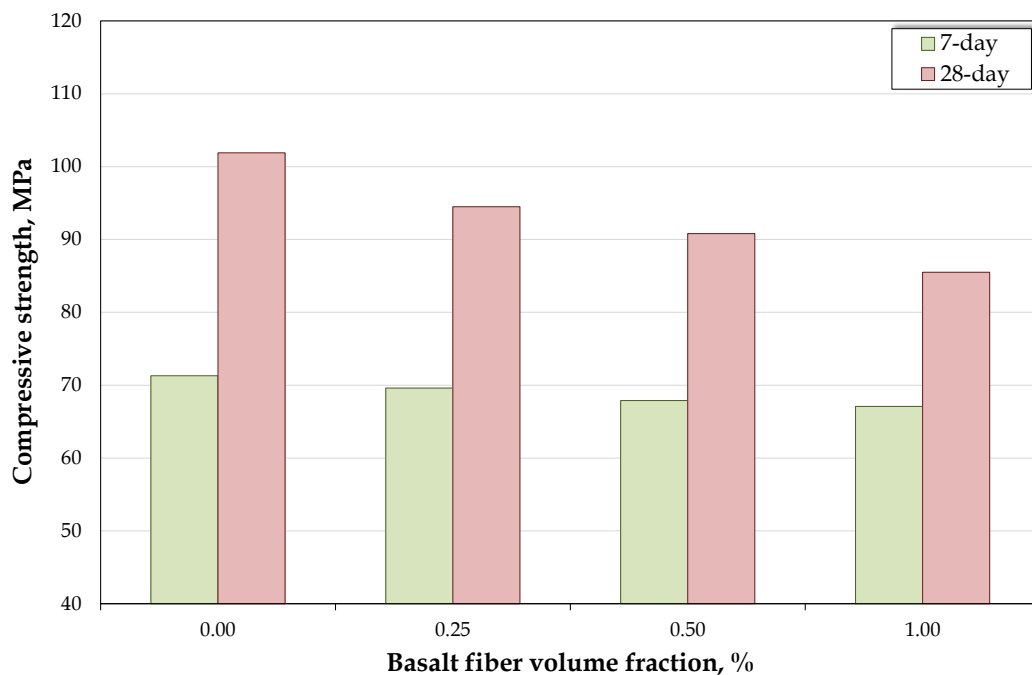


Figure 4.11. 7-day and 28-day compressive strength values of SCC mixtures versus basalt fiber volume fraction

The 7-day compressive strength values of the SCC mixtures produced in this study varied between 67 and 72 MPa while the 28-day compressive strength values were between 85 and 102 MPa. When Figure 4.11 was seen, it could be easily seen that the highest compressive strength values were procured in the plain SCC mixtures at both ages. The reduction percentages in the 7-day compressive strength due to basalt fiber addition were about 2.4, 4.8, and 5.9% for the basalt fiber volume fraction values of 0.25, 0.50, and 1.00%, respectively, whereas the decreasing rate in the 28-day compressive strength by the basalt fiber utilization were about 7.3, 10.9, and 16.1% for the basalt fiber volume fraction values of 0.25, 0.50, and 1.00%, respectively.

In addition to the compressive strengths tested at different ages, the compressive strengths at different temperature exposure were also tested during the experimental program of the current study. Five different temperature levels of ambient, 200, 300, 400, and 500 °C were designated to apply to the cylindrical SCC specimens. The change in compressive strength of SCC mixtures with respect to basalt fiber volume

fraction and temperature has been demonstrated in Figure 4.12. The 28-day specimens were exposed to these temperature levels for 3 hours and then, the compressive strength test was conducted. The results indicated that the compressive strength of the SCC mixtures were significantly affected by the temperature exposure. The systematical decreasing in the compressive strength was observed by the increasing of the temperature. The best compressive strength values were obtained at the ambient temperature. Especially, after 200 °C, there was a sudden dropping in the compressive strength as can be seen in Figure 4.12.

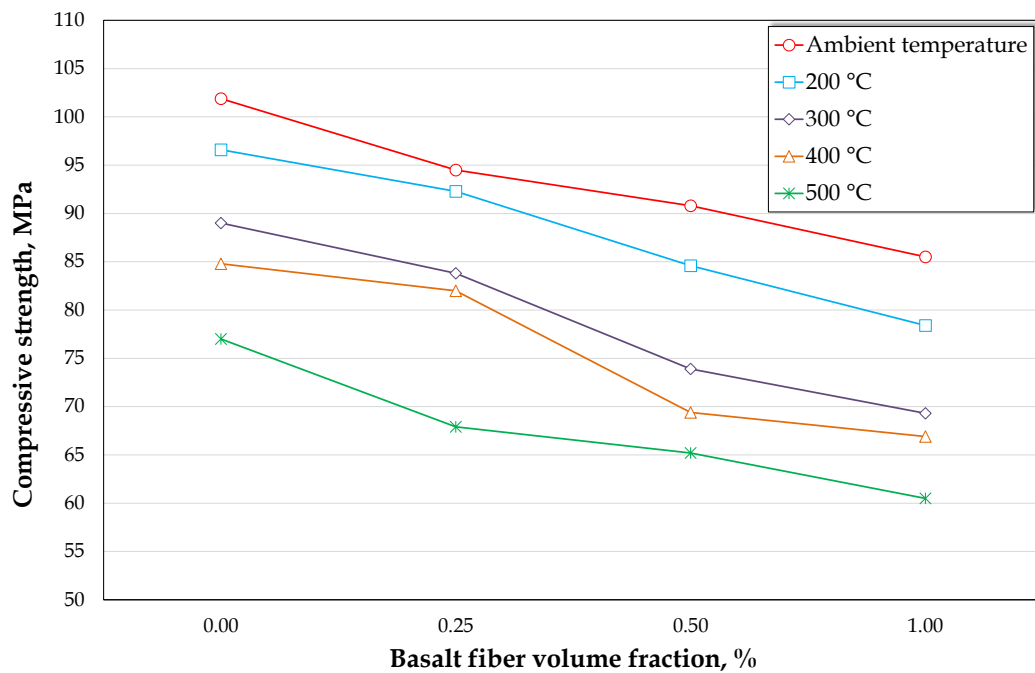
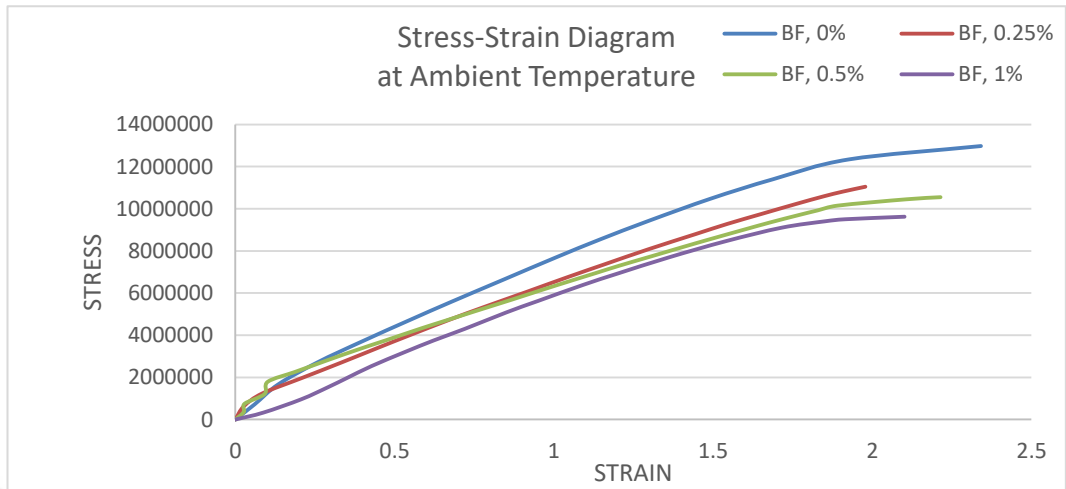


Figure 4.12. Variation in compressive strength of SCC mixtures concerning basalt fiber volume fraction and temperature

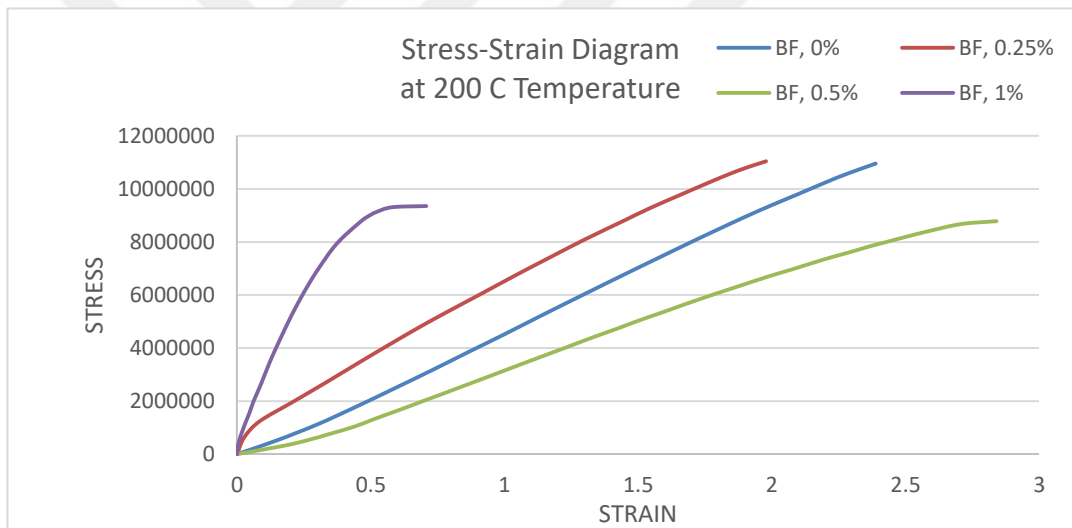
Apart from the compressive strength of the SCC mixtures, the compressive strength of the ordinary concrete that was employed in the production of the specimens of the slant shear strength specimens to represent the old concrete was also measured. The 7-day, 14-day, and 28-day compressive strength values of the ordinary concrete were 21.0, 26.5, and 30.5 MPa, respectively. The 28-day compressive strength value of 30.5 MPa provide the targeted compressive strength for the old concrete.

The behavior of concrete cylinder has been investigated by stress-strain relationships as given in Figure 4.13, it is obvious that the strain is decreased with introducing

basalt fibers. In general the strain reduction tendency is clearly observed with elevating in temperature.

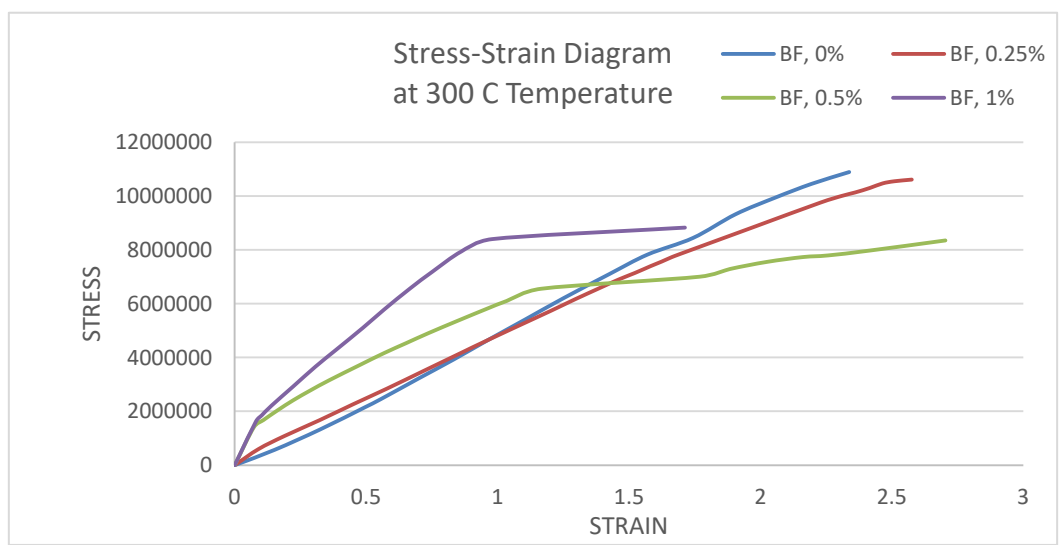


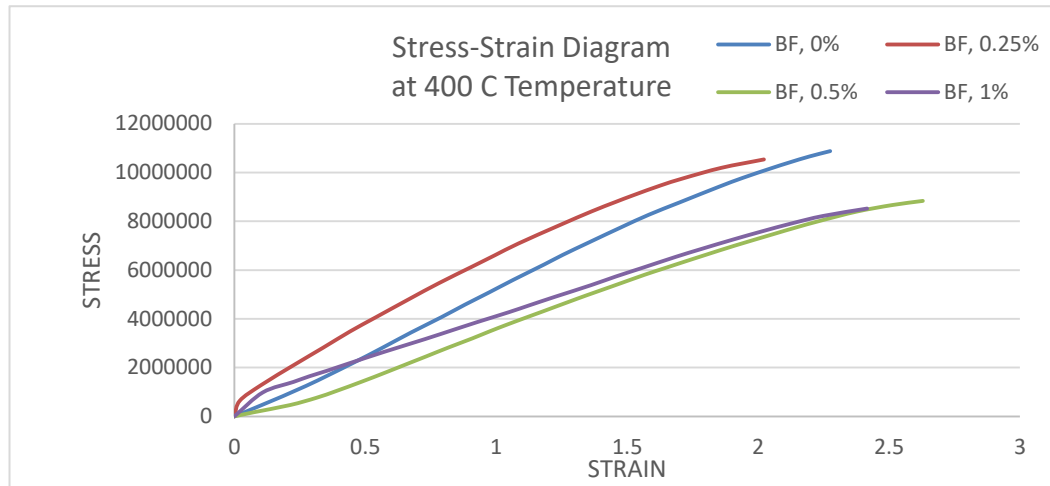
(a)



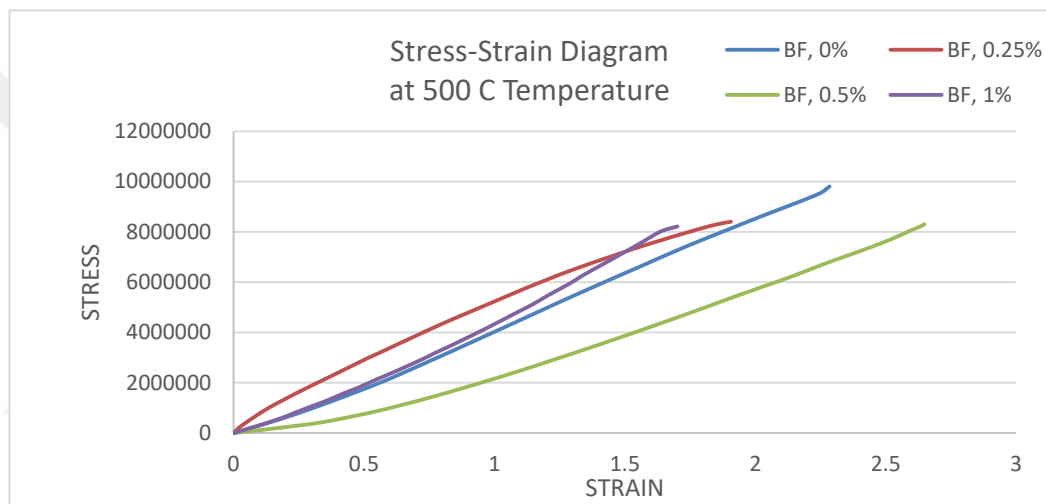
(b)

(c)





(d)



(e)

Figure 4.13. Stress-Strain curve of SCC mixtures concerning basalt fiber volume fraction and temperature: (a) At ambient Temperature, (b) At 200°C Temperature, (c) At 300°C Temperature, (d) At 400°C Temperature and (e) At 500°C Temperature

4.2.2 Elastic modulus

The effects of basalt fiber volume fraction and temperature on the elastic modulus of SCC mixtures have been indicated in Figure 4.14. The variation in the red line with circular mark given in this figure was given for the elastic modulus measured on the specimen at ambient temperature. The effect of basalt fiber on the SCC specimens can be obviously seen on the red line given in Figure 4.14. It can be easily said that no significant effect of basalt fiber on the elastic modulus was observed since there is a fluctuating in the elastic modulus with the increasing of the basalt fiber volume

fraction. Namely, there is no decreasing or increasing trend for elastic modulus concerning basalt fiber volume fraction increasing. However, it can be clearly seen that the elastic modulus of the mixtures decreased by the increasing of the temperature of the environment. The highest elastic modulus values were determined on the SCC specimens kept at the ambient temperature. The SCC mixture produced with the basalt fiber volume fraction of 0.50% has the elastic modulus of 36.4 GPa while that of 1.00% has the 31.5 GPa at the ambient temperature. These are the highest and lowest elastic modulus values for the SCC mixtures tested at ambient temperature. By increasing the temperature from the ambient to 500 °C caused the 36.6, 36.3%, 44.8, and 34.0% decrement in the elastic modulus of the SCC mixtures manufactured with the basalt fiber volume fractions of 0, 0.25, 0.50, and 1.00%, respectively.

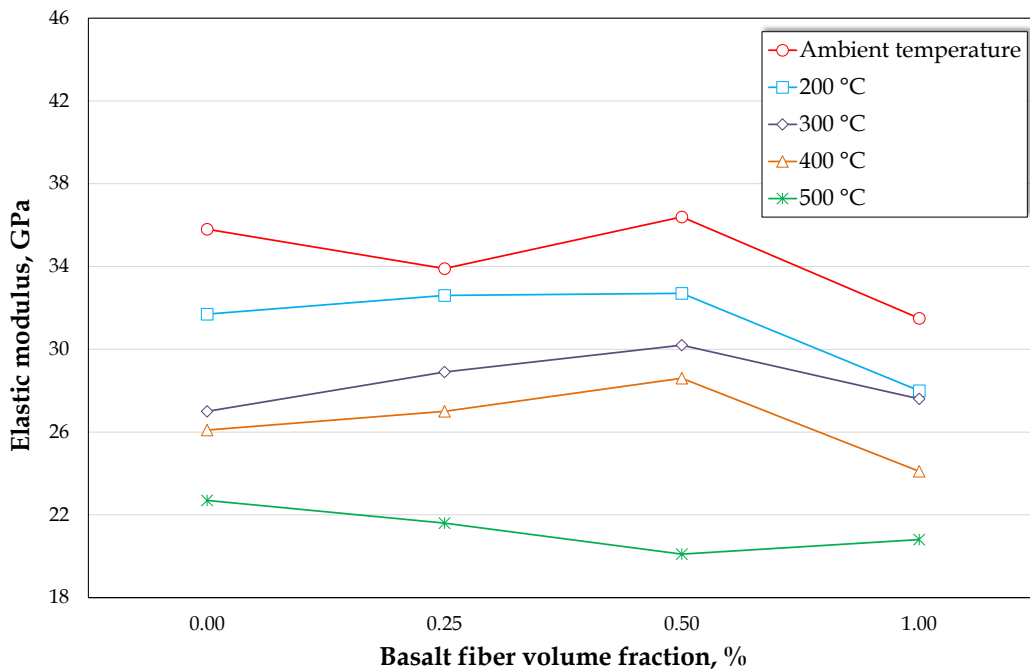


Figure 4.14. Variation in elastic modulus of SCC mixtures concerning basalt fiber volume fraction and temperature

4.2.3 Poisson's ratio

The Poisson's ratios measured for the SCC mixtures at ambient temperature have been submitted in Figure 4.15. as red line. Also, the Poisson's ratios measured at different temperature levels were given in this figure. The results indicated that slight impact of the temperature on the Poisson's ratio was observed. However, there was

an increasing trend for the SCC mixtures kept at ambient temperature up to the basalt fiber volume fraction of 0.50%, but, after this volume fraction, the decreasing in the Poisson's ratio was observed.

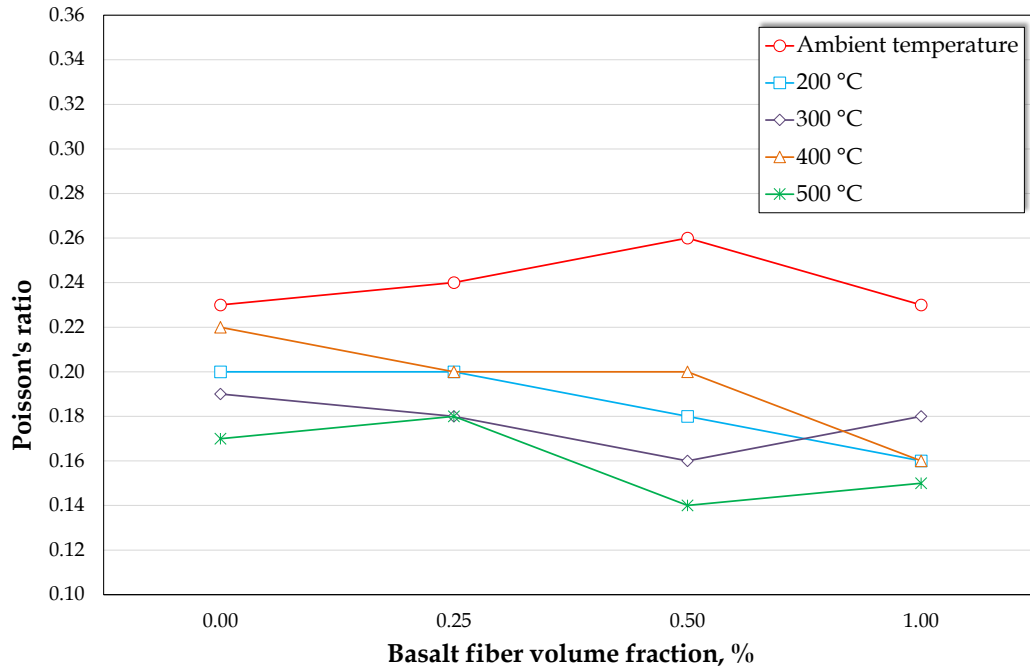


Figure 4.15. Variation in Poisson's ratio of SCC mixtures concerning basalt fiber volume fraction and temperature

4.2.4 Splitting tensile strength

Since the measurement of the direct tensile strength of the concrete is hard, generally, the tensile strength of the concrete is measured on the basis of either splitting tensile or flexural strength tests. In the current study, both, splitting tensile and flexural strength tests, were conducted to achieve supportive information about the influence of basalt fiber on the tensile behavior of the SCC mixtures. The results obtained from the splitting tensile strength test have been indicated in Figure 4.16. It was observed that the splitting tensile strength of the SCC mixtures increased by 0.25% basalt fiber addition, however, there was a decreasing trend in the splitting tensile strength after 0.25% basalt fiber volume fraction. It may be caused by the decreasing of the self compactibility of the concrete by higher basalt fiber incorporation. Another reason may be the coagulation of basalt fiber particles at higher volume fraction. At the ambient temperature level, the highest splitting tensile strength value of 7.32 MPa was achieved at the SCC mixture manufactured with

0.25% basalt fiber whilst the lowest value of 6.56 MPa was obtained at that produced with 1.00% basalt fiber. The basalt fiber having the particle with diameter in micro scale may be not well distributed in the cement matrix. So, the decreasing in the splitting tensile strength was measured after 0.25% volume fraction. In order to comprehend the tensile performance contribution of basalt fiber, the basalt fiber should be used more than 1.0% volume fraction.

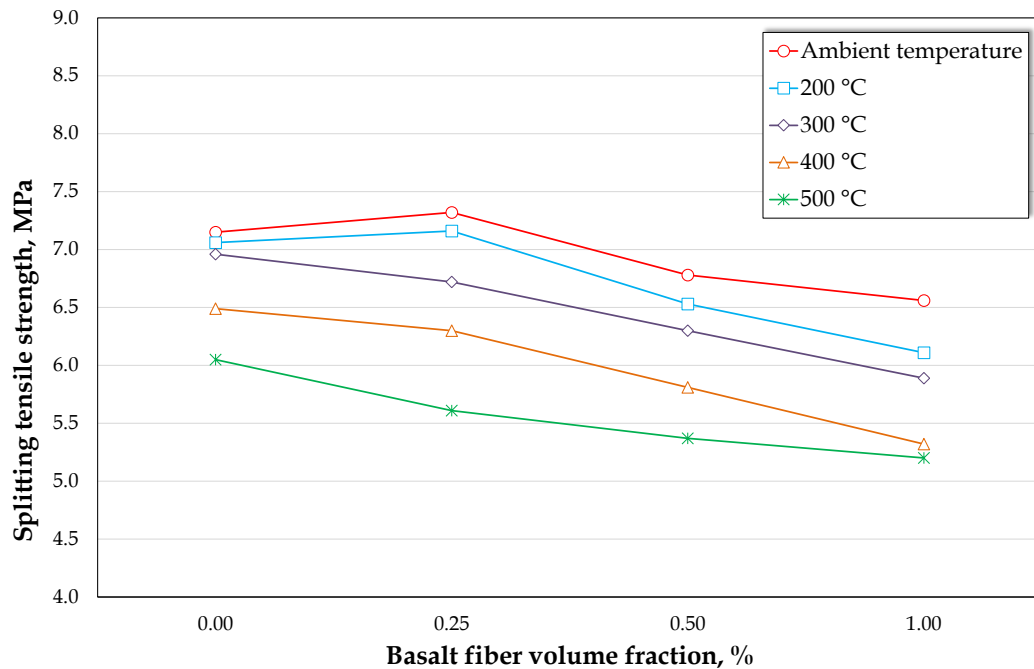


Figure 4.16. Variation in splitting tensile strength of SCC mixtures concerning basalt fiber volume fraction and temperature

In addition, when the effect of the temperature was investigated it would be clearly seen that the temperature adversely affected the splitting tensile strength. By increasing the temperature, a systematic reducing in the splitting tensile strength was observed. A sudden dropping in the splitting tensile strength at all basalt fiber volume fraction was seen especially after 300 °C. The splitting tensile strength values measured on the specimens exposed to 500 °C were 6.05, 5.61, 5.37, and 5.20 MPa for the SCC mixtures manufactured with the basalt fiber volume fraction of 0, 0.25, 0.50, and 1.00%, respectively. The reduction percentages in the splitting tensile strength were about 15.4, 23.4, 20.8, and 20.7% when the temperature was increased from ambient to 500 °C. The higher reduction rate may be related to the characteristics of basalt fiber. The temperature increase may have influenced the

basalt fiber inversely that resulted in a higher reduction rate of the splitting tensile strength of the SCC mixtures.

4.2.5 Flexural strength

The other test performed to evaluate the tensile behavior of the SCC mixtures is flexural strength test. The results obtained from this test regarding the basalt fiber volume fraction and temperature have been demonstrated in Figure 4.17. According to the test result, it can be expressed that basalt fiber utilization enhanced the flexural strength of the SCC. At the ambient temperature level, the highest flexural strength value of 8.91 MPa was attained in the SCC mixture manufactured with 1.00% basalt fiber whilst the lowest value of 8.24 MPa was procured in the plain SCC mixture. The flexural strength was increased as much as 8.1% when 1.00% basalt fiber was added. Besides, the worsening by the temperature exposure was also observed in the flexural strength. Since the flexural strength test is more similar to the direct tensile strength test, the tensile performance contributed by basalt fiber can be easily seen. The basalt fiber particles enhanced the cement paste of concrete under the flexural loads.

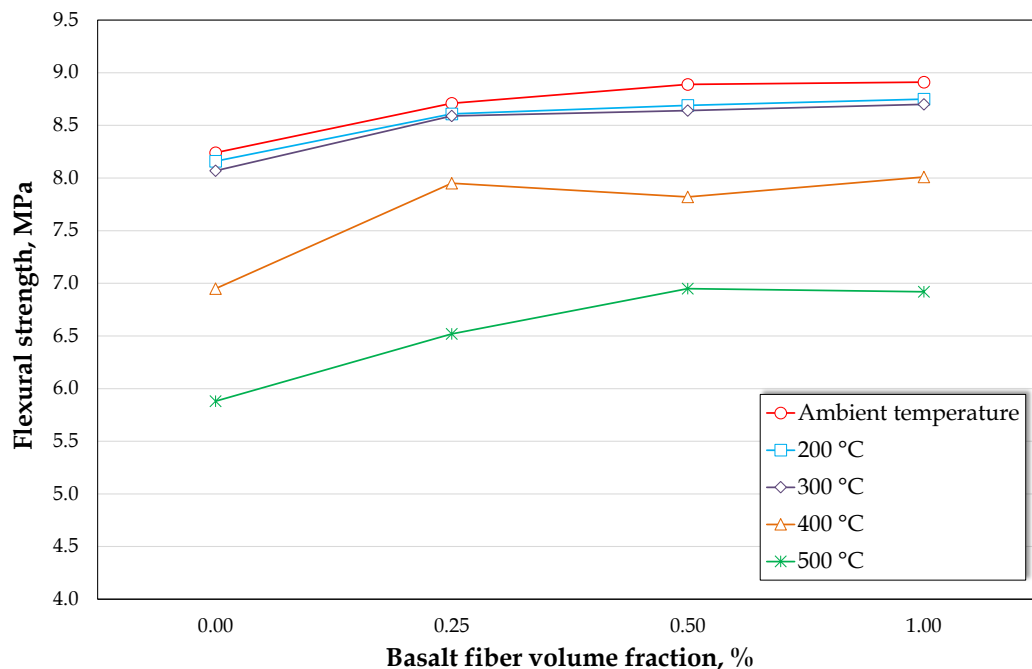


Figure 4.17. Variation in flexural strength of SCC mixtures concerning basalt fiber volume fraction and temperature

It was investigated that the flexural strength values at each fiber volume fraction were slightly decreased when the temperature was increased from ambient to 300 °C. However, a large reduction in the flexural strength was observed after 300 °C temperature exposure. The flexural strength values of the specimens exposed to 500 °C were 5.88, 6.52, 6.95, and 6.92 MPa for the SCC mixtures manufactured with the basalt fiber volume fraction of 0, 0.25, 0.50, and 1.00%, respectively. The reduction percentages in the flexural strength were about 28.6, 25.1, 21.8, and 22.3% when the temperature was increased from ambient to 500 °C.

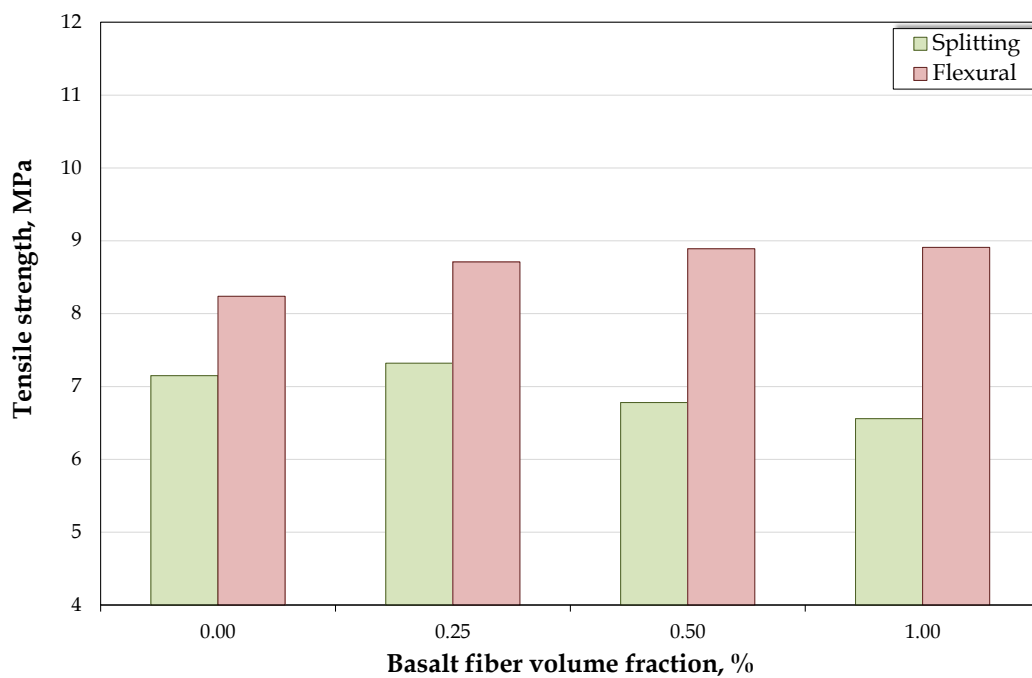


Figure 4.18. Splitting tensile and flexural strength values of SCC mixtures versus basalt fiber volume fraction

In order to express the relation between the splitting tensile and flexural strength of the SCC mixtures produced in this study, Figure 4.18 has been submitted. The splitting tensile and flexural strength values of the SCC mixtures at each basalt fiber content were comparatively indicated and it can be clearly comprehended that the flexural strength of the SCC mixtures, of which specimens were kept at the ambient temperature, is higher than the splitting tensile strength of the SCC mixtures. It is an expected finding that is well-known information about the relation between the splitting tensile and flexural strengths. Besides, when the results individually investigated, it can be seen that the increasing the basalt fiber volume fraction increased the tensile strength of SCC mixtures under flexural loads, however,

decreased the tensile strength of SCC mixtures under splitting loads. The main reason may be the difference between the tensile failures of both test methods. During the splitting tensile strength test, an axial load is applied to concrete that tries to split the concrete specimen, but, during the flexural strength test, a direct load that tries to bend the concrete specimen is applied. For this reason, the basalt fiber plays a role during the bending loads, yet, it can not play a role under a splitting load.

4.2.6 Slant shear strength

The slant shear strength values of the SCC mixtures combined with ordinary concrete that used to represent old concrete have been demonstrated in Figure 4.19. The casting surface between the old and new concretes were treated to improve the slant shear strength characteristic. Three different methods, of which photographic view was shown in Figure 3.5a, were used to make a surface treatment. The surface treatment methods applied in the current study are hole drilling, groove, and sand blasting. In addition to these surface treatment methods, in one series, the surface of the ordinary concrete was kept as casted, namely, no surface treatment was applied. The slant shear strength versus basalt fiber volume fraction for each surface textures can be seen in Figure 4.19.

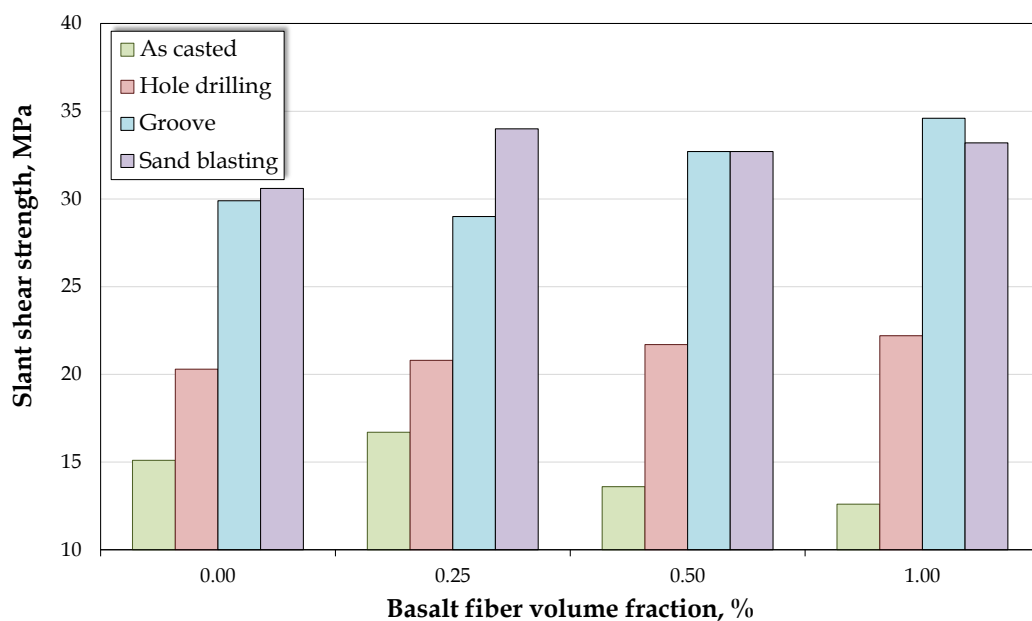
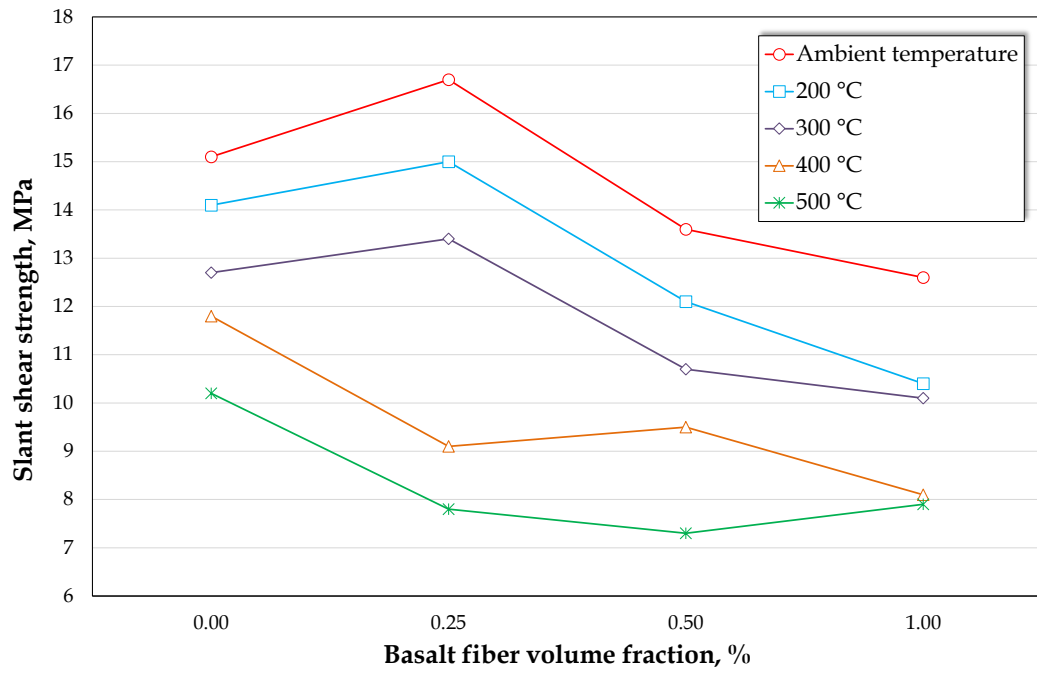


Figure 4.19. Slant shear strength values of SCC mixtures at ambient temperature versus basalt fiber volume fraction

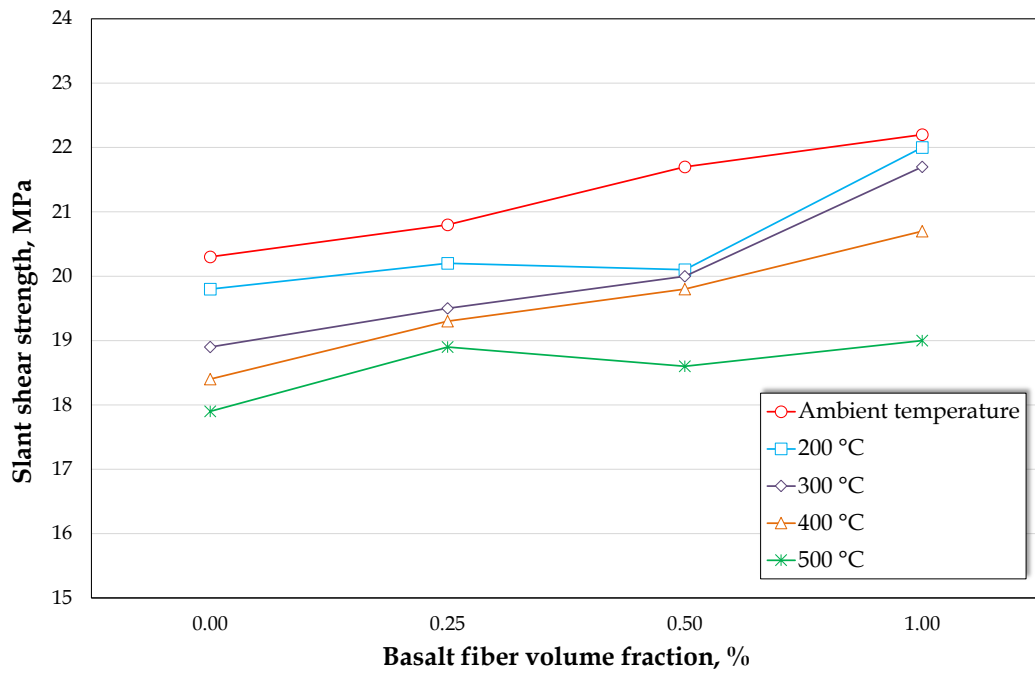
The lowest slant shear values were procured in the concretes, of which old concrete surfaces were not treated. Applying the surface treatment significantly enhanced the slant shear strength values. Besides, the SCC mixtures, which were employed to represent new concrete, produced with higher basalt fiber volume fraction had the lower slant shear strength values when no surface treatment was applied. But, the slant shear strength values were increased by the increasing the basalt fiber content when the surface treatment was applied to old concrete. The highest performance were observed in the groove and slant blasting surface treated specimens.

At the basalt fiber volume fraction of 0 and 0.25%, the slant shear strength values of the sand blasting surface treated specimens were higher than that of groove surface treated whereas at the basalt fiber volume fraction of 1.00%, the slant shear strength value of the groove surface treated specimens were higher than that of sand blasting surface treated. The slant shear strength at the basalt fiber volume fraction of 0.50% were equal to each other.

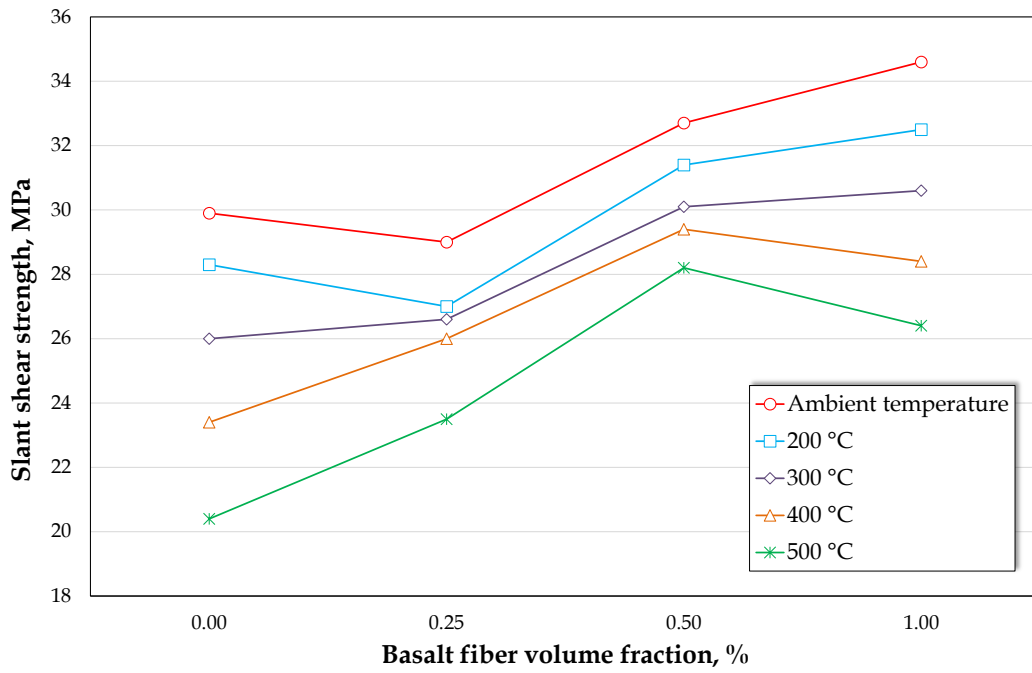
Additionally, the effect of the temperature on the slant shear strength was also experimentally investigated. The results achieved for each surface treatment method have been individually presented in Figures 4.20a-d. The slant shear strength change of the as casted specimens with respect to the temperature varying and basalt fiber volume fraction has been indicated in Figure 4.20a whereas that of drilled, grooved, and sand blasted specimens have been shown in Figures 4.20b, 4.20c, and 4.20d, respectively.



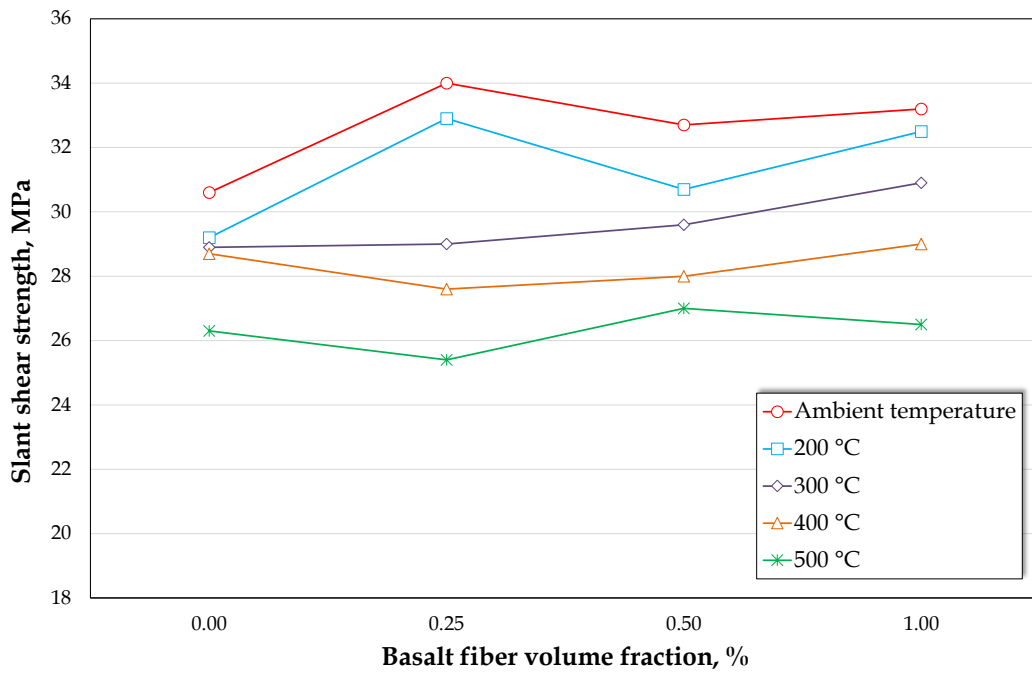
(a)



(b)



(c)



(d)

Figure 4.20. Variation in slant strength of SCC mixtures concerning basalt fiber volume fraction and temperature: (a) as casted, (b) hole drilling, (c) groove, and (d) sand blast

By increasing the temperature from ambient to 500 °C, it was observed that the slant shear strength values for as casted surfaced-specimens decreased about 32.5, 53.3,

46.3, and 37.3%. When the reduction rate in the other types of surface treatment was investigated it would be seen that the highest reduction rate belongs to as casted surfaced-specimens. Namely, it means that the specimens having no surface treatment were influenced by temperature more than the specimens having a surface treatment. The results also showed that the slant shear strengths of especially groove surfaced-specimens have been treated not only by surface treatment method but also the basalt fiber utilization. The SCC mixtures with basalt fiber filled the groove on the old concrete and an interlocking between old and new concretes was occurred. Therefore, it could be stated that the basalt fiber increased the resistance of the interlocking either. The similar effect of the basalt fiber could be seen in the drilled surfaced-specimens. But, it is not good as much as the groove surfaced-specimens. Possibly, if the greater holes were opened on the old concrete surface, the interlocking occurrence would be much more.

Apart from the slant shear strength test, it was also measured the axial strength of the ordinary concrete that represented the old concrete. The results achieved from this test with respect to the change of the temperature have been demonstrated in Figure 4.21. It was seen that the highest axial strength value of 26.1 MPa was measured at the ambient temperature. Increasing the temperature from the ambient to 500 °C resulted in the decreasing of the axial strength of the ordinary strength as much as 16.1% while the decreasing rate due to temperature increasing from ambient to 200, 300, and 400 °C were about 6.1, 12.3, and 13.4%, respectively. When the results of the axial strength test and slant shear strength test were compared it would be seen that the slant shear strength value of the groove and sand blasting surfaced-specimens were higher than the axial strength of the ordinary concrete. However, that of the as casted and hole drilled surfaced-specimens were less than the axial strength of the ordinary concrete.

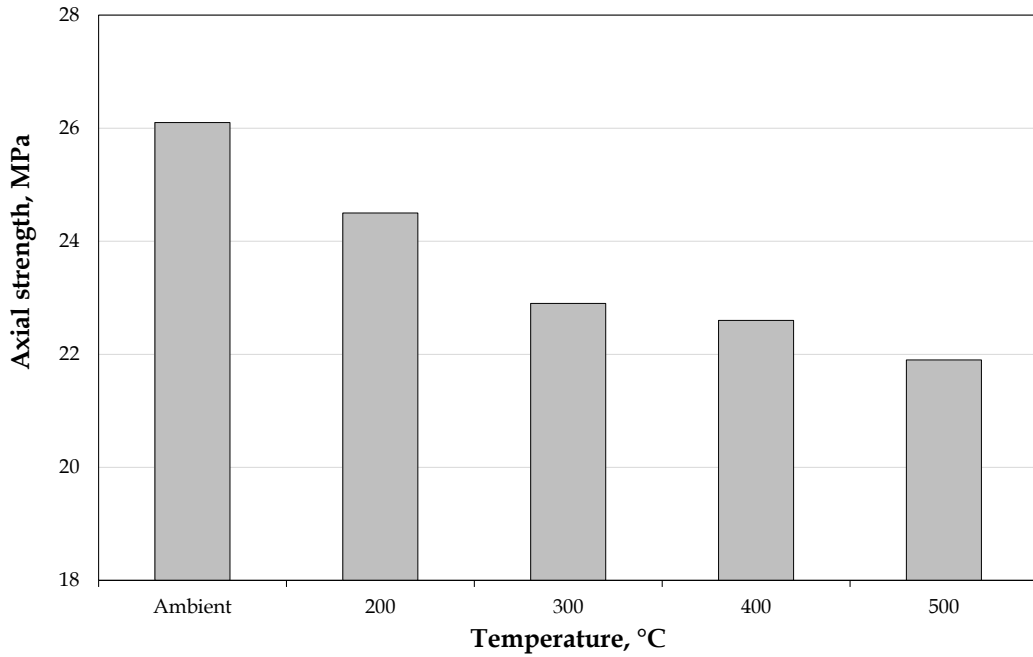


Figure 4.21. Axial strengths of old concrete versus temperature

Apart from the loading test of slant shear strength test, the visual observation on the testing specimen was also carried out. According to visual observation, four failure mode were designated for slant shear strength test specimens. The failure mode for each specimen has been individually presented in Table 4.1. In addition, the failure modes observed on these specimens have been photographically presented in Figure 4.22. The determined failure modes in the current study were the interfacial failure at the inclined surface between ordinary concrete and SCC mixture (IF abbreviation was used), the compression failure in the overlay layer (OL abbreviation) and the substrate layer (SL abbreviation), and columnar failure (CF abbreviation) in the hybrid concrete prism. In order to easily discernment, the failure modes were presented with different color in Table 4.1.

Table 4.1. Failure mode of slant shear strength test specimens

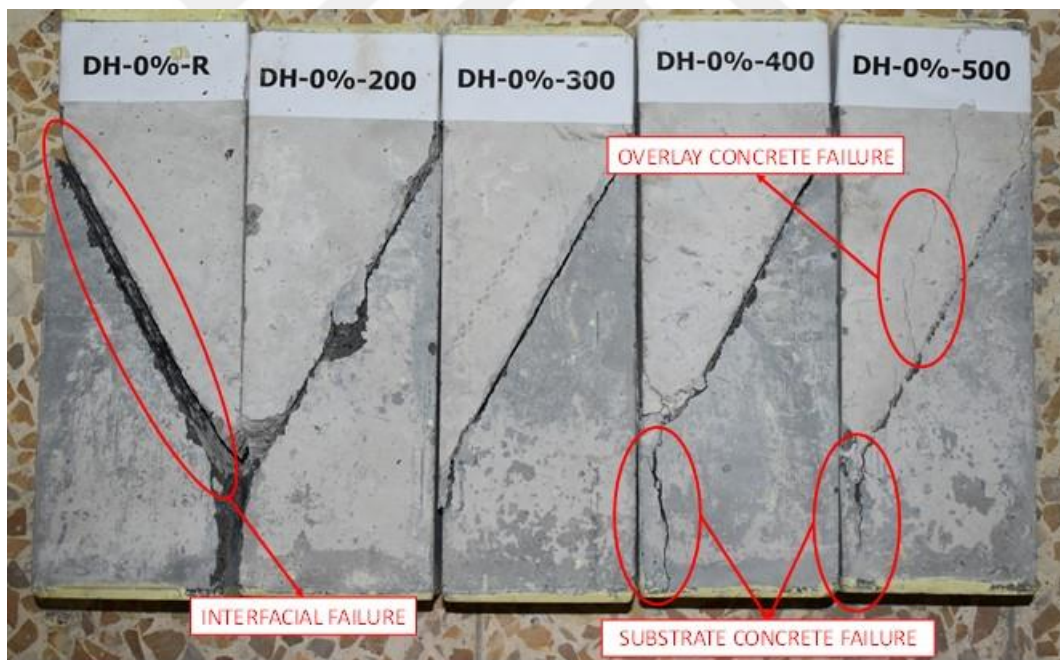
Surface treatment type	Temperature	Mix ID			
		SCC	SCC25	SCC50	SCC100
As casted	25				
	200	IF	IF	IF	IF
	300	OL	OL	OL SL	OL SL
	400				

	500				
Hole drilled	25				
	200	IF	IF	IF	IF
	300	OL	OL	OL	OL
	400	SL	SL	SL	SL
	500				
Grooved	25	OL	SL	OL-SL	OL-SL-CF
	200	SL		IF-OL-SL	
	300	OL-SL-CF	SL		CF
	400		CF	SL	SL
	500	SL	IF-OL-SL	SL	SL-CF
Sand blasted	25	SL-CF	IF-OL-SL	IF	IF-OL
	200			OL	
	300	OL	OL-CF	SL	OL-SL-CF
	400	SL	SL-CF	OL-SL	SL
	500	CF	SL	SL	IF-OL-SL

When Table 4.1 was investigated, it would be clearly comprehended that the specimens were failed due to the failing of the interfacial between the concrete surfaces and the failing of overlay concrete (SCC) in the mixtures without treatment. After the basalt fiber volume fraction of 0.25%, the failing of substrate concrete (ordinary concrete) was also observed. However, all specimens, on which hole drilling treatment was applied, were failed due to failing of the interfacial surface and overlay and substrate concretes.



(a)



(b)

Figure 4.22. Photographically indication of typical failure modes occurring on slant shear strength test specimens: (a) before test and (b) after test

The effect of temperature and basalt fiber volume fraction can be easily seen when the failure modes of the specimens, on which grooving and sand blasting treatments were applied, were investigated. When the table was considered, it can be obviously

seen that the failing of substrate and overlay concretes are generally observed failure mode in each treatment group. Especially, the failing of substrate concrete was observed when the surface between ordinary and self-compacting concretes were treated by the grooving and sand blasting methods. The lowest observed failure mode was columnar failure. Moreover, to indicate the failure modes on the testing specimens, Figure 4.22 has been presented. The aforementioned failure modes can be easily distinguished by observing the photos submitted in Figure 4.22.

4.3 Permeability tests

4.3.1 Sorptivity index

In order to show the effect of the basalt fiber utilization and content in the SCC production on the permeability properties, the sorptivity index of the SCC mixtures manufactured in this study were determined. According to the results achieved from this test, it can be said that the lower the sorptivity index value, the lower the capillary water absorption value. The sorptivity index values, which were given as sorptivity coefficients, versus basalt fiber volume fraction have been submitted in Figure 4.23. The results indicated that the greatest capillary water suction was observed in the plain SCC mixture, since its sorptivity coefficient value is the highest. The sorptivity coefficient values ranging between 0.055 and 0.090 $\text{mm}/\text{min}^{0.5}$ were measured in the current study. The lowest sorptivity index values of 0.055 $\text{mm}/\text{min}^{0.5}$ were measured in the SCC mixtures manufactured with basalt fiber volume fractions of 0.25 and 1.00%. The lowest sorptivity index values were determined for the SCC mixtures including basalt fiber.

The test result indicated that the rising of the basalt fiber volume fraction from 0.25 to 0.50% resulted in the increasing of the sorptivity index value, namely resulted in the increasing of the capillary water suction. However, the sorptivity index value decreased by the rising of the basalt fiber volume fraction from 0.50 to 1.00%. In this manner, although the sorptivity index value increased by the rising of the basalt fiber volume fraction from 0.25 to 0.50%, the sorptivity index value for the SCC mixture manufactured with basalt fiber volume fraction of 0.50% was still less than that of the plain SCC mixture. The reason behind the decreasing of the sorptivity index values by the basalt fiber addition may be due to the void filling ability of the basalt

fiber since the particle sizes of basalt fiber are in the micro-scale. However, utilization the basalt fiber more than volume fraction of 0.25% resulted in increasing of sorptivity coefficient. It may be due to the coagulation of basalf fiber particles. In order to better understanding of the effect of basalt fiber on sorptivity characteristics of both conventional and self-compacting concretes, a further study is required with incorporating the basalt fiber more than 1.0% volume fraction.

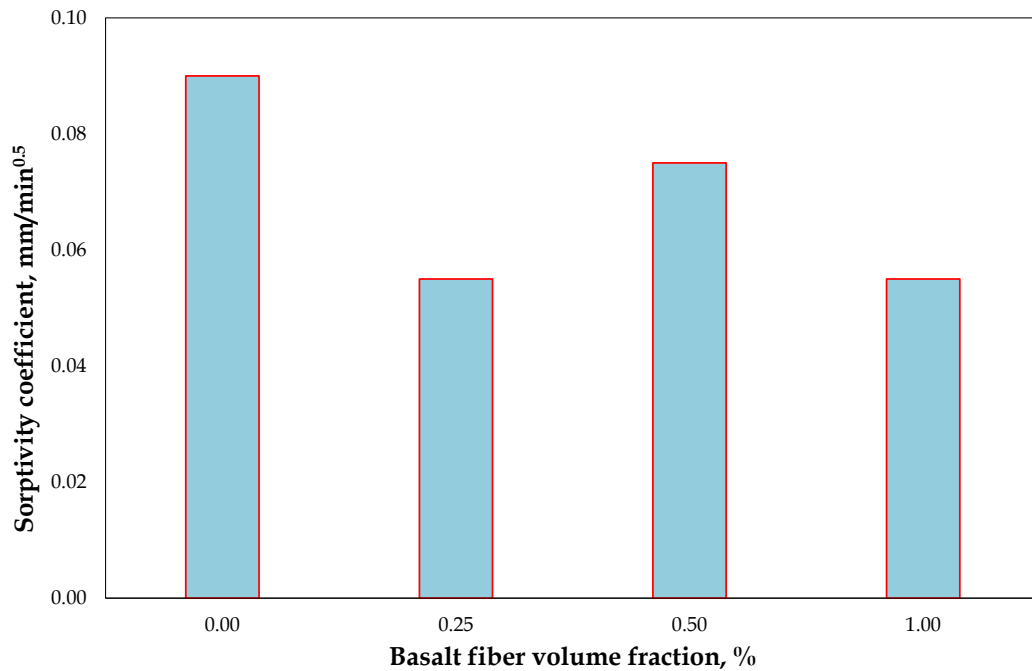


Figure 4.23. Sorptivity coefficients versus basalt fiber volume fraction

4.3.2 Water penetration depth

The water penetration depth values versus basalt fiber volume fraction have been graphically presented in Figure 4.24. The results achieved from this test were between 9.0 and 13.6 mm. The lowest water penetration depth value of 9.0 mm was measured in the plain SCC mixture while the highest water penetration depth value of 13.6 mm was measured in the SCC mixture manufactured with basalt fiber volume fraction of 0.50%.

The basalt fiber addition to the SCC mixture resulted in lower water penetration depth for the volume fraction of 0.25%, but then, it caused the increase of the water penetration depth. The basalt fiber utilization at the content of 0.25% resulted in the decreasing of the water penetration depth about 6% whereas the basalt fiber

utilization at the contents of 0.50 and 1.00% caused the increasing of the water penetration depth as much as 54.7 and 15.0%, respectively.

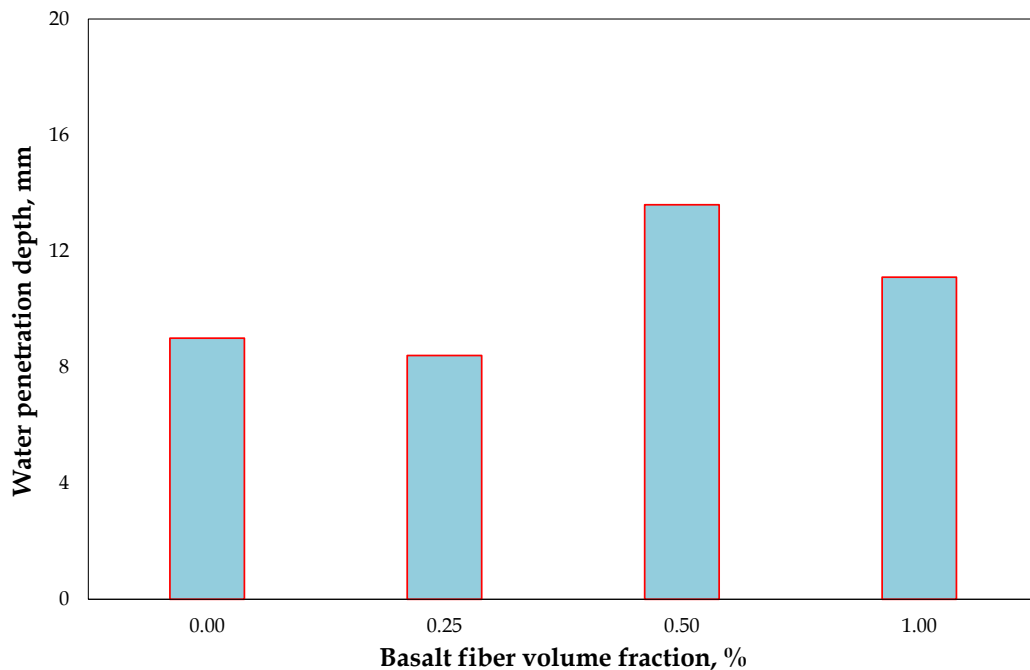


Figure 4.24. Water penetration depth versus basalt fiber volume fraction

4.3.3 Resistance to chloride ion penetration

The rapid chloride permeability test was conducted to state the resistance of the SCC mixtures without and with basalt fiber to chloride ion penetration. Figure 4.25 indicates the change in the resistance of the SCC mixtures to chloride ion penetration in terms of total charge passed versus basalt fiber volume fraction. The total charge passed values changing between 29 and 41 C were achieved during the performing of this test. The highest total charge passed value that means the lowest resistance to chloride ion penetration was measured in the plain SCC mixture whereas the lowest total charge passed value of 41 C was observed in the SCC mixture produced with the basalt fiber volume fraction of 0.25%. After this basalt fiber volume fraction value, the total charge passed values of the SCC mixtures indicated increasing trend. But their total charge passed values are less than that of the plain SCC mixture. Algin and Ozen (2018) also observed a similar effect of the basalt fiber on the chloride ion penetrability of the SCC mixtures. Besides, it was stated that the basalt fiber particles play a blocking role through the pores in the cement paste and therefore, the permeability of the concrete decreases (Algin and Ozen, 2018; Long et al. 2016).

Table 4.2. Total charge passed according to ASTM C1202 (2019)

Total charge passed (Coulombs)	Chloride ion penetrability
> 4000	High
2000 – 4000	Moderate
1000 – 2000	Low
100 – 1000	Very low
< 100	Negligible

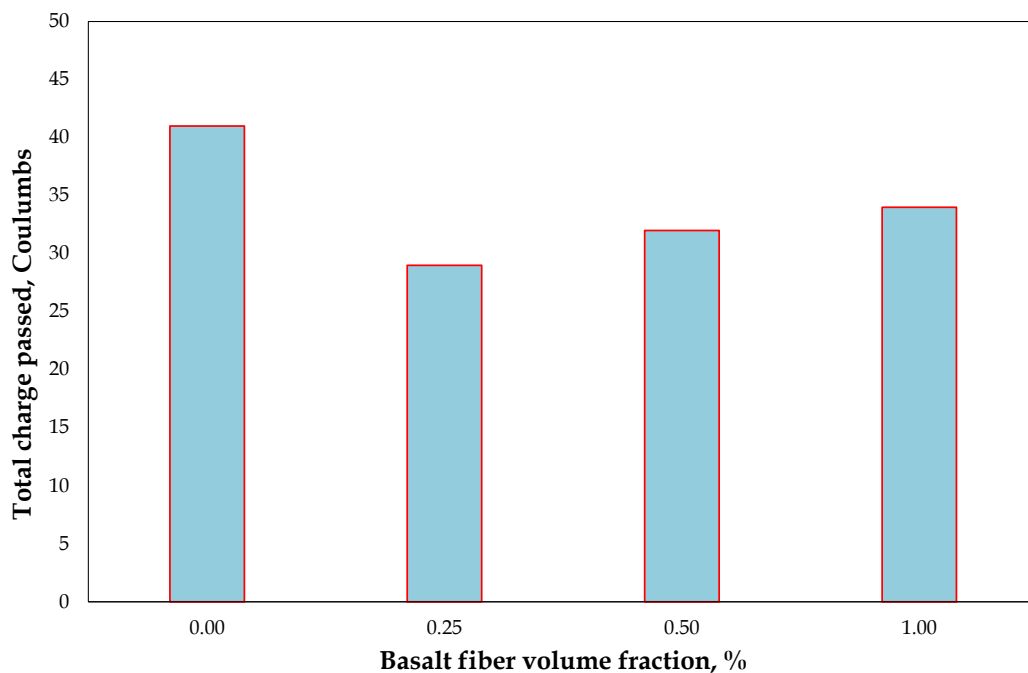


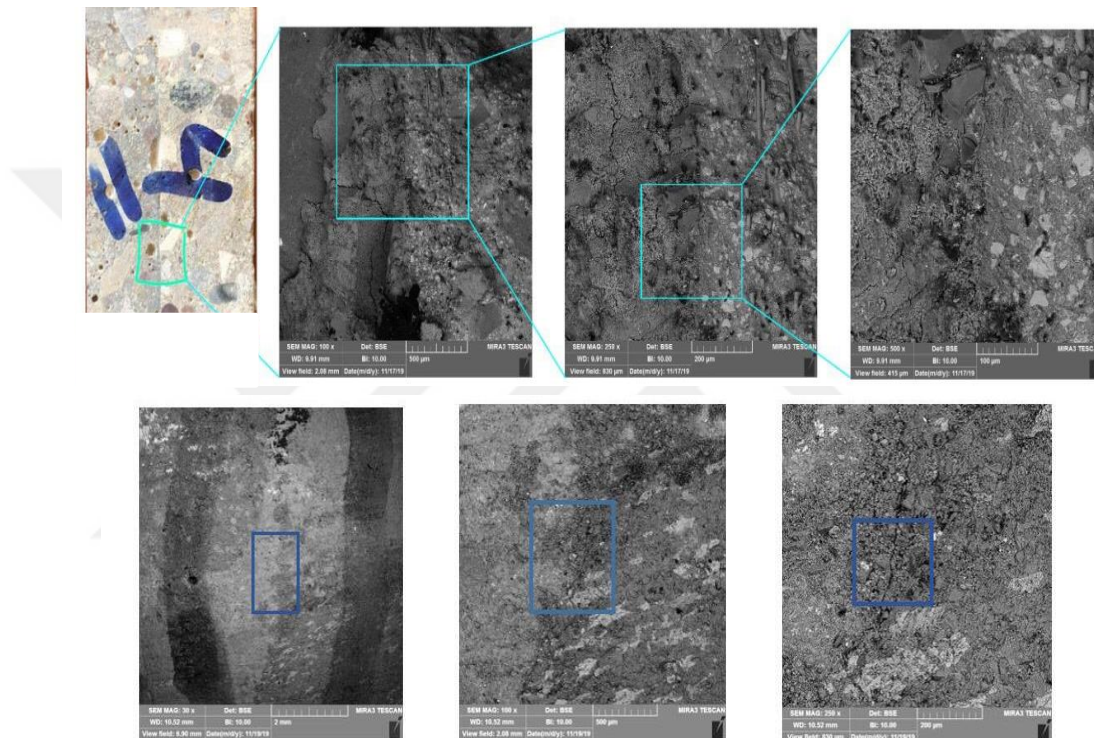
Figure 4.25. Effect of basalt fiber volume fraction on chloride permeability of SCC mixtures in terms of total charge passed

According to ASTM C1202, there is a classification for the concretes regarding the total charge passed values as tabulated in Table 4.2. When the SCC mixtures produced in this study are considered, it can be said that their chloride ion penetrability is negligible since all values measured in this study are less than 100 C. However, the effect of basalt fiber on chloride ion penetration resistance cannot be easily observed according to these results. Because the control mixture, namely plain SCC mixture, has negligible chloride ion permeability. Basalt fiber utilization firstly decreased the chloride ion permeability of SCC mixture since it consists of particles with diameter in micro scale by which the basalt fiber can fill the gaps in the SCC mixture. However, maybe due to the coagulation of basalt fiber particle, after 0.25%

volume fraction, there were a decreasing in the chloride ion permeability of SCC mixtures.

4.4 Scanning Electron Microscopy (SEM)

Figures 4.26 Show the micrograph of present SEM for the microstruction of the transition area between normal and basalt fiber concretes. According to the SEM photographs it is obvious that the overlay stays intact with insignificant cracks and



separated at the interfacial surface.

Figure 4.26. SEM micrographs of concrete samples incorporating Basalt fiber: 30x, 100x, 250x and 500x Magnifications

It is worth to mention that the samples SEM were taken from hybrid concrete specimens which were already tested in slant shear experiment. Thus, superior bond is demonstrated for composite samples with sand blasting preparation and grooving of interfacial surface preparation of normal concrete substrate. This is noticed in Figure 4.26, where micro cracks are induced in normal concrete part. Perfect permeability of high strength basalt concrete played remarkable role in enhancing the bond strength of composite (hybrid) concrete samples. Accordingly, better adhesion

and superior interlock have been achieved between old and new segments of hybrid concrete.



CHAPTER 5

STATISTICAL ANALYSIS

This section of the thesis involves the statistical evaluation of the influence of the independent parameters such as basalt fiber volume fraction and exposed temperature level on the dependent parameters such as compressive, splitting tensile, flexural, and slant shear strength as well as elastic modulus and Poisson's ratio. Therefore, a kind of an analysis of variance (ANOVA), which is the general linear model ANOVA, was employed in the statistical evaluation. The GLM-ANOVA decreases the control variance to quantify the controlling factor dominancy, which makes it a significant diagnostic and statistical analysis tool. The level of significance, by which the statistical significance of the independent variables on the dependent variables is specified, was designated as 0.05 to carry out the analysis in this study. A "Minitab" named software was handled to statistically examine the mechanical test results presented in Chapter 4 by means of the GLM-ANOVA technique. For the dependent variables like the compressive, splitting tensile, and flexural strength, elastic modulus, and Poisson's ratio, the independent variables were the basalt fiber volume fraction and temperature level. But in addition to the basalt fiber volume fraction and temperature level, the surface treatment methods were also assigned as the independent variable for the dependent variable like slant shear strength. For this, the dummy variables were used to designate the surface treatment methods. The p-value in the statistical analysis results represents the importance of the independent variables on the dependent variables. The independent variable can be considered a significant factor on the dependent variable in the case of the p-value of less than 0.05. Otherwise, the independent variable can be regarded an insignificant factor. In addition to p-value, the percent contributions of the independent variable on the dependent variable were also determined and reported in the following sections. This statistical parameter gives information about the effectiveness degree of the independent variable on the test results. Namely, the effectiveness of the independent variable to particular response becomes higher when the percent contribution value gets higher.

5.1 Statistical Evaluation of Compressive Strength

Table 5.1 indicates the statistical analysis results for the compressive strength test. It can be comprehended that the influence of both, basalt fiber volume fraction and temperature level on the compressive strength is statistical significance since the p-values for these independent variables are less than 0.05 as can be seen from Table 5.1.

Table 5.1. Statistical evaluation of compressive strength of SCC mixtures

Dependent variable	Independent variable	Sequential sum of squares	Computed F	P value	Significance	Contribution (%)
Compressive strength	BF*	922.24	84.39	0.000	YES	35.61
	T**	1623.99	111.45	0.000	YES	62.70
	Error	43.71	-	-	-	1.69
	Total	2589.95	-	-	-	-

* BF: basalt fiber volume fraction

** T: temperature level

Besides, it can be understood from the percent contribution values of basalt fiber volume fraction and temperature level that both independent parameters have meaningful contribution on the compressive strength of the SCC mixtures, however, the temperature level has more remarkable contribution on the compressive strength than the basalt fiber volume fraction since its percent contribution value is more than that of the basalt fiber volume fraction.

5.2 Statistical Evaluation of Elastic Modulus

The statistical analysis results for the elastic modulus test has been tabulated in Table 5.2. It can be comprehended that the influence of both, basalt fiber volume fraction and temperature level on the elastic modulus is statistical importance since the p-values for these independent variables are less than 0.05.

Moreover, it can be comprehended from the percent contribution values of basalt fiber volume fraction and temperature level that only the temperature level have meaningful contribution on the elastic modulus of the SCC mixtures, the contribution of the temperature level on the elastic modulus is much more than the basalt fiber

volume fraction since its percent contribution value is much more than that of the basalt fiber volume fraction. Accordingly, the contribution of the basalt fiber volume fraction can be underestimated when it was compared to the contribution of the temperature level.

Table 5.2. Statistical evaluation of elastic modulus of SCC mixtures

Dependent variable	Independent variable	Sequential sum of squares	Computed F	P value	Significance	Contribution (%)
Elastic modulus	BF*	28.313	5.29	0.015	YES	6.39
	T**	393.318	55.15	0.000	YES	88.78
	Error	21.394	-	-	-	4.83
	Total	443.025	-	-	-	-

* BF: basalt fiber volume fraction

** T: temperature level

5.3 Statistical Evaluation of Poisson's Ratio

The statistical analysis results for the Poisson's ratio test has been reported in Table 5.3. It can be comprehended that the influence of only temperature level on the Poisson's ratio is statistical significance since the p-value for temperature level is less than 0.05 while that of the basalt fiber volume fraction is more than 0.05.

Table 5.3. Statistical evaluation of Poisson's ratio of SCC mixtures

Dependent variable	Independent variable	Sequential sum of squares	Computed F	P value	Significance	Contribution (%)
Poisson's ratio	BF*	0.002175	3.00	0.073	NO	11.18
	T**	0.014380	14.88	0.000	YES	73.91
	Error	0.002900	-	-	-	14.91
	Total	0.019455	-	-	-	-

* BF: basalt fiber volume fraction

** T: temperature level

In addition, it can be understood from the percent contribution values of basalt fiber volume fraction and temperature level that only the temperature level have meaningful contribution on the Poisson's ratio of the SCC mixtures, the contribution

of the temperature level on the Poisson's is much more than the basalt fiber volume fraction since its percent contribution value is much more than that of the basalt fiber volume fraction. For this reason, it can be stated that the contribution of the basalt fiber volume fraction to the Poisson's ratio can be underestimated.

5.4 Statistical Evaluation of Splitting Tensile Strength

Table 5.4 shows the statistical analysis results for the splitting tensile strength test. It can be comprehended that the influence of both, basalt fiber volume fraction and temperature level on the splitting tensile strength is statistical significance since the p-values for these independent variables are less than 0.05 as can be seen from Table 5.4.

Table 5.4. Statistical evaluation of splitting tensile strength of SCC mixtures

Dependent variable	Independent variable	Sequential sum of squares	Computed F	P value	Significance	Contribution (%)
Splitting tensile strength	BF*	2.7435	46.74	0.000	YES	33.98
	T**	5.0952	65.10	0.000	YES	63.11
	Error	0.2348	-	-	-	2.91
	Total	8.0735	-	-	-	-

* BF: basalt fiber volume fraction

** T: temperature level

Besides, it can be understood from the percent contribution values of basalt fiber volume fraction and temperature level that both independent parameters have meaningful contribution on the splitting tensile strength of the SCC mixtures, however, the temperature level has more important contribution on the splitting tensile strength than the basalt fiber volume fraction since the percent contribution value of temperature level is more than that of the basalt fiber volume fraction.

5.5 Statistical Evaluation of Flexural Strength

The statistical analysis results for the flexural strength test has been submitted in Table 5.5. It can be understood that the influence of both, basalt fiber volume fraction and temperature level on the flexural strength is statistical significance since both independent variables have the p-values of less than 0.05. Furthermore, it can be

comprehended from the percent contribution values of basalt fiber volume fraction and temperature level that only the temperature level have meaningful contribution on the flexural of the SCC mixtures, the contribution of the temperature level on the flexural strength is much more than the basalt fiber volume fraction since its percent contribution value is much more than that of the basalt fiber volume fraction. Therefore, it can be noted that the contribution of the basalt fiber volume fraction to the flexural strength can be underestimated.

Table 5.5. Statistical evaluation of flexural strength of SCC mixtures

Dependent variable	Independent variable	Sequential sum of squares	Computed F	P value	Significance	Contribution (%)
Flexural strength	BF*	2.0156	36.11	0.000	YES	13.47
	T**	12.7230	170.96	0.000	YES	85.04
	Error	0.2233	-	-	-	1.49
	Total	14.9619	-	-	-	-

* BF: basalt fiber volume fraction

** T: temperature level

5.6 Statistical Evaluation of Slant Shear Strength

The statistical analysis results for the slant shear strength test has been reported in Table 5.6. It can be comprehended that the influence of all independent variables on the slant shear strength is statistical significance since the p-values of the surface treatment method, basalt fiber volume fraction, and temperature level are less than 0.05.

Moreover, it can be comprehended from the percent contribution values of surface treatment method, basalt fiber volume fraction, and temperature level that the most meaningful contribution on the slant shear strength of the SCC mixtures belongs to the surface treatment method, the contribution of this independent variable on the slant shear strength is much more than the basalt fiber volume fraction and temperature level since their percent contribution values are much less than that of the surface treatment method. In this context, the contributions of these independent variables, in particular the basalt fiber volume fraction, can be underestimated.

Table 5.6. Statistical evaluation of Slant shear strength of SCC mixtures

Dependent variable	Independent variable	Sequential sum of squares	Computed F	P value	Significance	Contribution (%)
Slant shear strength	ST*	4255.52	501.71	0.000	YES	89.18
	BF**	23.75	2.80	0.000	YES	0.50
	T***	297.26	26.28	0.000	YES	6.23
	Error	195.09	-	-	-	4.09
	Total	4771.61	-	-	-	-

*ST: surface treatment method

**BF: basalt fiber volume fraction

*** T: temperature level

CHAPTER 6

MODELING

6.1 Introduction to Gene Expression Programming

The description of soft computing can be done as a total of techniques aiming the utilization of the uncertainty and toleration for erroneous to procure the robustness, low solution cost, and tractability (Zadeh, 1994). The engineering and financial estimation problems can be considered in the soft computing technique application areas.

Genetic algorithms, which utilize the populations of individuals and select them according to their formation and present the genetic diversity by employing genetic operators, and genetic programming, which carries out the same processes as genetic algorithms but can be considered a generalized form of genetic algorithms (Gen and Cheng, 1997), are much-used soft computing techniques. Genetic programming that was suggested by Koza (1992) is basically the genetic algorithms implementation to computer programs. Gene expression programming (GEP), which was devised by Ferreira (2001), can be regarded the developed shape of genetic algorithms and programming since the same mechanisms in the genetic algorithms and programming are handled by GEP. However, the using of the expressions of discovered knowledge and/or learned models makes the GEP a novel technique, by which it creates the computer programs (Li et al., 2005). Therefore, it could be stated that the GEP is the enhanced form of genetic algorithms and programming. Koza (1992) present the flowchart of gene expression algorithm as given in Figure 6.1.

The description of problem at the beginning is very crucial in the genetic algorithm and programming since this process is the main issue lying beneath them. Then, the program endeavors to solve the problems in the problem-independent mode (Koza, 1997; Gen and Cheng, 1997). However, the GEP creates the different sized and encoded shaped computer programs, then chromosomes are imported, and the fitness of each individual is determined based on the solution quality. On the basis of the

solution, the same genetic operator with minor differences are employed by these three techniques mentioned above (Güneyisi et al., 2014).

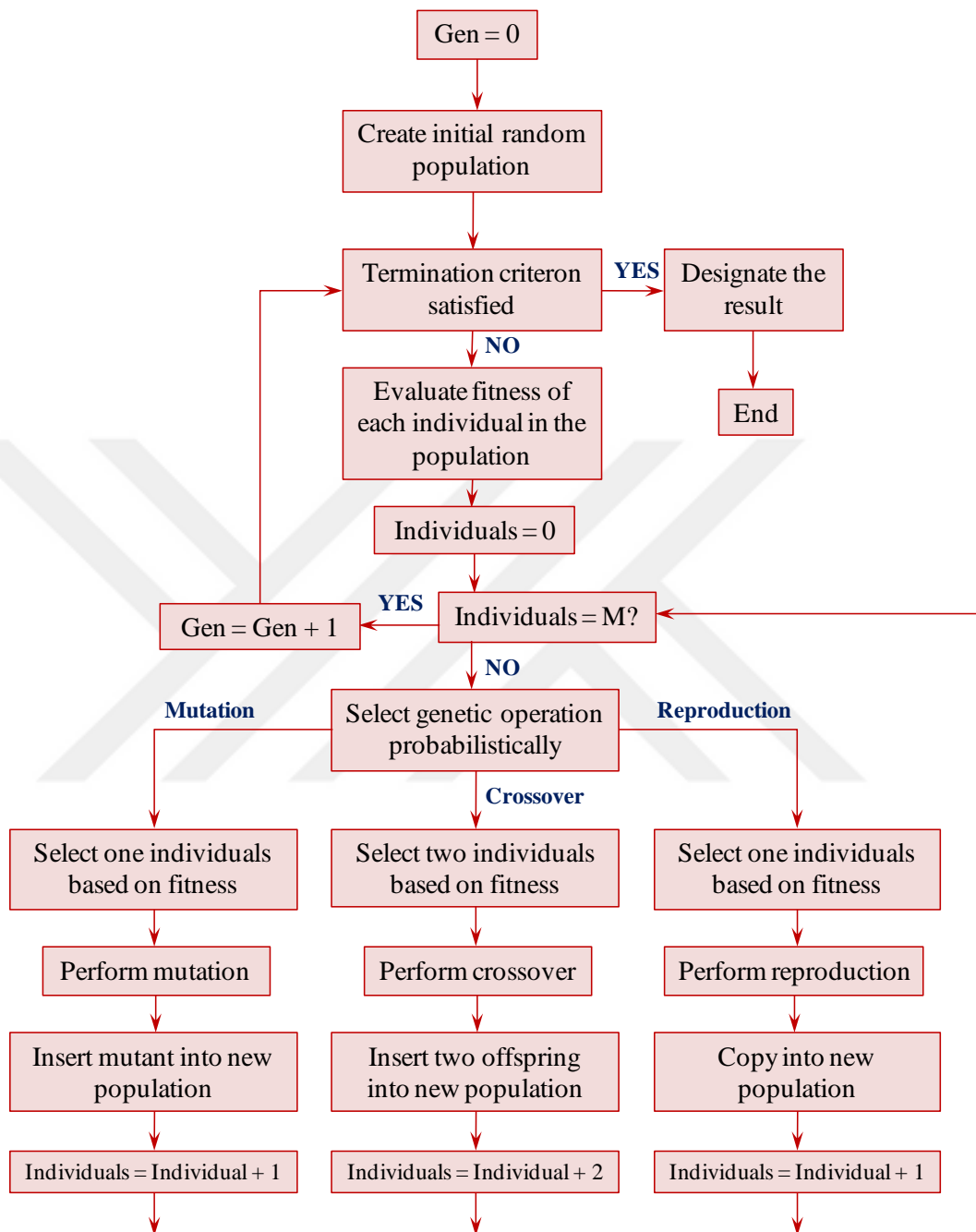


Figure 6.1. The flowchart presentation of a genetic programming paradigm (Koza, 1992)

Open reading frames, which let better expression of structural organization, are employed by the GEP. Ferreira (2001) called the open reading frames as K-expressions, of which name comes from the Karva language. The K-expressions is one of the remarkable advantage of GEP since it procure an opportunity to infer the

phenotype obtained from the gene sequences. Additionally, the GEP allow to translation of K-expressions to expression trees that are the diagramming illustration of the phenotype of GEP sequence as shown in Figure 6.2. Otherwise, the inverse process such as translation of ET to K-expression is also possible. For instance, the following mathematical expression can be:

$$\sqrt{(a - b)/(a + b)} \quad (6.1)$$

predicated in the K-expression or in the expression tree as below:

$$\begin{array}{l} 01234567 \\ Q/-+abab \end{array} \quad (6.2)$$

where Q represents the square root.

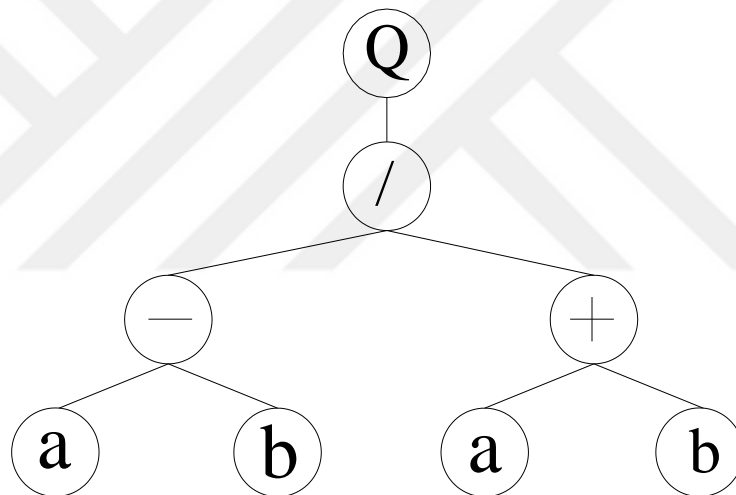


Figure 6.2. Typical configuration of expression tree

6.2 Proposed Model

The experimental test results achieved from the current study for elastic modulus, splitting tensile strength, flexural strength, and slant shear strength tests were used in the generation of GEP models.

In this study, three GEP models were created to estimate the elastic modulus, splitting tensile strength, flexural strength, and slant shear strength of the SCC mixtures. In total, the current study provides four new models that estimate individually the elastic modulus, splitting tensile strength, flexural strength, and slant shear strength. The exposed temperature, basalt fiber volume fraction, and

compressive strength of SCC mixture were employed as independent variable in the generation of GEP models for the elastic modulus, splitting tensile strength, and flexural strength whereas in addition to these independent variables, the surface texture characteristic of specimens was also designated as independent parameter in the creation of GEP model for slant shear strength.

Table 6.1. Input and output experimental data of elastic modulus, splitting tensile strength, and flexural strength for train and test set

No	T*	BF*	f_c^*	E^*	f_{split}^*	f_{flex}^*
1	25	0	101.9	35.8	7.15	8.24
2		0.25	94.5	33.9	7.32	8.71
3		0.5	90.8	36.4	6.78	8.89
4		1	85.5	31.5	6.56	8.91
5		0	96.6	31.7	7.06	8.16
6	200	0.25	92.3	32.6	7.16	8.61
7		0.5	84.6	32.7	6.53	8.69
8		1	78.4	28.0	6.11	8.75
9		0	89.0	27.0	6.96	8.07
10	300	0.25	83.8	28.9	6.72	8.59
11		0.5	73.9	30.2	6.30	8.64
12		1	69.3	27.6	5.89	8.70
13		0	84.8	26.1	6.49	6.95
14	400	0.25	82.0	27.0	6.30	7.95
15		0.5	69.4	28.6	5.81	7.82
16		1	66.9	24.1	5.32	8.01
17		0	77.0	22.7	6.05	5.88
18	500	0.25	67.9	21.6	5.61	6.52
19		0.5	65.2	20.1	5.37	6.95
20		1	60.5	20.8	5.20	6.92

* T: temperature; BF: basalt fiber volume fraction; f_c : compressive strength; E: elastic modulus; f_{split} : splitting tensile strength; f_{flex} : flexural strength.

Totally, in the generation of GEP models for the elastic modulus, splitting tensile strength, and flexural strength, 20 data were employed while 80 data were used in the creation of GEP model for the slant shear strength. These data were randomly divided into two groups as train and test dataset in the generation of all models. The

test dataset was approximately 25% of total data whilst the remained of total data was used in the train dataset. Experimental test results of elastic modulus, splitting tensile strength, and flexural strength have been submitted in Table 6.1. Besides, the test results of slant shear strength have been presented in Table 6.2. The bold data in these tables shows the test data.

Table 6.2. Input and output experimental data of slant shear strength for train and test set

No	T*	BF*	f_c^*	ST*	f_{slant}^*	ST*	f_{slant}^*	ST*	f_{slant}^*	ST*	f_{slant}^*
1		0	101.9		15.1		20.3		29.9		30.6
2	25	0.25	94.5		16.7		20.8		29.0		34.0
3		0.5	90.8		13.6		21.7		32.7		32.7
4		1	85.5		12.6		22.2		34.6		33.2
5		0	96.6		14.1		19.8		28.3		29.2
6	200	0.25	92.3		15.0		20.2		27.0		32.9
7		0.5	84.6		12.1		20.1		31.4		30.7
8		1	78.4		10.4		22.0		32.5		32.5
9		0	89.0		12.7		18.9		26.0		28.9
10	300	0.25	83.8		13.4		19.5		26.6		29.0
11		0.5	73.9	1**	10.7	2**	20.0	3**	30.1	4**	29.6
12		1	69.3		10.1		21.7		30.6		30.9
13		0	84.8		11.8		18.4		23.4		28.7
14	400	0.25	82.0		9.1		19.3		26.0		27.6
15		0.5	69.4		9.5		19.8		29.4		28.0
16		1	66.9		8.1		20.7		28.4		29.0
17		0	77.0		10.2		17.9		20.4		26.3
18	500	0.25	67.9		7.8		18.9		23.5		25.4
19		0.5	65.2		7.3		18.6		28.2		27.0
20		1	60.5		7.9		19.0		26.4		26.5

* T: temperature; BF: basalt fiber volume fraction; f_c : compressive strength; TT: surface treatment type; f_{slant} : slant shear strength.

** 1: as casted surface; 2: hole drilled surface; 3: grooved surface; 4: sand blasted surface.

Moreover, in order to identify the surface texture types of slant shear strength test, dummy variables were used. For normal surface, namely surface without treatment, was designated as one (1) while the others, hole drilling, grooving, and sand blasting

were selected as two (2), three (3), and four (4), respectively. They were also indicated in Table 6.2.

GeneXproTools 4.0 named software was employed in the generation of empirical models for elastic modulus, splitting tensile strength, flexural strength, and slant shear strength. The derivation was done by using simple function sets such as addition, subtraction, multiplication, division, square root, and arctangent. In addition, the number of chromosome and genes were designated as 60 and 4, respectively, in the generation of each mathematical model while the head size chosen as 10 for all models. The details of parameters used in the GEP algorithms have been submitted in Table 6.3.

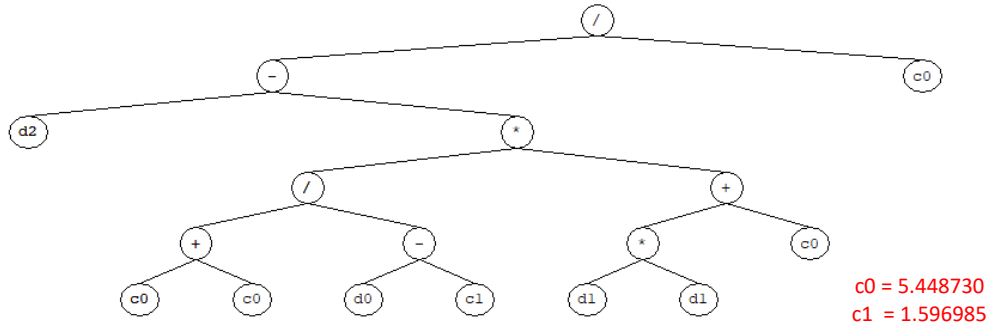
Table 6.3. Parameters employed in model derivation

P1	Function set	+, -, *, /, Sqrt,
P2	Number of generation	299999
P3	Chromosomes	60
P4	Head size	10
P5	Number of genes	4
P6	Linking function	Addition
P7	Constants per gene	2
P8	Lower/upper bound of constants	-10/10
P9	Mutation rate	0.044
P10	Inversion rate	0.1
P11	One-point recombination rate	0.3
P12	Two-point recombination rate	0.3
P13	Gene recombination rate	0.1
P14	Gene transposition rate	0.1

6.3 GEP Model for Elastic Modulus

The expression trees of mathematical GEP model derived for elastic modulus by using the experimental test results given in Table 6.1 have been indicated in Figure 6.3.

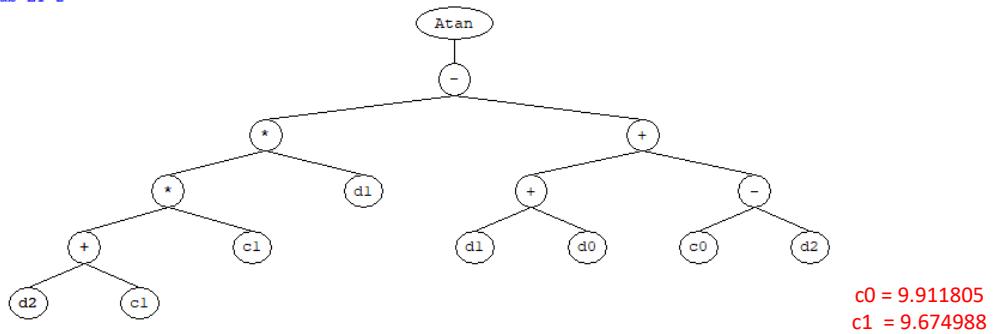
Sub-ET 1



c0 = 5.448730
c1 = 1.596985

(a)

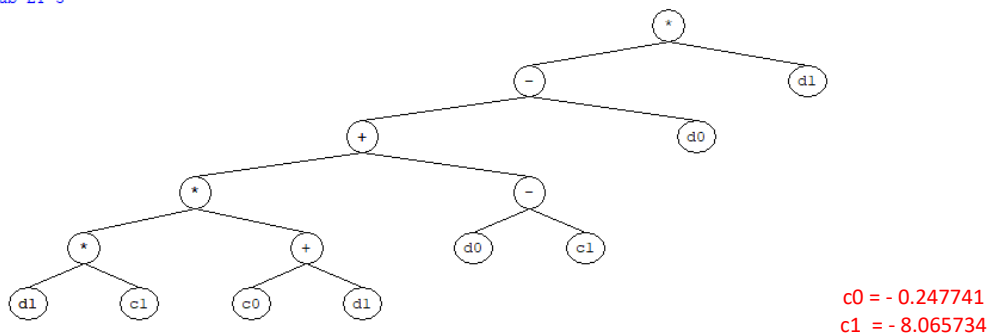
Sub-ET 2



c0 = 9.911805
c1 = 9.674988

(b)

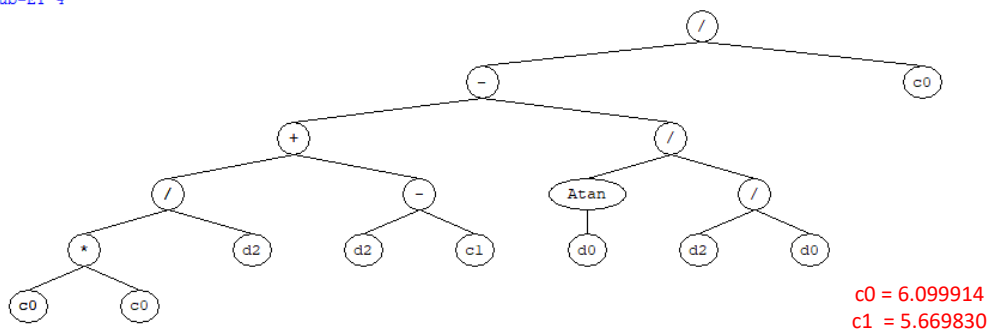
Sub-ET 3



c0 = -0.247741
c1 = -8.065734

(c)

Sub-ET 4



c0 = 6.099914
c1 = 5.669830

(d)

Figure 6.3. Expression trees for GEP model of elastic modulus: a) Function 1, b) Function 2, c) Function 3, and d) Function 4

In addition, the empirical predictive model for each function achieved from the expression trees are presented in the following equations:

$$E = E_1 + E_2 + E_3 + E_4 \quad (6.3)$$

$$E_1 = \frac{d_2 - \frac{10.89746xd_1^2 + 59.37731723}{d_0 - 1.596985}}{5.44873} \quad (6.3a)$$

$$E_2 = \tan^{-1}((9.674988xd_2 + 93.6053928)xd_1 - d_1 - d_0 + d_2 - 9.911805) \quad (6.3b)$$

$$E_3 = d_1(0.247741 - 8.065734xd_1x(d_1 - 0.247741)) \quad (6.3c)$$

$$E_4 = \frac{\frac{37.20895081 - d_0x \tan^{-1}(d_0)}{d_2} + d_2 - 5.66983}{6.099914} \quad (6.3d)$$

where;

E : modulus of elasticity (in GPa)

d_0 : exposed temperature (in °C)

d_1 : basalt fiber volume fraction (in %)

d_2 : concrete compressive strength (in MPa)

The elastic modulus of SCC mixtures exposed to temperature was estimated by using the formula given above. The normalized elastic modulus values that means the experimental elastic modulus divided by predicted elastic modulus with respect to experimental elastic modulus have been indicated in Figure 6.4. The normalized elastic modulus gives an idea about the estimation capability of the mathematical model. A good scattering of normalized values means a good estimation capability. However, firstly, it is needed to be known how good scattering can be comprehended. For this reason, the normalization line limits should be decided at the beginning. When the narrow limitation values such as $\pm 10\%$ were chosen, the evaluation of estimation performance of model would be well comprehended. In this study, $\pm 10\%$ normalization limit values were selected to indicate the estimation capability of model. When Figure 6.4 is observed, it can be easily seen that all normalized values, train and test data, are dispersed between the normalization limits

that means the prediction performance of empirical GEP model can be considered good.

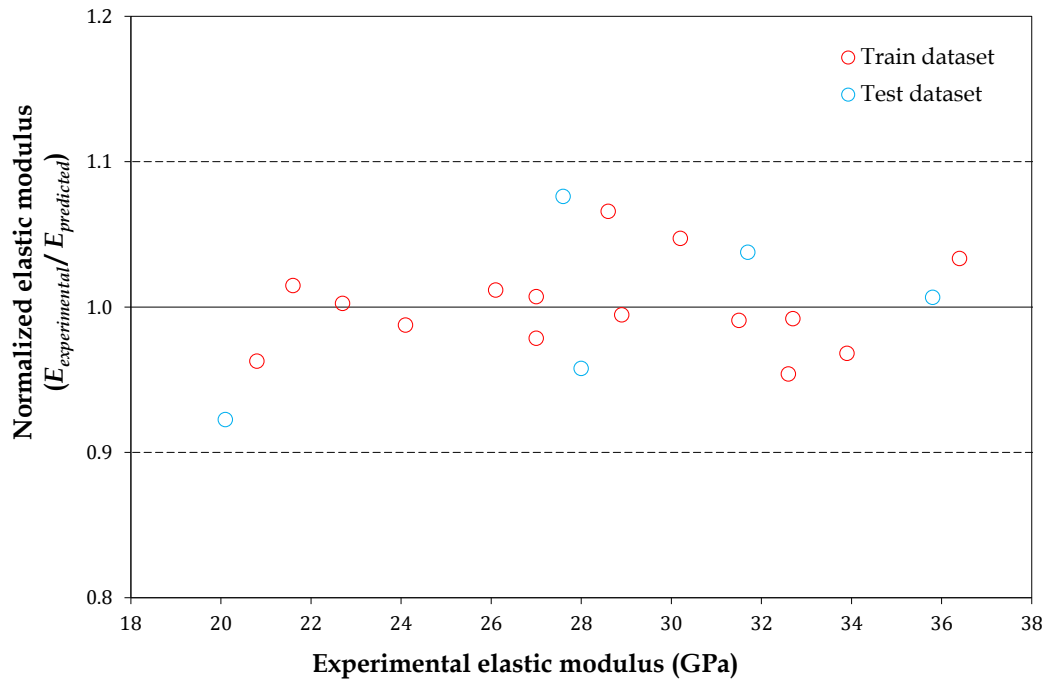
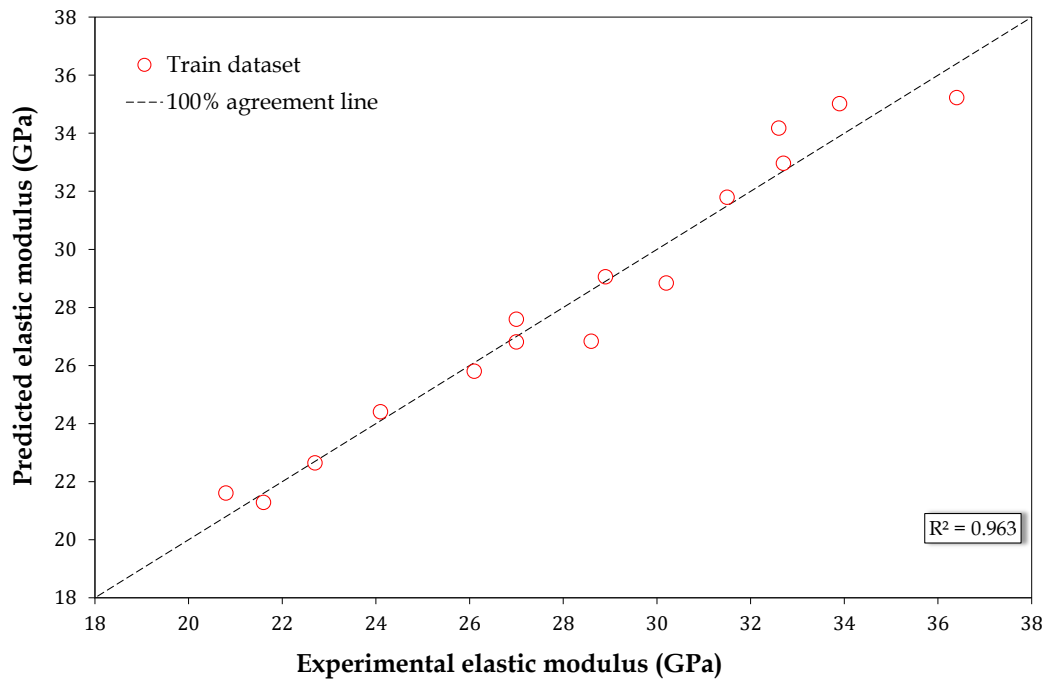
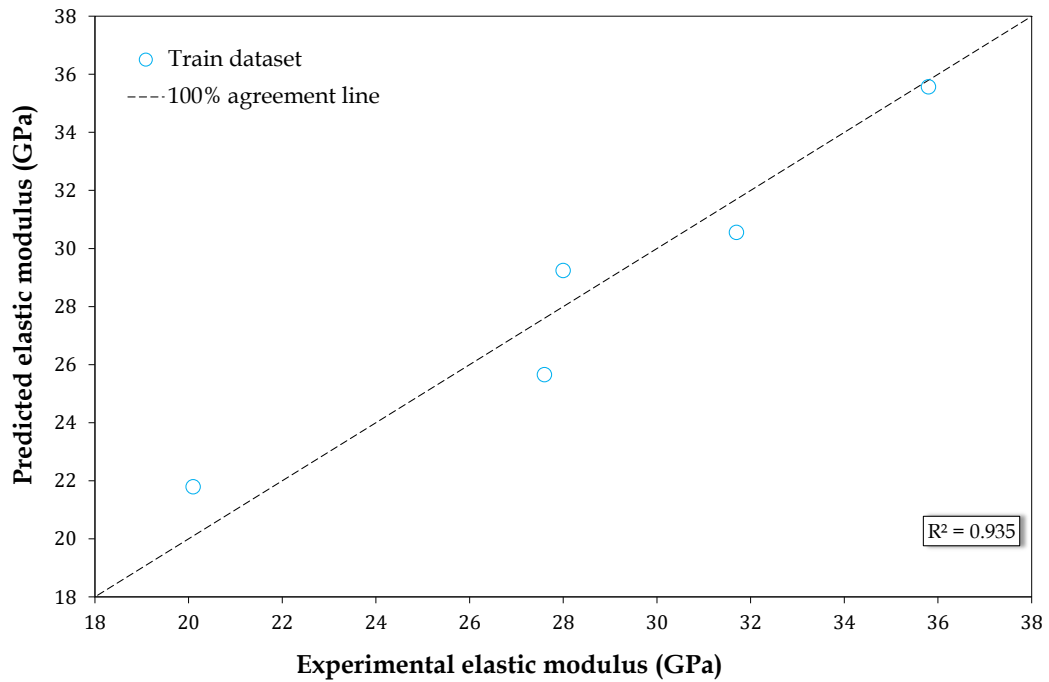


Figure 6.4. Estimation performance of empirical GEP model concerning experimental result



(a)



(b)

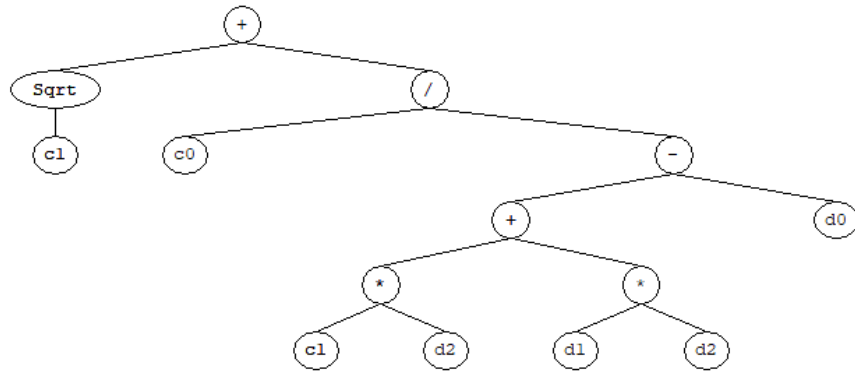
Figure 6.5. Predicted versus experimental elastic modulus values for: a) train and b) test datasets

Another parameter that indicates the prediction capability of proposed GEP model is R-squared value. Therefore, the predicted versus experimental elastic modulus values for train and test datasets have been plotted in Figures 6.5a and 6.5b, respectively. Besides, the R-squared values for train and test datasets were also presented in these figures. The graphs obviously indicate that the predicted and experimental elastic modulus values are well distributed on the 100%-agreement line. In addition, the R-squared values of 0.963 and 0.935 were achieved in the proposed model. It means that the mathematical model has good and robust prediction capability since the R-squared value of test dataset is very near to that of train dataset. The R-squared value of 0.963 also reveal that there is a strong correlation between the experimental and predicted elastic modulus values.

6.4 GEP Model for Splitting Tensile Strength

The expression trees of mathematical GEP model derived for splitting tensile strength by using the experimental test results given in Table 6.1 have been indicated in Figure 6.6. In addition, the empirical predictive model for each function achieved from the expression trees are presented in the following equations:

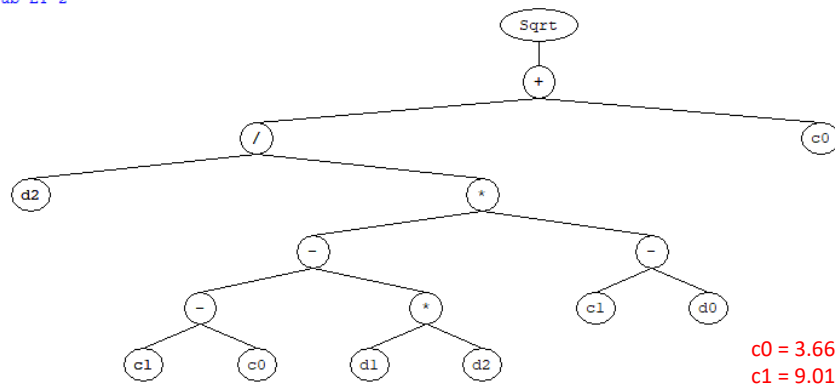
Sub-ET 1



c0 = 8.336487
c1 = 3.985047

(a)

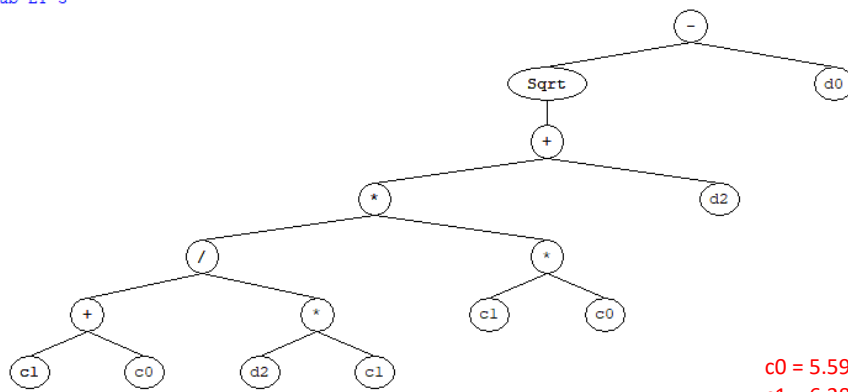
Sub-ET 2



c0 = 3.666351
c1 = 9.011840

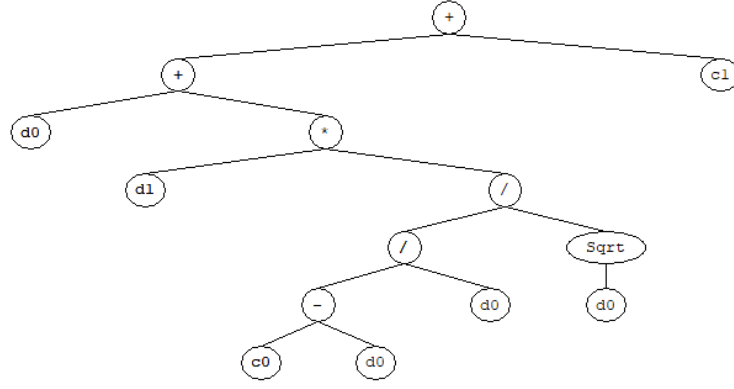
(b)

Sub-ET 3



c0 = 5.597992
c1 = 6.288910

(c)



$$\begin{aligned} c0 &= 6.107544 \\ c1 &= -6.556854 \end{aligned}$$

(d)

Figure 6.6. Expression trees for GEP model of splitting tensile strength: a) Function 1, b) Function 2, c) Function 3, and d) Function 4

$$f_{split} = f_{s1} + f_{s2} + f_{s3} + f_{s4} \quad (6.4)$$

$$f_{s1} = 1.996258 + \frac{8.336487}{3.985047xd_2 + d_1xd_2 - d_0} \quad (6.4a)$$

$$f_{s2} = \sqrt{\frac{d_2}{(5.345489 - d_1xd_2)x(9.01184 - d_0)} + 3.666351} \quad (6.4b)$$

$$f_{s3} = \sqrt{\frac{66.5427823}{d_2} + d_2} - d_0 \quad (6.4c)$$

$$f_{s4} = d_0 + d_1x \left(\frac{6.107544 - d_0}{\sqrt{d_0^3}} \right) - 6.556854 \quad (6.4d)$$

where;

f_{split} : splitting tensile strength (in MPa)

The splitting tensile strength of SCC mixtures exposed to temperature was predicted by using the formula given above. The normalized splitting tensile strength values that means the experimental splitting tensile strength divided by predicted with respect to experimental splitting tensile strength have been shown in Figure 6.7. The normalized splitting tensile strength provides an idea about the estimation capability of the mathematical model. In this study, $\pm 10\%$ normalization limit values were selected to indicate the estimation capability of mathematical GEP model. When

Figure 6.7 is seen, it can be easily noticed that all normalized values, train and test data, are scattered between the normalization limits that means the prediction performance of empirical GEP model can be considered good.

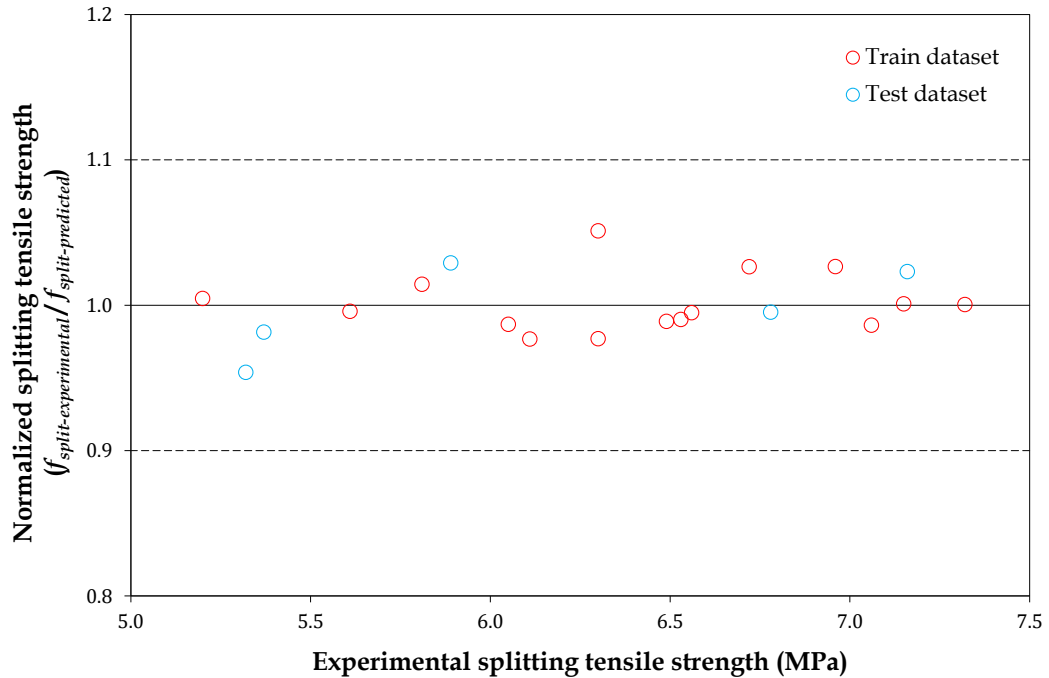
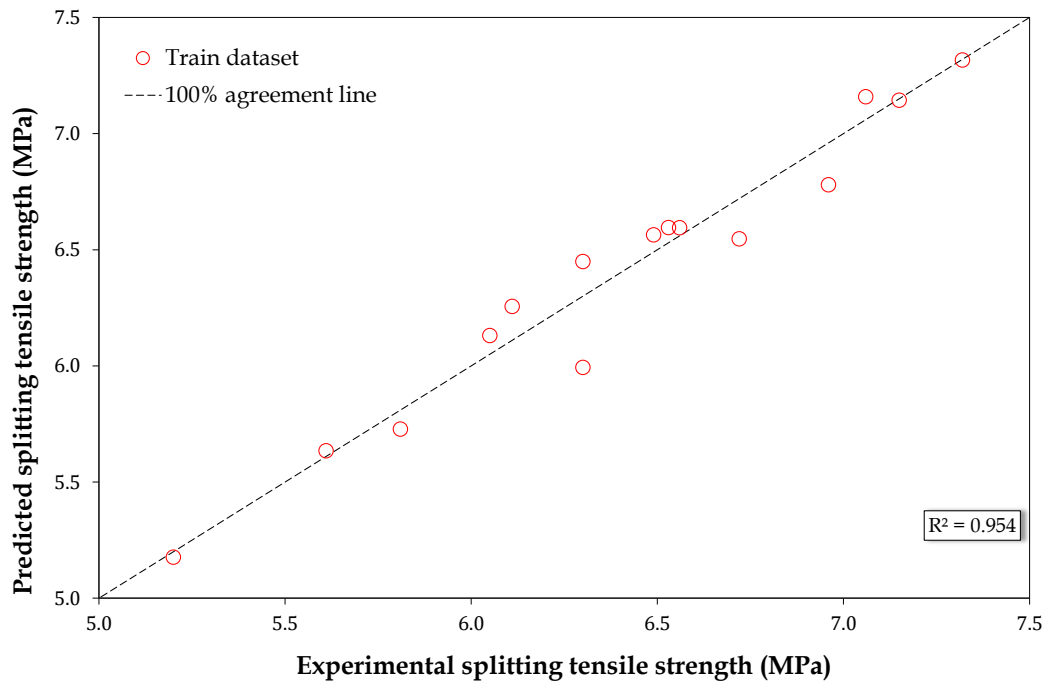


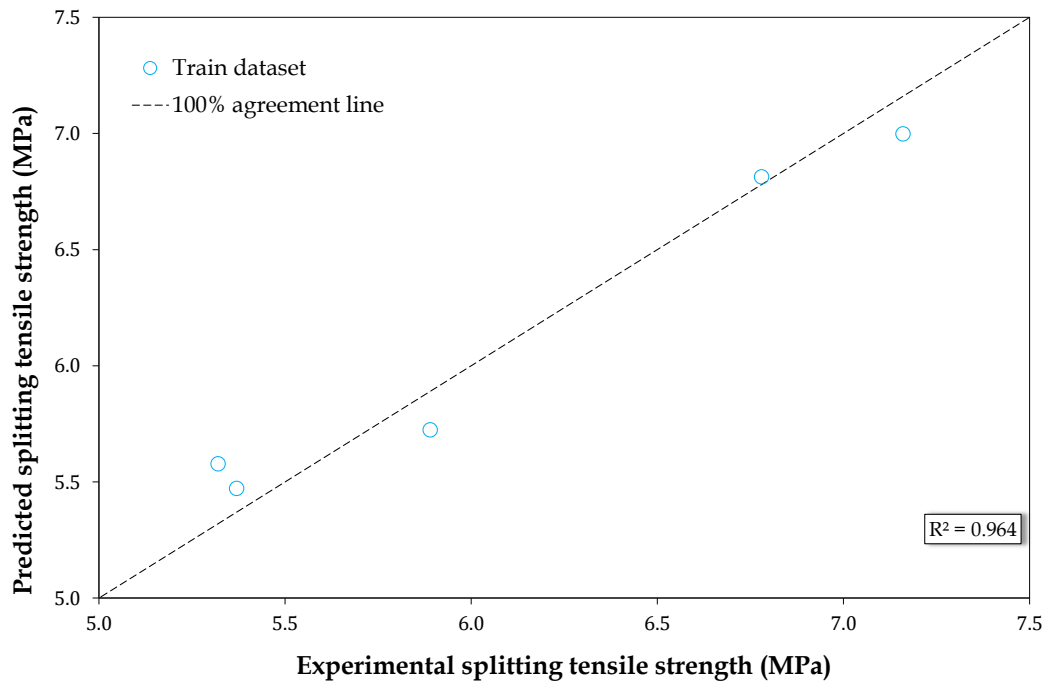
Figure 6.7. Estimation performance of empirical GEP model concerning experimental result

In addition, the predicted versus experimental splitting tensile strength values for train and test datasets have been plotted in Figures 6.8a and 6.8b, respectively. R-squared value is another parameter that indicates the prediction capability of proposed GEP model. Therefore, the R-squared values for train and test datasets were also presented in these figures. The graphs obviously show that the predicted and experimental splitting tensile strength values are well distributed on the 100%-agreement line. In addition, the R-squared values of 0.954 and 0.964 were achieved in the proposed model. It means that the mathematical model has good and robust prediction capability since the R-squared value of test dataset is greater than that of train dataset. The R-squared values procured for this empirical model also emphasize

that there is a strong correlation between the experimental and predicted splitting tensile strength values.



(a)



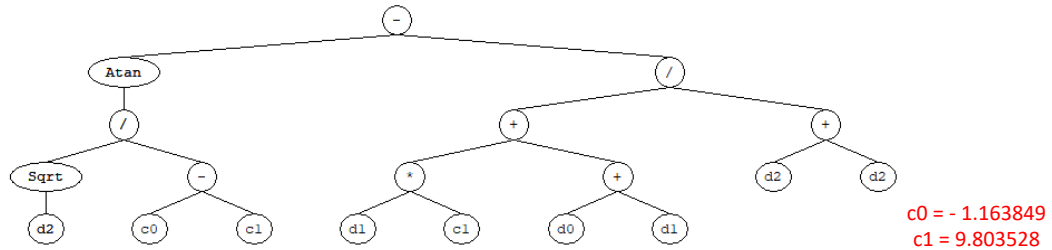
(b)

Figure 6.8. Predicted versus experimental splitting tensile strength values for: a) train and b) test datasets

6.5 GEP Model for Flexural Strength

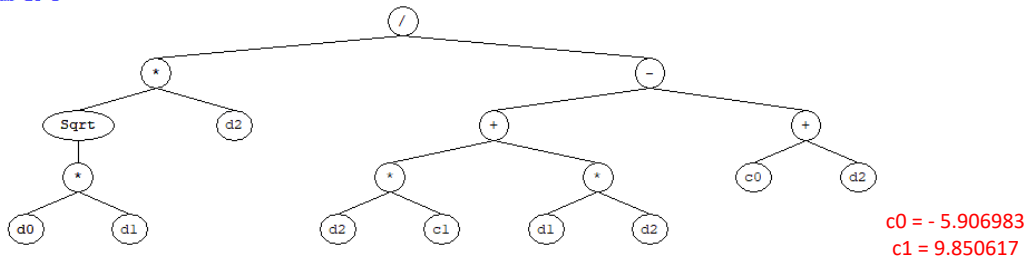
The expression trees of mathematical GEP model derived for flexural strength by using the experimental test results given in Table 6.1 have been indicated in Figure 6.9.

Sub-ET 1



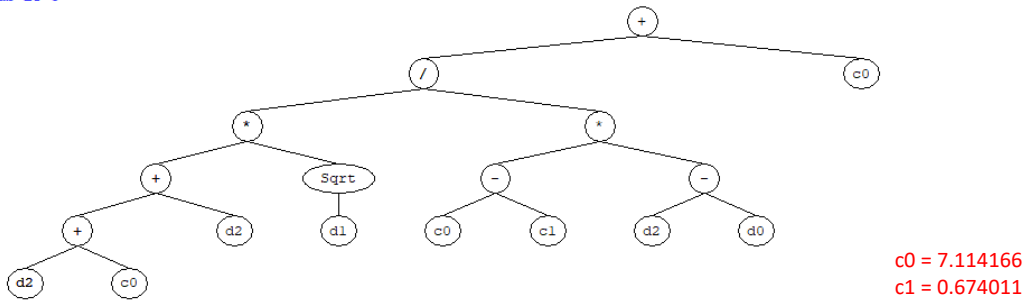
(a)

Sub-ET 2



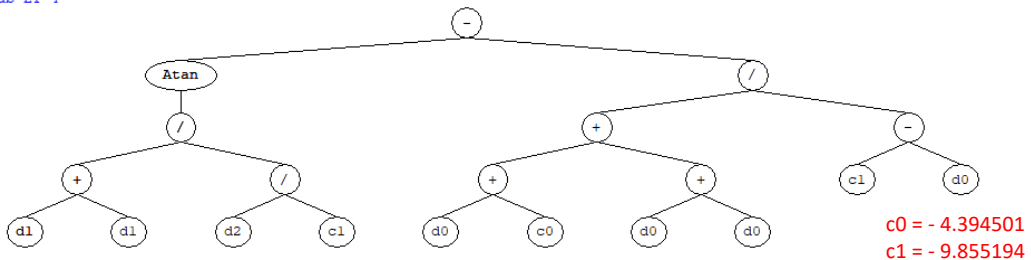
(b)

Sub-ET 3



(c)

Sub-ET 4



(d)

Figure 6.9. Expression trees for GEP model of flexural strength: a) Function 1, b) Function 2, c) Function 3, and d) Function 4

In addition, the empirical predictive model for each function achieved from the expression trees are presented in the following equations:

$$f_{flex} = f_{f1} + f_{f2} + f_{f3} + f_{f4} \quad (6.5)$$

$$f_{f1} = \tan^{-1}\left(-\frac{\sqrt{d_2}}{10.967377}\right) - \frac{d_0 + d_1 + 9.803528x d_1}{2x d_2} \quad (6.5a)$$

$$f_{f2} = \frac{d_2 \sqrt{d_0 x d_1}}{9.850617x d_2 + d_1 x d_2 + 5.906983 - d_2} \quad (6.5b)$$

$$f_{f3} = \frac{(2x d_2 + 7.114166)x \sqrt{d_1}}{6.440155x(d_2 - d_0)} + 7.114166 \quad (6.5c)$$

$$f_{f4} = \tan^{-1}\left(-\frac{8.789002x d_1}{d_2}\right) + \frac{3x d_0 - 4.394501}{d_0 + 9.855194} \quad (6.5d)$$

where;

f_{flex} : flexural strength (in MPa)

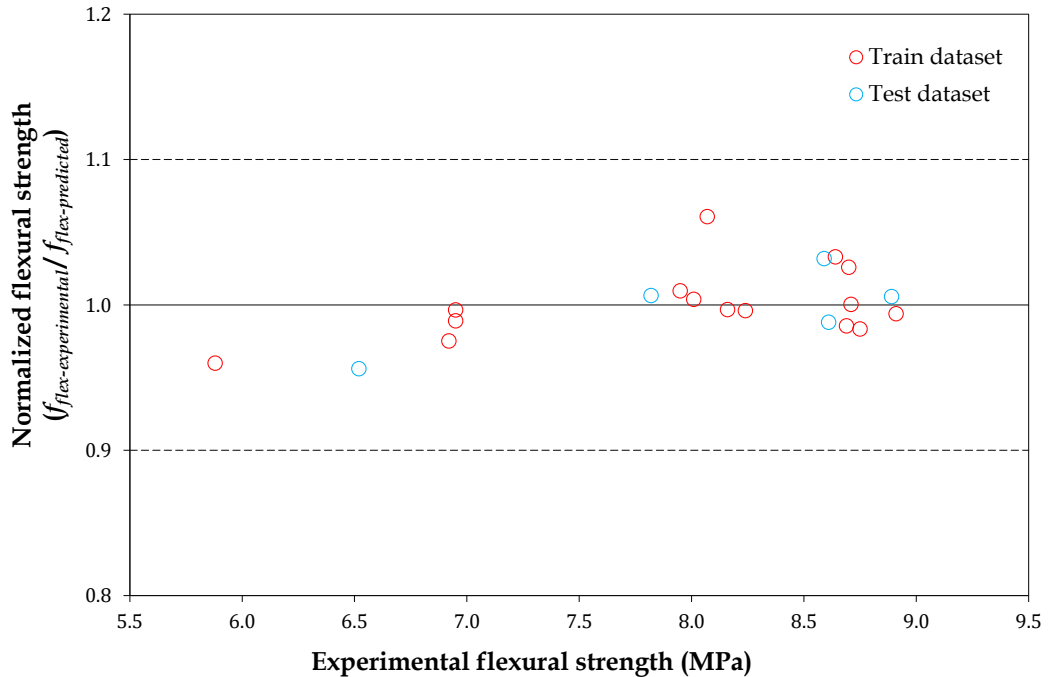
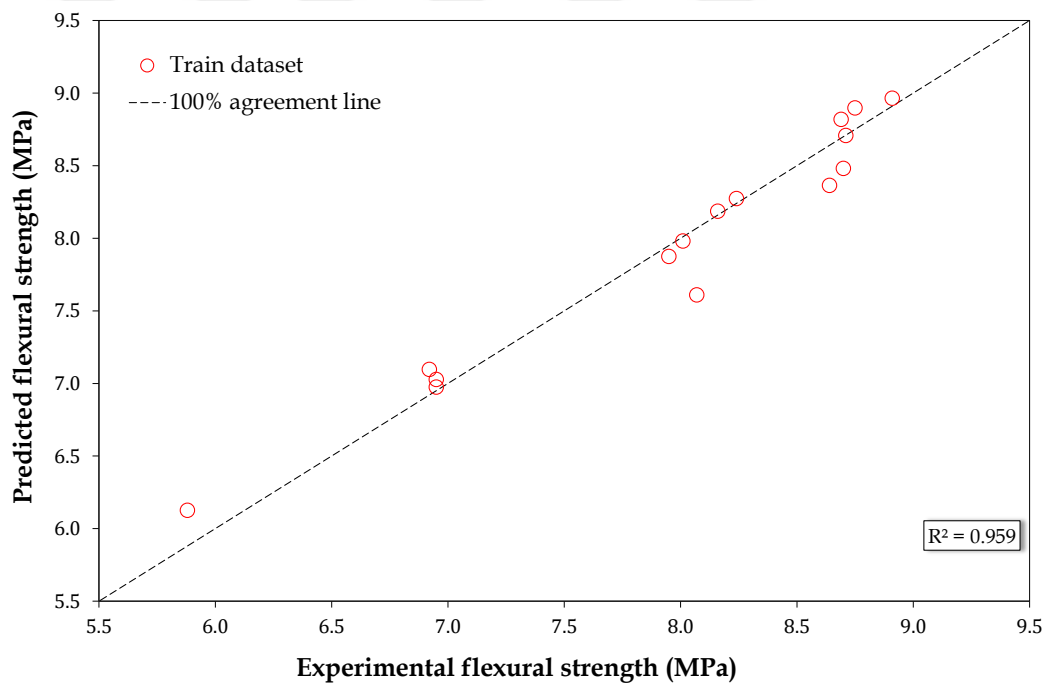


Figure 6.10. Estimation performance of empirical GEP model concerning experimental result

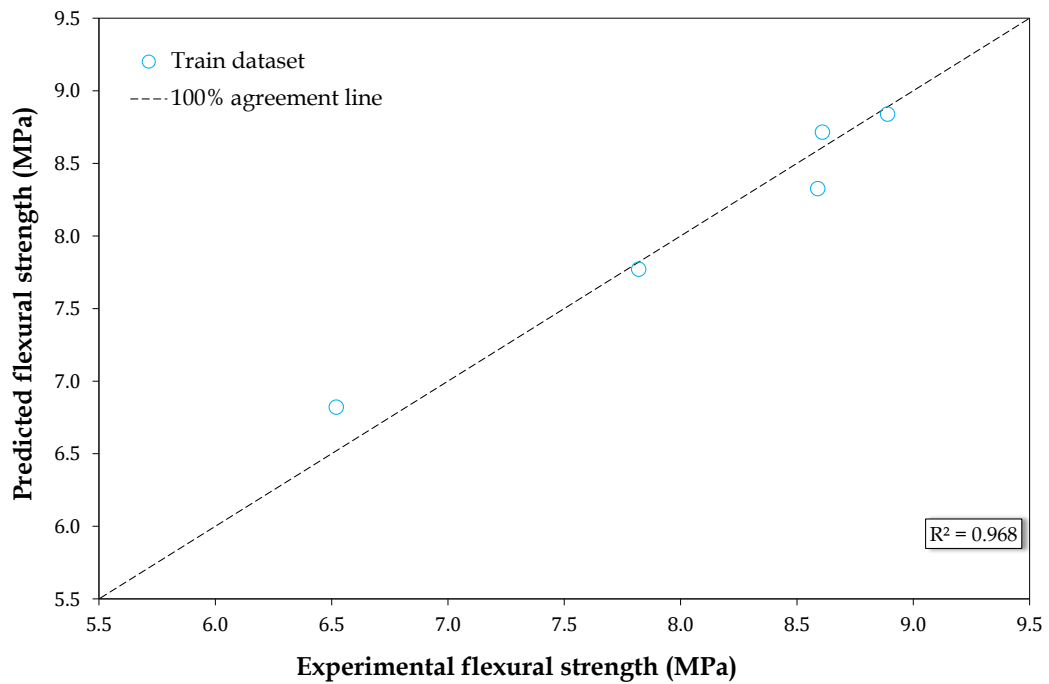
The flexural strength of SCC mixtures exposed to temperature was predicted by using the formula given above. The normalized flexural strength values that signifies the experimental flexural strength divided by predicted with respect to experimental

flexural strength have been shown in Figure 6.10. The normalized flexural strength ensures an idea about the estimation capability of the mathematical model. In this study, $\pm 10\%$ normalization limit values were chosen to demonstrate the prediction performance of empirical GEP model. When Figure 6.10 is observed, it can be easily seen that all normalized values, train and test data, are dispersed between the normalization limits that signifies the estimation capacity of proposed GEP model can be regarded good.

In addition to normalized values, the predicted versus experimental flexural strength values for train and test datasets have been plotted in Figures 6.11a and 6.11b, respectively. R-squared value is another parameter that presents the estimation performance of proposed GEP model. Therefore, the R-squared values for train and test datasets were also submitted in Figures 6.11a and 6.11b.



(a)



(b)

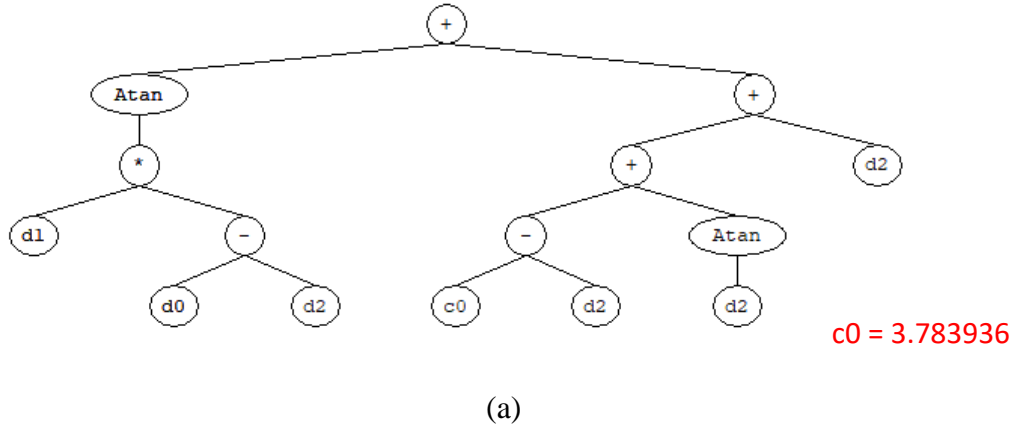
Figure 6.11. Predicted versus experimental flexural strength values for: a) train and b) test datasets

The graphs obviously demonstrate that the predicted and experimental flexural strength values are well distributed on the 100%-agreement line. In addition, the R-squared values of 0.959 and 0.968 were obtained in the proposed GEP model. It signifies that the empirical model has good and robust prediction performance since the R-squared value of test dataset is greater than that of train dataset. The R-squared values attained for this mathematical model also impress that there is a strong correlation between the experimental and predicted flexural strength values.

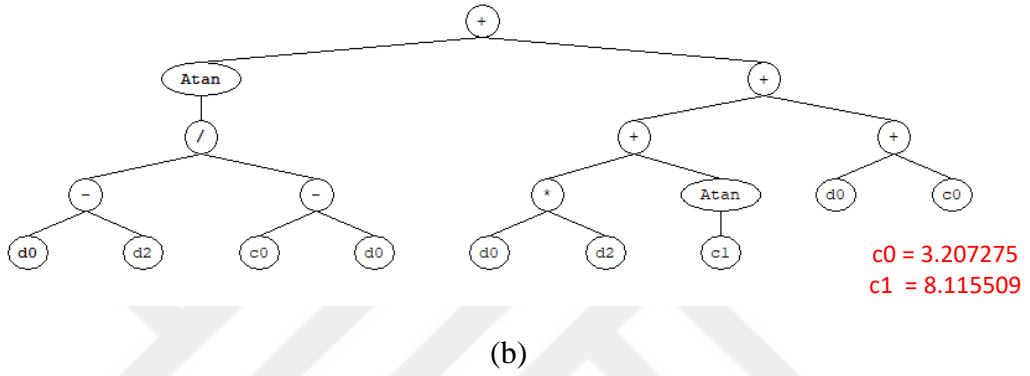
6.6 GEP Model for Slant Shear Strength

The expression trees of mathematical GEP model derived for slant shear strength by using the experimental test results given in Table 6.2 have been indicated in Figure 6.12.

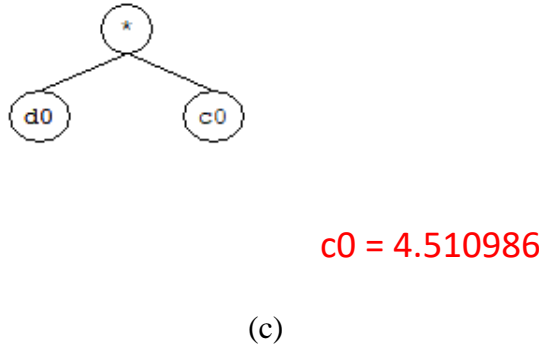
Sub-ET 1



Sub-ET 2



Sub-ET 3



Sub-ET 4

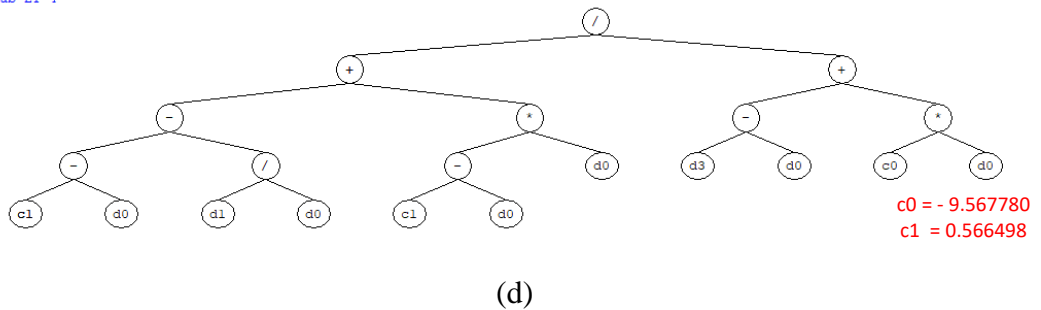


Figure 6.12. Expression trees for GEP model of slant shear strength: a) Function 1, b) Function 2, c) Function 3, and d) Function 4

In addition, the empirical predictive model for each function achieved from the expression trees are presented in the following equations:

$$f_{slant} = f_{ss1} + f_{ss2} + f_{ss3} + f_{ss4} \quad (6.6)$$

$$f_{ss1} = \tan^{-1}(d_1 x (d_0 - d_2)) + \tan^{-1}(d_2) + 3.783936 \quad (6.6a)$$

$$f_{ss2} = \tan^{-1}\left(\frac{d_0 - d_2}{3.207275 - d_0}\right) + d_0 x d_2 + d_0 + 4.655468483 \quad (6.6b)$$

$$f_{ss3} = 4.510986 x d_0 \quad (6.6c)$$

$$f_{ss4} = \frac{0.566498 - d_0 - \frac{d_1}{d_0} - d_0 x (9.56778 + d_0)}{d_3 - d_0 - 9.56778 x d_0} \quad (6.6d)$$

where;

f_{slant} : slant shear strength (in MPa)

d_0 : surface treatment type

d_1 : exposed temperature (in °C)

d_2 : basalt fiber volume fraction (in %)

d_3 : concrete compressive strength (in MPa)

The slant shear strength of SCC mixtures exposed to temperature was predicted by handling the aforementioned formula. The normalized slant shear strength values that can be explained as the experimental slant shear strength divided by predicted with respect to experimental slant shear strength have been shown in Figure 6.13.

The normalized slant shear strength signifies an idea about the estimation capableness of the proposed GEP model. In this study, $\pm 10\%$ normalization limit values were designated to show the prediction capableness of proposed GEP model. When Figure 6.13 is observed, it can be easily seen that nearly all normalized values, train and test data, are dispersed between the normalization limits that means the estimation capacity of empirical GEP model can be considered good. In addition to normalized values, the predicted versus experimental flexural strength values for train and test datasets have been plotted in Figures 6.14a and 6.14b, respectively. R-

squared value is another parameter that presents the estimation performance of proposed GEP model. Therefore, the R-squared values for train and test datasets were also submitted in these figures.

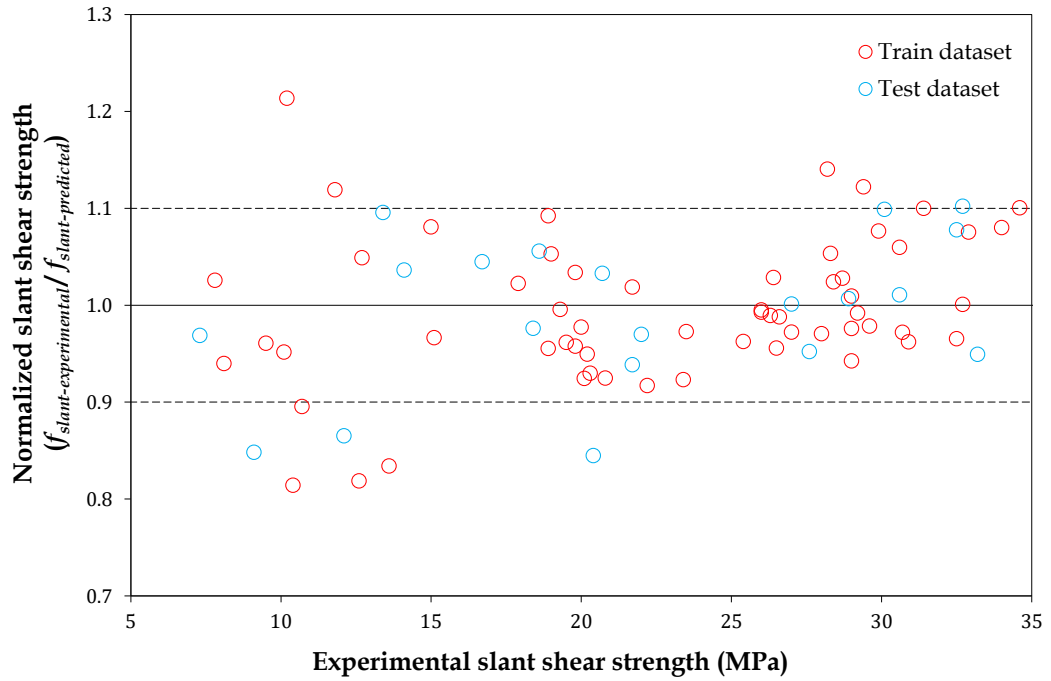
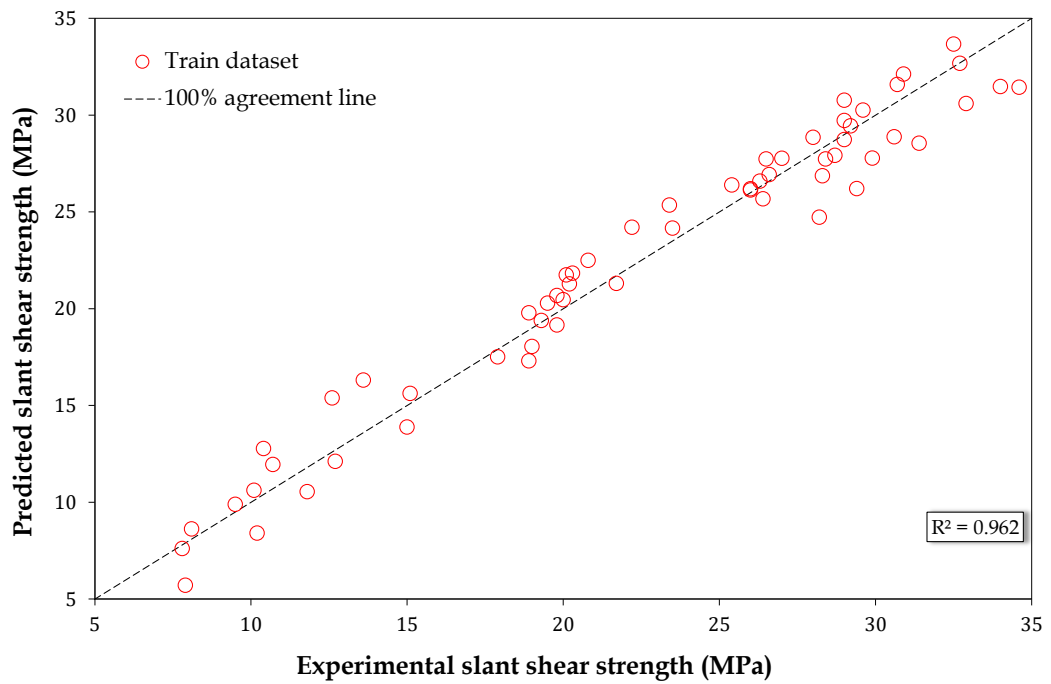
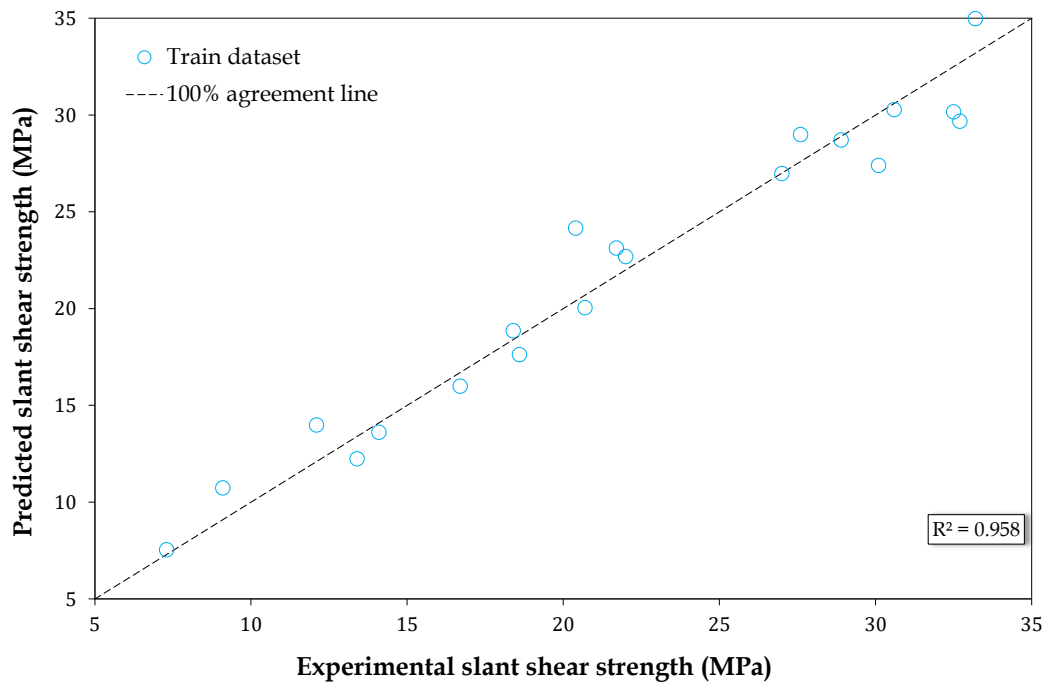


Figure 6.13. Estimation performance of empirical GEP model concerning experimental result



(a)



(b)

Figure 6.14. Predicted versus experimental slant shear strength values for: a) train and b) test datasets

The graphs obviously demonstrate that the predicted and experimental slant shear strength values are well distributed on the 100%-agreement line. In addition, the R-squared values of 0.962 and 0.958 were obtained in the empirical GEP model. It means that the proposed model has good and robust estimation performance since the R-squared value of test dataset is almost same with that of train dataset. The R-squared values attained for this mathematical model also indicate that there is a strong correlation between the experimental and predicted slant shear strength values.

CHAPTER 7

CONCLUSIONS

The study herein covers the experimental test results of self-compacting concrete (SCC) involving basalt fiber and exposed to the different level of temperature. The characteristics of SCC was determined in terms of fresh and hardened state tests. The fresh state tests performed in this study were the slump flow diameter and time, V-funnel flow time, L-box height ratio, and J-ring flow diameter, time, and height difference. However, the hardened properties of SCC mixtures were examined based on the mechanical and permeability properties. The compressive strength, elastic modulus, Poisson's ratio, splitting tensile and flexural strengths, and slant shear strength tests were carried out to observe the mechanical properties whereas the sorptivity index, water penetration depth, and rapid chloride permeability tests were conducted to examine the permeability properties. Based on the test results reported in Chapter 4, statistical evaluation given in Chapter 5, and modelling submitted in Chapter 6, the following findings have been drawn:

7.1 Fresh Workability:

- a) According to the fresh state test results, it can be concluded that the SCC mixtures confirming the EFNARC committee specifications can be manufactured with the basalt fiber till volume fraction of 1.0%.
- b) Slump flow test indicated that the utilization of basalt fiber and increasing its content caused lower slump flow diameter and time values. Especially after 0.25% basalt fiber volume fraction, dramatically reduction in flowability of SCC mixtures was observed.
- c) J-ring test supporting the slump flow test result also revealed that there is a significant negative effect of basalt fiber on the fresh characteristics of SCC. However, this negative effect caused by basalt fiber can be minimized at certain level by changing the amount of superplasticizer. A similar trend was

- d) Observed in both, slump flow and J-ring tests, by increasing of basalt fiber volume fraction.
- e) A delaying in slump flow and J-ring flow times were seen by addition of and increasing the content of basalt fiber. Since the indirect viscosity of concrete is measured by performing these tests, it can be stated that basalt fiber addition resulted in the decreasing of viscosity.
- f) Another indirect viscosity measurement method is V-funnel flow time test and according to this test, it was shown that the basalt fiber utilization has also a negative effect on the viscosity of the SCC. However, the SCC mixtures manufactured in this study conform the EFNARC committee guidelines and specifications.
- g) In addition to the flowability and viscosity of the SCC mixtures, the passing ability of the concrete mixtures produced in this study was also measured by L-box height ratio and J-ring height difference. According to these results, it can be concluded that the SCC mixtures were in the passing ability class range that was recommended by the EFNARC committee although there was a reduction in these test results by basalt fiber addition to the SCC mixture.

7.2 Compressive Strength:

- a) The compressive strength results measured on the 7 and 28-day concrete samples revealed that the 7-day compressive strength values of the SCC mixtures are about $75\pm 5\%$ of the 28-day compressive strength values. It was observed at the compressive strength of both ages that the basalt fiber addition to the SCC decreased the compressive strength values at both ages. Although there is a decreasing in the compressive strength of SCC mixtures by basalt fiber utilization, it is hard to state any certain conclusion about the influence of microfibers on the compressive strength of concrete.
- b) Besides, the compressive strengths of cylindrical specimens exposed to the 3-hour different temperature level of ambient, 200, 300, 400, and 500 °C were also tested. The systematical decreasing in the compressive strength was

observed by the increasing of the temperature. Especially, after 200 °C, there was a sudden reduction in the compressive strength.

7.3 Modulus of Elasticity:

- a) The effects of basalt fiber volume fraction and temperature on the elastic modulus of SCC mixtures were also experimentally investigated. It can be easily said that no significant effect of basalt fiber on the elastic modulus was observed since there is a fluctuating in the elastic modulus with the increasing of the basalt fiber volume fraction. However, it can be clearly seen that the elastic modulus of the mixtures decreased by the increasing of the temperature of the environment.

7.4 Poisson's ratios:

- a) The Poisson's ratios for the SCC mixtures at various basalt fiber volume fractions and different temperature were also measured during this thesis. A slight impact of the temperature on the Poisson's ratio was observed in this study. However, there was an increasing trend for the SCC mixtures kept at ambient temperature up to the basalt fiber volume fraction of 0.50%, but, after this volume fraction, the decreasing in the Poisson's ratio was observed.

7.5 Splitting Tensile:

- a) Moreover, it was observed that the splitting tensile strength of the SCC mixtures increased by 0.25% basalt fiber addition, however, there was a decreasing trend in the splitting tensile strength after 0.25% basalt fiber volume fraction. It may be caused by the decreasing of the self-compactibility of the concrete by higher basalt fiber incorporation. When the effect of the temperature was investigated it would be clearly seen that the temperature adversely affected the splitting tensile strength. By increasing the temperature, a systematic reducing in the splitting tensile strength was observed.
- b) The other test performed to evaluate the tensile behavior of the SCC mixtures is flexural strength test. According to the test result, it can be expressed that basalt fiber utilization enhanced the flexural strength of the SCC. Besides, the

worsening by the temperature exposure was also observed in the flexural strength. It was investigated that the flexural strength values at each fiber volume fraction were slightly decreased when the temperature was increased from ambient to 300 °C. However, a large reduction in the flexural strength was observed after 300 °C temperature exposure.

7.6 Slant shear strength:

- a) The slant shear strength values of the SCC mixtures combined with ordinary concrete that used to represent old concrete were measured and a surface treatment was applied to the casting surface between the old and new concretes in order to improve the slant shear strength characteristic. The surface treatment methods applied in the current study were hole drilling, groove, and sand blasting. In addition to these surface treatment methods, in one concrete series, the surface of the ordinary concrete was kept as casted, namely, no surface treatment was applied.
- b) The lowest slant shear values were procured in the concretes, of which old concrete surfaces were not treated. Applying the surface treatment significantly enhanced the slant shear strength values. Besides, the SCC mixtures, which were employed to represent new concrete, produced with higher basalt fiber volume fraction had the lower slant shear strength values when no surface treatment was applied.
- c) The highest slant shear strength values were observed in the groove and slant blasting surface treated specimens. At the basalt fiber volume fraction of 0 and 0.25%, the slant shear strength values of the sand blasting surface treated specimens were higher than that of groove surface treated whereas at the basalt fiber volume fraction of 1.00%, the slant shear strength value of the groove surface treated specimens were higher than that of sand blasting surface treated.
- d) Also, the effect of the temperature on the slant shear strength was also experimentally investigated. The specimens having no surface treatment were influenced by temperature more than the specimens having a surface treatment.
- e) Apart from the loading test of slant shear strength test, the visual observation on the testing specimen was also carried out. It would be clearly

comprehended that the specimens were failed due to the failing of the interfacial between the concrete surfaces and the failing of overlay concrete (SCC) in the mixtures without treatment. After the basalt fiber volume fraction of 0.25%, the failing of substrate concrete (ordinary concrete) was also observed. However, all specimens, on which hole drilling treatment was applied, were failed due to failing of the interfacial surface and overlay and substrate concretes.

7.7 Sorptivity Index:

- a) The sorptivity index of the SCC mixtures manufactured in this study were determined to show the effect of the basalt fiber utilization on the permeability properties. The results indicated that the greatest capillary water suction was observed in the plain SCC mixture, since its sorptivity coefficient value is the highest. The lowest sorptivity index values were determined for the SCC mixtures including basalt fiber. The reason behind the decreasing of the sorptivity index values by the basalt fiber addition may be the void filling ability of the basalt fiber since the particle sizes of basalt fiber are in the micro-scale.

7.8 Water Penetration Depth:

- a) The results achieved from the water penetration depth test indicated that the lowest water penetration depth value was measured in the plain SCC mixture while the highest water penetration depth value was measured in the SCC mixture manufactured with basalt fiber volume fraction of 0.50%. . The basalt fiber utilization at the content of 0.25% resulted in the decreasing of the water penetration depth whereas the basalt fiber utilization at the contents of 0.50 and 1.00% caused the increasing of the water penetration depth.

7.9 Resistance to chloride ion penetration:

- a) The rapid chloride permeability test was conducted to state the resistance of the SCC mixtures without and with basalt fiber to chloride ion penetration. The highest total charge passed value that means the lowest resistance to chloride ion penetration was measured in the plain SCC mixture whereas the lowest total charge passed value of 41 C was observed in the SCC mixture

produced with the basalt fiber volume fraction of 0.25%. After this basalt fiber volume fraction value, the total charge passed values of the SCC mixtures indicated increasing trend. According to ASTM C1202, the SCC mixtures produced in this study can be considered the negligible chloride ion penetrability.

REFERENCES

- Abdelrahman, A., Rizkalla, S. (1997). Serviceability of concrete beams prestressed by carbon fiber-reinforced-plastic bars. *American concrete institute Structural Journal*. 94(4), 447–454.
- Abdolhosseini Qomi, M. J., KrakowiaK, K. J., Bauchy M., Stewart, R., Jagannathan, D., Brommer, D. B., Baronnet, A., Buehle, M. J., Yip, S., Ulm, F-J, Van, Vlie, K. J. and Pellenq, R. J. M. (2014). Combinatorial molecular optimization of cement hydrates. *Nature communications*, 5, 1-10.
- Abu-Tair, AI., Rigden, SR., Burley, E. (1996). Testing the bond between repair materials and concrete substrate. *American concrete institute Materials Journal*. 553-558.
- ACI 211. (2002). Standard Practice for Selecting Proportions for Normal, Heavyweight, and Mass Concrete, ACI Committee Reports, Guides, Standard Practices, and Commentaries, USA, www.concrete.org
- Adebar, P., Mindess, S., Pierre, D., Olund. (1997). Shear Tests of Fiber Concrete Beams without Stirrups, *American concrete institute Structural Journal*. (94) 1: 68-76.
- Alaee, F. J., Karihaloo, B.L. (2003). Retrofitting of reinforced concrete beams with CARDIFRC. *Journal of Composites for Construction*. 7 (3), 174-186.
- Alcocer, S.M., Jirsa, J.O. (1993). Strength of Reinforced Concrete Frame Connections Rehabilitated by Jacketing. *American concrete institute Structural journal*. 90 (3) 249-261.
- Algin, Z., Ozen, M. (2018). The properties of chopped basalt fibre reinforced self-compacting concrete. *Construction and Building Materials*, 186: 678-85.

Ali, YAZ., Ambalavanan, R. (1999). Flexural behaviour of reinforced concrete beams repaired with styrene-butadiene rubber latex, silica fume and methylcellulose repair formulations. *Magazine of concrete research*. **51**: 113–120.

Alocer, S., Jirsa, J. (1990). Assessment of the response of reinforced concrete frame connections redesigned by jacketing. In: Proceedings of the Fourth US National. *Conference on Earthquake Engineering*. **3**: 295-304.

Arivalagan, S. (2012). Study on the compressive and split tensile strength properties of basalt fiber concrete members, *Global Journal of Researches in Engineering Civil and Structural Engineering*. 12(4).

Armelin, H.S., Banthia, N. (1997). Prediction of Flexural Post Cracking Performance of Steel Fiber Reinforced Concrete from the Full Out of Single Fibers. *American concrete institute Materials Journal*. 94(1): 18-31.

Arslan, M.A. (2016). Effects of basalt and glass fiber chopped fibers addition on fracture energy and mechanical properties of ordinary concrete: CMOD measurement. *Construction and Building Materials*. **114**: 383-91.

Ashour, S.A., Mahmood, K., Wafa, F.F. (1997). Influence of Steel Fibers and Compression Reinforcement on Deflection of High-Strength Concrete Beams. *American concrete institute Structural Journal*. 94(6): 611-624.

ASTM. American Society for Testing and Materials. (2019). ASTM C1202-19. Standard Test Method for Electrical Indication of Concrete's Ability to Resist Chloride Ion Penetration, ASTM International, West Conshohocken, PA, www.astm.org

ASTM. American Society for Testing and Materials. (2017). ASTM C1621 / C1621M-17. Standard Test Method for Passing Ability of Self-Consolidating Concrete by J-Ring, ASTM. International, West Conshohocken, PA, www.astm.org

ASTM. American Society for Testing and Materials. (2018). ASTM C192 / C192M-18. Standard Practice for Making and Curing Concrete Test Specimens in the Laboratory, ASTM International, West Conshohocken, PA, www.astm.org

ASTM. American Society for Testing and Materials. (2018). ASTM C39/C39M-18. Standard Test Method for Compressive Strength of Cylindrical Concrete Specimens, ASTM International, West Conshohocken, PA, www.astm.org

ASTM. American Society for Testing and Materials. (2014). ASTM C469/C469M-14. Standard Test Method for Static Modulus of Elasticity and Poisson's Ratio of Concrete in Compression, ASTM International, West Conshohocken, PA, www.astm.org

ASTM. American Society for Testing and Materials. (2017). ASTM C496 / C496M-17. Standard Test Method for Splitting Tensile Strength of Cylindrical Concrete Specimens, ASTM International, West Conshohocken, PA, www.astm.org

ASTM. American Society for Testing and Materials. (2018). ASTM C78 / C78M-18. Standard Test Method for Flexural Strength of Concrete (Using Simple Beam with Third-Point Loading), ASTM International, West Conshohocken, PA, www.astm.org

ASTM. American Society for Testing and Materials. (2013). ASTM C882 / C882M-13a. Standard Test Method for Bond Strength of Epoxy-Resin Systems Used With Concrete By Slant Shear, ASTM International, West Conshohocken, PA, www.astm.org

Atutis, M., Valivonis, J., Atutis, E. (2015). Analysis of serviceability limit state of GFRP prestressed concrete beams. *Composite Structures*. **134**: 450–459.

Atutis M., Valivonis J., Atutis E. (2018). Experimental study of concrete beams prestressed with basalt fiber reinforced polymers. Part I: Flexural behavior and serviceability. *Composite Structures*. **183**: 114-123.

Austin, S., Robins, P., Pan, V. (1995). Tensile bond testing of concrete repairs. *Materials and Structures*. **28**: 249-259.

Azad, A., Hakeem, I. (2013). Flexure behavior of hybrid high performance concrete construction. Research, Development, and Practice in Structural of the substrate surface. *Construction and Building Materials*. 18(9): 675-681.

Wei, B., Cao, H., Song, S. (2010). Environmental resistance and mechanical performance of basalt and glass fibers. *Materials Science and Engineering*. 527(18–19): 4708 – 4715.

Banthia, N., Gupta, R. (2004). Hybrid fiber reinforced concrete (HFRC): fiber synergy in high strength matrices. *Materials and Structures*. 37 (10): 707–716.

Basaltex. (2019)

http://www.basaltex.com/files/cms1/basalt-fibres-as-reinforcement-forcomposites_ugent.pdf

Berozashvili, M. (2001). continuous reinforcing fibers are being offered for construction, civil engineering and other composites applications. *Advanced material. composite news, composite worldwide*. 21(6): 5-6.

Bett, B.J., Klingner, R.E., Jirsa, J.O. (1988). Lateral load response of strengthened and repaired reinforced concrete columns. *American concrete institute Structural Journal*. 85(5): 499-508.

Borhan, T.M. (2012). Properties of glass concrete reinforced with short basalt fiber. *Materials and Design*. 42:(265–271).

Borhan, T.M. (2013). Thermal and mechanical properties of basalt fibre reinforced concrete. *World Academy of Science, Engineering and Technology International Journal of Civil and Environmental Engineering*. 7(4): 334–7, <https://doi.org/10.5281/zenodo.1058277>.

Brandt, A.M. (2008). Fiber reinforced cement-based (FRC) composites after over 40 years of development in building and civil engineering. *Composite Structures*, 86: 3-9.

Bruhwiller, E., Denarie, E. (2008). Rehabilitation of concrete structures using ultra-High Performance Fiber Reinforced Concrete. The Second International. Symposium on Ultra High Performance Concrete. Kassel, Germany.

Brigante, D. (2014). *New Composite Materials: Selection, Design, and Application*, Springer International. Publishing, Switzerland.

- C., High, H.M., Seliem, A., El-Safty, S.H., Rizkalla. (2015). Use of basalt fibers for concrete structures. *Construction and Building Materials*. **96**: 37–46.
- C., Jiang, K., Fan, F., Wu, D., Chen. (2014). Experimental study on the mechanical properties and microstructure of chopped basalt fibre reinforced concrete. *Materials Design*. **58** :187–193.
- D. Kralj. (2009). Experimental study of recycling lightweight concrete with aggregates containing expanded glass. *Process Safety and Environmental Protection*. **87(4)**: 267–273.
- D.J., Hannant. (2003). Fibre reinforced concrete, in: J. Newman, B.S. Choo (Eds.), *Advanced Concrete Technology-processes*, An Imprint of Elsevier, Oxford. 146–163.
- D.P., Dias, C., Thaumaturgo. (2005). Fracture toughness of geopolymeric concretes reinforced with basalt fibers. *Cement and Concrete Composites*. **27**: 49–54.
- D.Y., Yoo, J.H., Lee, Y.S., Yoon. (2013). Effect of fiber content on mechanical and fracture properties of ultra-high performance fiber reinforced cementitious composites. *Composite Structures*. **106**: 742–753.
- D.Y., Yoo, Y.S., Yoon, N., Banthia. (2015). Predicting the post-cracking behavior of normal- and high-strength steel-fiber-reinforced concrete beams. *Construction and Building Materials*. **93**: 477–485.
- Denarie, E., Bruhwiler, E. (2006). Structural Rehabilitation with ultra-high performance fiber reinforced Concrete. *Restoration of buildings and monuments*. **12(5-6)**: 453-468.
- Dias, D.P., Thaumaturgo, C. (2005). Fracture toughness of geopolymeric concretes reinforced with basalt fibres. *Cement and Concrete Composites*. **27(1)**: 49–54.
- Dong, J.F., Wang, Q.Y., Guan, Z.W. (2017). Material properties of basalt fibre reinforced concrete made with recycled earthquake waste. *Construction and Building Materials*. **130**: 241-251.
- EFNARC. (2005). Specification and guidelines for self-compacting concrete. Free pdf copy downloadable from <http://www.efnarc.org>

Elshafie, S., Boulbibane, M., Whittleston, G. (2016). Mechanical Performance of reinforced concrete with different proportions and length of basalt fiber. *Journal of Material Science and Engineering*.

Emmons, PH. (1994). Concrete Repair and Maintenance. In: Part Three: Surface Repair, Section 6: Bonding Repair Materials to Existing Concrete. MA: R.S. Means Company. 154-163.

F., Bayramov, C., Tasdemir, M.A., Tasdemir. (2004). Optimisation of steel fiber reinforced concretes by means of statistical response surface method. *Cement and Concrete Composites*. **26**, 665–675.

F., Rezaie, S.M., Farnam. (2015). Fracture mechanics analysis of pre-stressed concrete sleepers via investigating crack initiation length. *Engineering Failure Analysis*. 58 (Part 1) 267–280.

F.U.A., Shaikh. (2013). Review of mechanical properties of short fiber reinforced geopolymer composites. *Construction and Building Materials*. **43**: 37–49.

Farhat, F., Nicolaidis, D., Kanellopoulos, A., Karihaloo, B. (2010). Behavior of RC Beams Retrofitted with CARDIFRC after thermal Cycling. *Journal of Material in Civil Engineering*. 22 (**21**).

Farhat, F., Nicolaidis, D., Kanellopoulos, A., Karihaloo, B. (2007). High performance fiber reinforced cementitious composite (CARDIFRC) Performance and application to retrofitting. *Engineering Fracture Mechanics*. 74(**1-2**). 151-167.

Ferreira, C. (2001). Gene expression programming; a new adaptive algorithm for solving problems. *Complex Systems*. 12(**2**): 87–129.

Fiore, V., Di Bella, G., Valenza, A. (2011). Glass-basalt/epoxy hybrid composites for marine applications. *Materias and Design*. **32**: 2091–2099.

Garbacz, A., Gorka, M., Courard, L. (2005). Effect of concrete surface treatment on adhesion in repair systems. *Magazine of Concrete Research*. 57(**1**): 49-60.

Gaythwaite, J.W. (2004). Design of marine facilities for the berthing, mooring and repair of vessels. American Society of Civil Engineers.

Gen, M., Cheng, R. (1997). Genetic Algorithms and Engineering Design, Wiley, Hoboken, NJ, USA.

Ghali A. (2014). Circular storage tanks and silos. CRC Press.

Graybeal, B.A. (2009). UHPC making strides, Public Roads, Federal. Highway Administration, McLean, VA, **72**: 17-21.

Graybeal., B.A. (2006). Material. Property Characterization of Ultra-High Performance Concrete, Report No. FHWA-HRT-06-103, Federal. Highway Administration, Washington, DC.

Güneyisi, E.M., Mermerdaş, K., Güneyisi, E., Gesoğlu, M. (2014). Numerical modeling of time to corrosion induced cover cracking in reinforced concrete using soft-computing based methods. *Materials and Structures*. 48(6):1739-1756.

Habel, K. (2004). Structural behavior of composite UHPFRC-concrete elements Doctoral. Thesis, Swiss Federal Institute of Technology. Lausanne, Switzerland.

Habel, K., Viviani, M., Denarie, E., Bruhwiler, E. (2006). Development of the mechanical properties of an Ultra-High Performance Fiber Reinforced Concrete. *Cement and Concrete Research*. 36(7): 1362-1370.

Haido, J. H. (2011). Nonlinear Dynamic Analysis Of Steel Fiber Reinforced Concrete Beams And Slabs. PhD thesis, Universiti Sains Malaysia.

Haido, J. H., Dinkha, Y. Z., Abu-Bakar, B. H. (2018) Slant shear strength of hybrid concrete made with old and new parts using reactive and inert waste powders. *Academic Journal of Nawroz University*. 7(4). 236-244.

Harris, D.K., Sarkar, J., Ahlborn, T.M. (2011). Interface Bond Characterization of Ultra-High Performance Concrete Overlays. *Paper presented at the Transportation Research Board 90th Annual Meeting*.

Hindo, K.R. (1990). In-place bond testing and surface preparation of concrete. *Concrete Int.* (April). 127-129.

http://www.basaltex.com/files/cms1/basalt-fibres-as-reinforcement-forcomposites_ugent.pdf. 2019

Huang, Zhang, Bin, Wang, Aoyu, Xie, Yazhen, Qi. (2017). Experimental study on dynamic mechanical properties and constitutive model of basalt fiber reinforced concrete. *Construction and Building Materials*. **152**: 154-167.

Huaxin, Liu, Jianwei, Yang, Xiangqing, Kong, Xuxu, Xue. (2017). Basic Mechanical Properties of Basalt Fiber Reinforced Recycled Aggregate Concrete. *The open civil engineering journal*. **11**: 43-53.

J. Ma, X. Qiu, L. Cheng, Y. Wang. (2011). Experimental research on the fundamental Mechanical properties of presoaked basalt fiber concrete, in: Lieping Ye, Peng Feng, Qingrui Yue (Eds.), *Advances in FRP Composites in Civil Engineering*, Springer, Berlin, Heidelberg. 85–88.

J., Michels, R., Christen, D., Waldmann. (2013). Experimental and numerical investigation on postcracking behavior of steel fiber reinforced concrete. *Engineering Fracture Mechanics*. **98**: 326–349.

J., Sim, C., Park, D.Y., Moon. (2005). Characteristics of basalt fiber as a strengthening material for concrete structures. *Composite Part B: Engineering*. **36** (6–7) 504–512.

J.F., Dong, Q.Y., Wang, Z.W., Guan. (2017). The influence of cooling processes on the corrosion performance of the rebar scale. *Construction and Building Materials*. 241-251.

Jiang, C., Fan, K., Wu, F., Chen, D. (2014). Experimental study on the mechanical properties and mixrostructure of chopped basalt fibre reinforced concrete. *Materials and Design*. **58**: 187-93.

Julio, E.N.B.S., Branco, F.A.B., Silva, V.D. (2004). Concrete-to-concrete bond strength influence of the roughness of the substrate surface. *Construction and Building Materials*. **18**(9), 675-681.

Jun, W., Ye, Z. (2010). Experimental research on mechanical and working properties of non-dipping chopped basalt fiber reinforced concrete, in: 3rd International Conference on Information Management, Innovation Management and Industrial Engineering, China. 635–637.

- Kamutha, Dr.R., I.syedali Fathima, Dr.K., Vijai. (2017). Experimental Investigation on Properties of Basalt Fiber Reinforced Geopolymer Concrete. *Journal of Mechanical and Civil Engineering*. 14(3): 105-109
- K. Zielinski, P. Olszewski. (2005). The impact of basalt fiber on selected physical and mechanical properties of cement mortar. *Betonwerk Fertigteil Technik*. 771 (3): 28-33.
- K., Arunagiri, P., Elanchezhiyan, V., Marimuthu, G., Arunkumar, P., Rajeswaran. UG. (2017). Mechanical Properties of Basalt Fiber Based Geopolymer Concrete. International. *Journal of Science Engineering and Technology Research*. 6 (4): 2278-7798.
- K.P. Mehta, P.J.M. Monteiro. (2006). Concrete: Microstructure, Properties and Materials, 3rd ed., McGraw-Hill. 146–163.
- Kabay, N. (2014). Abrasion resistance and fracture energy of concretes with basalt fiber. *Construction and Building Materials*. 50: 95–101.
- Kizilkanat, A.B., Kabay, N., Akyüncü, V., Chowdhury, S., Akça, A.H. (2015). Mechanical properties and fracture behavior of basalt and glass fiber reinforced concrete: An experimental study. *Construction and Building Materials*. 100: 218-24.
- Koza, J.R. (1992). Genetic Programming; on the Programming of Computers by Means of Natural Selection, MIT Press, Cambridge, MA, USA.
- L.S. Hsu, C.T.T. Hsu. (1994). Stress-strain behavior of steel-fiber high-strength concrete under compression. *American concrete institute Structure Journal*. 91 (4): 448–457.
- Lees, J.M., Burgoyne, C.J. (1999). Experimental study of influence of bond on flexural behavior of concrete beams pretensioned with aramid fiber reinforced plastics. *American concrete institute Structure Journal*. 96(3): 377–385.
- Li, B.X., Chen, M.X., Cheng, F., Liu, L.P. (2004). The mechanical properties of polypropylene fiber reinforced concrete. *Journal of Wuhan University of Technology Material Science*. 11(19):68–71.

- Li, V.C. (2003). On engineered cementitious composites (ECC). *Journal of Advanced Concrete Technology*. **1**: 215-230.
- Li, V.C., Wang, S., Wu, C. (2001). Tensile strain-hardening behavior of polyvinyl alcohol engineered cementitious composite (PVA-ECC). *American concrete institute Materials Journal*. **98**: 483-492.
- Li, X., Zhou, C., Xiao, W., Nelson, P.C. (2005). Prefix gene expression programming. In Proceedings of Late Breaking Paper at the Genetic and Evolutionary Computation Conference, Washington, DC, USA.
- Long, W., Mai, Z., Shi, J., Zhao, T., Peng, W. (2016). Research on chloride penetration resistance of hybrid fiber reinforced self-compacting concrete, 5th International Conference on Durability of Concrete Structures, Shenzhen University, Shenzhen, Guangdong Province, P.R. China.
- Lopresto, V., Leone, C., De Iorio, I. (2011). Mechanical characterization of basalt fiber reinforced plastic. *Composite Part B: Engineering*. **42**:717–723.
- Lu, Z., Xian, G., Li, H. (2015). Effects of exposure to elevated temperatures and subsequent immersion in water or alkaline solution on the mechanical properties of pultruded basalt fiber-reinforced polymer plates. *Composite Part B: Engineering*. **77**: 421-30.
- Lu, X.B., Hsu., C.T.T. (2006). Behaviour of high strength concrete with and without steel fiber reinforcement in triaxial compression, *Cement and Concrete Research*. **36** (9): 1679–1685.
- M. Di Ludovico, A. Prota, G. Manfredi. (2010). Structural upgrade using basalt fibers for concrete confinement. *Journal of Composite for Construction*. **14** (5): 541–552.
- M.G., Alberti, A., Enfedaque, J.C., Gálvez. (2016). Fracture mechanics of polyolefin fiber reinforced concrete: study of the influence of the concrete properties, casting procedures, the fiber length and specimen size. *Engineering Fracture Mechanics*. **154**: 225–244.

- Markovic, I. (2006). High-performance hybrid-fiber concrete: development and utilization, PhD thesis, Delft University of Technology.
- Mingchao, W. (2008). Chemical Durability and Mechanical Properties of Alkali-proof Basalt Fiber and its Reinforced Epoxy Composites. *Journal of Reinforced Plastics and Composites*. 27(4): 393-407
- Momayez, A., Ehsani, M.R., Ramezani-pour, A.A., Rajaie, H. (2005). Comparison of methods for evaluating bond strength between concrete substrate and repair materials. *Cement and Concrete Research*. 35(4), 748–757.
- Mu, B., Meyer, C., Shimanovich, S. (2002). Improving the interface bond between fiber mesh and cementitious matrix. *Cement and Concrete Research*. 32(5): 783–787.
- N. Kabay. (2014). Abrasion resistance and fracture energy of concretes with basalt fiber. *Construction and Building Materials*. 50:95–101.
- Naaman, A.E, Reinhardt, H.W. (2006). Proposed classification of HPFRC composites based on their tensile response. *Materials and Structures*. 39: 547-555.
- Naaman, A.E., Homrich, J.R. (1989). Tensile stress-strain properties of SIFCON. *American concrete institute Materials Journal*. 86: 244-251.
- P., Asokan, M., Osmani, A.D.F. (2009). Price, Assessing the recycling potential. of glass fiber reinforced plastic waste in concrete and cement composites. *Journal of Cleaner Production*. 17 (9): 821–829.
- Palmieri, A., Matthys, S., Tierens, M. (2009). Basalt fibers: mechanical properties and applications for concrete structures. Concrete solutions: proceedings of the international conference on concrete solutions. CRC Press/Balkema.165-169.
- Pellenq, R.J.M., Kushima, A., Shahsavari, R., Vliet, K.J.V., Buehler, M.J. (2009). A realistic molecular model of cement hydrates. *Proceedings of the National Academy of Sciences*. 106: 16102-16107.
- Pfeifer, C.G., Moeser, B., Giebson, C., Stark, J. (2009). Durability of ultra-high-performance concrete, Tenth ACI International. Conference on Recent Advances in Concrete Technology and Sustainability Issues, No. SP-261-1.

Ramakrishnan, V. (1993). Recent Advancements in Concrete Fiber Composites. ACI-Singapore Chapter-Special. Publication, July 19.

Ramakrishnan, V. (1997a). Performance Characteristics and Applications of High - Performance Synthetic Fiber Reinforced Concretes, Proceedings of the International Workshop on High Strength Concrete and Structural Strengthening, Singapore, Nov. **29**:33-54.

Ramakrishnan, V., (1997b). Structural Applications of Polyolefin Fiber Reinforced concrete," American Concrete Institute, Spring Convention, Session on "Structural Application of Fiber Reinforced Concrete, Seattle, Washington, April 6-11. (Accepted for publication in the proceedings.)

Ramakrishnan, V., Neeraj, S., Tolmare, Vladimir B. Brik. (1998). Performance Evaluation of 3-D Basalt Fiber Reinforced Concrete & Basalt Rod Reinforced Concrete. Final. Report for Highway IDEA Project 45, Transportation Research Board, 79.

Ramirez, J.L., Barcena, J.M., Urreta, J.I., Sanchez, J.A. (1991). Repair of concrete columns with partial Localized damages. Report T 2.1 and 2.2 BREU-0186-C, April.

Rodriguez, M., Park, R. (1994). Seismic load tests on reinforced concrete columns strengthened by jacketing. *American concrete institute Structural journal*. (March-April): 150-159.

Rossi, P. (2002). Development of new cement composite material for construction, Innovation And Developments in Concrete Materials and Construction.

Rossi, P. (1997). High performance multimodal fiber reinforced cement composites (HPMFRCC): the LCPC Experience. *American concrete institute Material. Journal*. 478–483.

S.J., Jin, Z.L., Li, J., Zhang, Y.L, Wang. (2014). Experimental study on the performance of the basalt fiber concrete resistance to freezing and thawing. *Applied and Mechanic Materials*. 584-586: (1304-1308)

S.T., Tassew, A.S., Lubell. (2014) Mechanical properties of glass fiber reinforced ceramic concrete. *Construction and Building Materials*. **51**: (215–224).

Sakhavand, N., Muthuramalingam, P., Shahsavari, R. (2013). Toughness governs the rupture of the interfacial H-bond assemblies at a critical. length scale in hybrid materials . *Langmuir*. 29(**25**): 8154-8163.

Santos, P.M.D., Julio, E.N.B. (2011). Factors affecting bond between new and old concrete. *American concrete institute Material Journal*. 108(**4**): 449-456.

Sarkar, J. (2010). Characterization of the bond strength between ultra-high performance concrete substrates. Master of Science: Civil Engineering. Michigan Technological. University.

Sarsam, K.F., Mohammed. (2014). M.H. Load-Deflection Behavior of Hybrid Beams Containing Reactive Powder Concrete and Conventional. *Concrete Journal of Engineering and Development*. 18(**3**): 118-147.

Saucier, F., Pigeon, M. (1991). Durability of new-to-old concrete bonding. In: Proceedings of the ACI International. Conference Evaluation and Rehabilitation of Concrete Structures and Innovations in Design, Hong Kong. **1**: 689-707.

Sen, R., Shahawy, M., Rosas, J., Sukumar, S. (1998). Durability of aramid pretensioned elements in a marine environment. *American concrete institute Structural Journal*. 95(**5**): 578–586.

Serbescu, A., Guadagnini, M., Pilakoutas, K. (2014). Mechanical characterization of basalt FRP rebars and long-term strength predictive model. *Journal of Composites for Construction*. 19(**2**): 04014037.

[http://dx.doi.org/10.1061/\(ASCE\)CC.1943-5614.0000497](http://dx.doi.org/10.1061/(ASCE)CC.1943-5614.0000497).

Shahin, Y., Köksal, F. (2011). The influences of matrix and steel fiber tensile strengths on the fracture energy of high-strength concrete. *Construction Building Materials*. 25 (**4**): 1801–1806.

Shahsavari, R., Sakhavand, N. (2016). Hybrid cementitious materials: nanoscale modelling and characterization. Woodhead publishing series in civil and structural engineering, Elsevier.

Shin, H-C., Wan, Z. (2010). Interfacial Properties between New and Old Concretes. Second International Conference on Sustainable Construction Materials and Technologies. Ancona, Italy.

Shi, J., Chen, Z., Shao, S., Zheng, J. (2014). Experimental and numerical study on effective thermal conductivity of novel form-stable basalt fiber composite concrete with PCMs for thermal storage. *Applied thermal engineering*. **66**: 156–161.

Silfwerbrand, J. (1990). Improving concrete bond in repaired bridge decks *Concrete Int*:(September). 121-126.

Sivakumar, A., Santhanam, M. (2007). Mechanical properties of high strength concrete reinforced with metallic and non-metallic fibers. *Cement and Concrete Composites*. (8): 603–608.

Stoppenhagen, D.R., Jirsa, J.O., Wyllie, L.A. (1995). Seismic repair and strengthening of a severely damaged concrete frame. *American concrete institute Structural Journal*. (March• April):177-187.

Talbot, C., Pigeon, M., Beaupre, D., Morgan, DR. (1994). Influence of surface preparation on long-term bonding of shotcrete. *American concrete institute Structural Journal*: (November-December). 560-566.

Tayeh, B.A., Abu-Bakar, B.H., Johari, M.A.M., Voo, Y.L. (2013). Utilization of ultra-high performance fiber concrete (UHPFC) for rehabilitationa review. *Procedia Engineering*. **54**: (525-538).

Tayeh, B.A., Abu Bakar, B.H., Megat Johari, M.A., Voo Y.L. (2012). Mechanical and permeability properties of the interface between normal concrete substrate and ultra-high performance fiber concrete overlay. *Construction and Building Materials*. **36**: (538–548).

Torres, L., Sharaky, I., Barris, C., Baeba, M. (2013). Experimental study of the influence of adhesive properties and bond length on the bond of NSM FRP Bars in Concrete. *Journal of Civil Engineering Management*. **22(6)**: 808–817.

TS-EN 12390-8. (2002). Testing Hardened Concrete-Part 8: Depth of Penetration of Water under Pressure. Institute of Turkish Standards, Ankara, Turkey.

- Tsinker, G. (1997). Handbook of port and harbor engineering. Springer.
- Tumadhir, M., Borhan. (2013). World Academy of Science, Engineering and Technology International. *Journal of Civil and Environmental Engineering*. 7(4).
- U.A.S. Faiz. (2013). Review of mechanical properties of short fibre reinforced geopolymer composites. *Construction and Building Materials*. **43**: 37–49.
- Vaysburd, A., Emmons, P. (2000). How to make today's repairs durable for tomorrow-corrosion protection in concrete repair. *Construction and Building Materials*. 14(4): 189-197.
- W., Li, J., Xu. (2009). Mechanical properties of basalt fiber reinforced geopolymeric concrete under impact loading. *Materials Science and Engineering*. **505**: 178–186.
- Weimin, Li., Jinyu, Xu. (2009). Impact characterization of basalt fiber geopolymeric concrete using a 100-mm-diameter split Hopkinson pressure bar. *Material science and engineering*. (513-514): 145-153.
- Warren A (2013) Report on Engineering Fibers.
- Wille, K., Naaman, A.E., Parra-Montesinos, G.J. (2011). Ultra-high performance concrete with compressive strength exceeding 150 MPa (22 ksi): A simpler way. *American concrete institute Materials Journal*. **108**: 46-54.
- Wu J, Li H, Xian G. (2010). Influence of elevated temperature on the mechanical and thermal performance of BFRP rebar. CICE 2010. In: 5th int. Conf. FRP composites in Civil engineering. Beijing: Tsinghua University Press. 69-72.
- X., Hu, T., Shen. (2005). The applications of the CBF in war industry and civil fields. *Hi-Tech Fiber and Application*. **30**: 7–13.
- Y., Uchida, N., Kurihara, K., Rokugo, W., Koyanagi. (1995). Determination of tension softening diagrams of various kinds of concrete by means of numerical analysis in: F.H. Wittmann (Ed.), *Fracture Mechanics of Concrete Structures*, Aedificatio Publishers, Freiburg, Germany. 17–30.

Yuan, Y.S., Marosszeky, M. (1991). Major factor influence the performance of structural repair Evaluation and rehabilitation of concrete structures and innovations in design, Proceedings of ACI international Conference, Hong Kong. 128–150.

Yoo, D.Y., J.H. Lee, Y.S. Yoon. (2013). Effect of fiber content on mechanical and fracture properties of ultra-high performance fiber reinforced cementitious composites. *Composites Structures*. **106**: (742–753).

Yoo, D.Y., Y.S. Yoon, N. Banthia. (2015). Predicting the post-cracking behavior of normal- and high-strength steel-fiber-reinforced concrete beams. *Constrion and Building Materials*. 93: 477–485.

Z.G., Yan, H.H., Zhu, J.W., Ju. (2013). Behaviour of reinforced concrete and steel fiber reinforced concrete shield TBM tunnel linings exposed to high temperatures. *Constrion and Building Materials*. **38**: 610–618

Zadeh, L.A. (1994). Soft computing and fuzzy logic. *IEEE Software*. **6**: 48–56.

PERSONAL INFORMATION

Name and surname : Samadar Salim MAJEED

Nationality : Iraqi

Birth place and date : Iraq- Duhok / 1989

Marital status : Married

Phone number : +9647504594636

Email : samadar7090@gmail.com

EDUCATION

	Graduate school	Year
Master	College of Engineering/ Civil Department Gaziantep University - Turkey	2015
Bachelor	College of Engineering/ Civil Department Duhok University - Iraq	2011
High school	Alla typical Secondary school	2007

WORK EXPERIENCE

Years	Place	Enrollment
2015 -Present	Nawroz University	Ass. Lecturer at Architectural Department and Head of Engineering and Maintenance Department
2011-2015	Saril Company	Supervisor Engineer

PUBLICATIONS

FOREIGN LANGUAGE

English, Turkish, Arabic and Kurdish